EPRI | ELECTRIC POWER RESEARCH INSTITUTE

2007-349 BWR Vessel & Internals Project (BWRVIP)

November 21, 2007

Document Control Desk
U. S. Nuclear Regulatory Commission
11555 Rockville Pike
Rockville, MD 20852

Attention: John Honcharik

Subject: Project No. 704 – BWRVIP-108NP: BWR Vessel and Internals Project, Technical Basis for the Reduction of Inspection Requirements for the Boiling Water Reactor Nozzle-to-Vessel Shell Welds and Nozzle Blend Radii

Reference: BWRVIP letter 2002-323 from Carl Terry (BWRVIP Chairman) to Document Control Desk (NRC), "Project No. 704 – BWRVIP-108: BWR Vessel and Internals Project, Technical Basis for the Reduction of Inspection Requirements for the Boiling Water Reactor Nozzle-to-Vessel Shell Welds and Nozzle Blend Radii," dated November 25, 2002.

Enclosed are five (5) copies of the non-proprietary report "BWRVIP-108NP: BWR Vessel and Internals Project, Technical Basis for the Reduction of Inspection Requirements for the Boiling Water Reactor Nozzle-to-Vessel Shell Welds and Nozzle Blend Radii," EPRI Technical Report 1016123, November 2007. This report is being transmitted to the NRC as a means of exchanging information with the NRC for the purpose of supporting generic regulatory improvements related to inspections of BWR nozzle-to-vessel shell welds and nozzle blend radii.

The enclosed non-proprietary report supersedes the proprietary version of this report transmitted to the NRC by the BWRVIP letter referenced above. The content of the enclosed report is identical to that of the proprietary version. The BWRVIP is providing this non-proprietary version to facilitate use of the information in the report in public forums by the NRC and other organizations such as the ASME Code.

If you have any questions on this subject please call Bob Geier (Exelon, BWRVIP Assessment Committee Technical Chairman) at 630.657.3830.

Sincerely,

Rick Libra

Rick Libra
Exelon
Chairman, BWR Vessel and Internals Project

D058

Extra copies sent TO PM

PALO ALTO OFFICE
3420 Hillview Avenue, Palo Alto, CA 94304-1395 USA • 650.855.2000 • Customer Service 800.313.3774 • www.epri.com

EPRI | ELECTRIC POWER RESEARCH INSTITUTE

BWRVIP-108NP: BWR Vessel and Internals Project

Technical Basis for the Reduction of Inspection Requirements for the Boiling Water Reactor Nozzle-to-Vessel Shell Welds and Nozzle Blend Radii

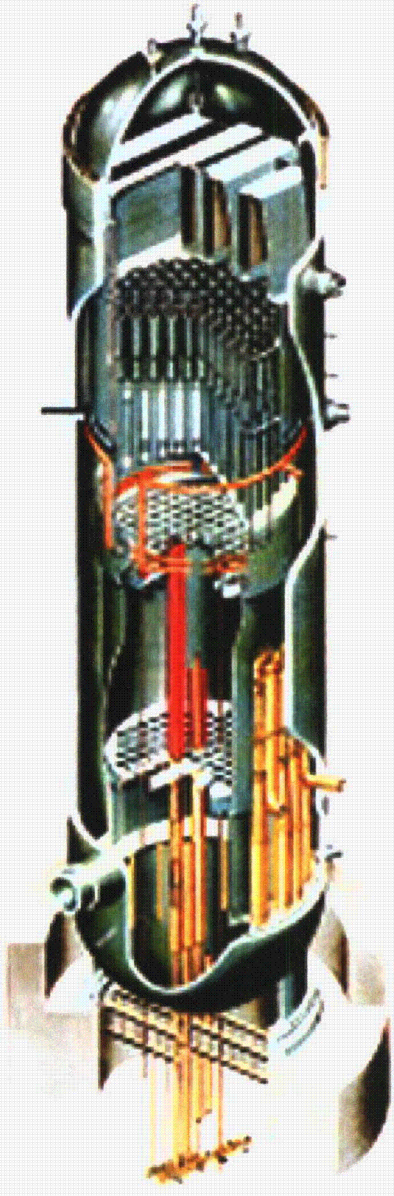

BWRVIP-108NP: BWR Vessel and Internals Project

Technical Basis for the Reduction of Inspection Requirements for the Boiling Water Reactor Nozzle-to-Vessel Shell Welds and Nozzle Blend Radii

1016123

Technical Report, November 2007

EPRI Project Manager
R. Carter

ELECTRIC POWER RESEARCH INSTITUTE
3420 Hillview Avenue, Palo Alto, California 94304-1338 • PO Box 10412, Palo Alto, California 94303-0813 • USA
800.313.3774 • 650.855.2121 • askepri@epri.com • www.epri.com

DISCLAIMER OF WARRANTIES AND LIMITATION OF LIABILITIES

THIS DOCUMENT WAS PREPARED BY THE ORGANIZATION(S) NAMED BELOW AS AN ACCOUNT OF WORK SPONSORED OR COSPONSORED BY THE ELECTRIC POWER RESEARCH INSTITUTE, INC. (EPRI). NEITHER EPRI, ANY MEMBER OF EPRI, ANY COSPONSOR, THE ORGANIZATION(S) BELOW, NOR ANY PERSON ACTING ON BEHALF OF ANY OF THEM:

(A) MAKES ANY WARRANTY OR REPRESENTATION WHATSOEVER, EXPRESS OR IMPLIED, (I) WITH RESPECT TO THE USE OF ANY INFORMATION, APPARATUS, METHOD, PROCESS, OR SIMILAR ITEM DISCLOSED IN THIS DOCUMENT, INCLUDING MERCHANTABILITY AND FITNESS FOR A PARTICULAR PURPOSE, OR (II) THAT SUCH USE DOES NOT INFRINGE ON OR INTERFERE WITH PRIVATELY OWNED RIGHTS, INCLUDING ANY PARTY'S INTELLECTUAL PROPERTY, OR (III) THAT THIS DOCUMENT IS SUITABLE TO ANY PARTICULAR USER'S CIRCUMSTANCE; OR

(B) ASSUMES RESPONSIBILITY FOR ANY DAMAGES OR OTHER LIABILITY WHATSOEVER (INCLUDING ANY CONSEQUENTIAL DAMAGES, EVEN IF EPRI OR ANY EPRI REPRESENTATIVE HAS BEEN ADVISED OF THE POSSIBILITY OF SUCH DAMAGES) RESULTING FROM YOUR SELECTION OR USE OF THIS DOCUMENT OR ANY INFORMATION, APPARATUS, METHOD, PROCESS, OR SIMILAR ITEM DISCLOSED IN THIS DOCUMENT.

ORGANIZATION(S) THAT PREPARED THIS DOCUMENT

Structural Integrity Associates

Electric Power Research Institute

NOTE

For further information about EPRI, call the EPRI Customer Assistance Center at 800.313.3774 or e-mail askepri@epri.com.

CITATIONS

This report was prepared by

Structural Integrity Associates
3315 Almaden Expressway, Suite 24
San Jose, CA 95118-1557

Principal Investigators
M. Herrera
S. Tang

Electric Power Research Institute
3420 Hillview Avenue
Palo Alto, CA 94303

Principal Investigator
L. Becker

This report describes research sponsored by the Electric Power Research Institute (EPRI) and its BWRVIP participating members.

The report is a corporate document that should be cited in the literature in the following manner:

BWRVIP-108NP: BWR Vessel and Internals Project, Technical Basis for the Reduction of Inspection Requirements for the Boiling Water Reactor Nozzle-to-Vessel Shell Welds and Nozzle Blend Radii. EPRI, Palo Alto, CA: 2007. 1016123.

PRODUCT DESCRIPTION

This report presents the technical basis to reduce inspection requirements of Boiling Water Reactor (BWR) Reactor Pressure Vessel (RPV) nozzle-to-shell welds and nozzle blend radii. Currently, BWR RPV welds are inspected per American Society of Mechanical Engineers (ASME) Boiler and Pressure Vessel (B&PV) Code, Section XI requirements, which requires 100% inspection each 10-year interval. This project provides the technical basis for the reduction of the nozzle-to-shell welds and nozzle blend radii to 25% of the nozzles every 10 years. The 25% coverage refers to 25% of the nozzles for each nozzle type, e.g., 1 of 4 core spray nozzles would be inspected. This report is the non-proprietary version of 1003557.

Results & Findings

Field experience has shown that very few indications have been discovered at the nozzle-to-shell weld. In addition, excluding the feedwater and control rod drive return lines (CRDRL) nozzles, very few indications have been seen at nozzle blend radius locations. Thus, field inspection results support the reduction of inspection requirements of the nozzle-to-shell weld and blend radius locations. For any cracks in the nozzle blend radius region, the results show that the conditional failure probability of the nozzles—due to a low temperature overpressure (LTOP) event—are very small ($<1x10^{-6}$ for 40 years), even without any inservice inspection. At the nozzle-to-vessel shell weld, the conditional probability of failure—due to the LTOP event—is also very small ($<1x10^{-6}$ for 40 years), with or without any in-service inspection.

Challenges & Objectives

Current requirements for the inspection of the nozzle-to-shell welds and nozzle blend radii are costly and result in significant radiation exposure to examiners. The performance of NDE has improved substantially such that there is a high reliability of detecting flaws that can challenge the structural integrity of BWR nozzles and their associated welds. Knowledge of improved NDE capabilities, coupled with fracture mechanics, provides the technical basis to justify reduction of inspections while maintaining safety.

Applications, Values & Use

The 25% sampling level provides a significant cost savings and reduces worker dose exposure. Several utilities have estimated that the proposed reduction of inspection requirements would result in a savings of up to $750,000 per 10-year interval, not including exposure considerations. The dose exposure has been estimated at approximately 75% of the current exposure.

EPRI Perspective

The BWR Vessel and Internals Project (BWRVIP) successfully completed a project to eliminate the requirement for inspection of RPV circumferential welds (TR-105697). The results of the

PFM evaluation contributed significantly to the technical justification for elimination of circumferential weld inspections. This project utilizes and benefits from a similar methodology, thereby extending the application of EPRI-developed technology.

Approach

The project team evaluated the available field inspection data and performance demonstration data for BWR nozzles. They selected representative nozzles for the evaluation, including core spray, main steam, and recirculation inlet and outlet nozzles. Probabilistic fracture mechanics (PFM) and deterministic fracture mechanics (DFM) calculations were performed to assess the reliability of the nozzles after implementing the revised inspection approach. The PFM code—VIPER—developed by the BWRVIP with a successful first use in TR-105697, employs Monte Carlo methods to assess the reliability of a BWR RPV having flaw distributions, material properties, fluence distributions, and several other parameters, which are assumed to be randomly distributed. A DFM evaluation was also performed to demonstrate that expected flaws, based on field experience, would not jeopardize the structural integrity of the vessel. A flaw is selected that bounds any expected flaws based on field inspection results. Using appropriate material properties, a deterministic linear elastic fracture mechanics evaluation is performed to demonstrate that failure is not expected.

Keywords

Boiling water reactor
Reactor pressure vessel
Stress corrosion cracking
Probabilistic fracture mechanics

CONTENTS

1 BACKGROUND 1-1

1.1 Introduction 1-1

2 INSPECTION HISTORY AND EXAMINATION EFFECTIVENESS BASED ON PERFORMANCE DEMONSTRATIONS 2-1

2.1 Examination Effectiveness 2-1

2.1.1 Detection 2-1

2.1.2 Sizing 2-5

2.1.3 Flaw Acceptability Evaluation in Light of Examination Uncertainties 2-7

2.2 Inspection History 2-12

2.2.1 Manufacturing and Preservice Inspection 2-12

2.2.2 Nozzle Inner-Radius Inservice Examinations 2-12

2.2.3 Inservice Inspection of Nozzle-to-Vessel Welds 2-12

2.2.4 Inspection History 2-13

2.3 Conclusions 2-13

3 SURVEY OF BWR NOZZLES, DATA COLLECTION AND SELECTION OF REPRESENTATIVE NOZZLES FOR ANALYSIS 3-1

3.1 Vessel Geometry and Design Features 3-1

3.2 Vessel/Vessel Nozzle Materials and Fabrication 3-4

3.3 Nozzles and Penetration Design Features 3-5

3.4 Selection of Nozzles for Evaluation 3-6

4 NOZZLE STRESS ANALYSIS 4-1

4.1 Analysis 4-3

4.1.1 Finite Element Models 4-3

4.1.2 Material Properties 4-6

4.1.3 Loads and Boundary Conditions 4-7

4.2 Results of Stress Analysis 4-17

5 PROBABILISTIC FRACTURE MECHANICS EVALUATION 5-1
5.1 Methodology 5-1
5.2 Design Inputs 5-1
5.3 Assumptions 5-3
5.4 Fatigue Crack Growth 5-3
5.5 Stress Results and Fatigue Cycle Loadings 5-8
5.5.1 Core Spray Nozzle 5-8
5.5.2 Main Steam Nozzle 5-9
5.5.3 Recirculation Inlet Nozzle 5-9
5.5.4 Recirculation Outlet Nozzle 5-10
5.6 Probabilistic Fracture Mechanics Evaluation Results 5-10
5.7 Results of Analyses 5-11
5.7.1 Inspection Sampling of 0% (No Inspection) 5-13
5.7.2 Inspection Sampling of 25% 5-13
5.7.3 Inspection Sampling of 90% 5-14

6 DETERMINISTIC FRACTURE MECHANICS EVALUATION 6-1

7 SUMMARY 7-1

8 REFERENCES 8-1

LIST OF FIGURES

Figure 2-1 Probability of Detection Performance for Passed and Passed Plus Failed Candidates for Appendix VIII Supplement 4, from the Outside Surface. Both Automated and Manual Techniques are Included 2-3
Figure 2-2 Probability of Detection for Manual, Automated and Combined (ALL), Considering All Candidates (Pass Plus Failed) 2-4
Figure 2-3 Probability of Detection for Manual, Automated, and Combined (ALL), Considering Only Passed Candidates 2-4
Figure 2-4 Histogram of Depth Successful Sizing Candidate Test Scores, Appendix VIII, Supplement 4. Examinations were Performed Both from the Inside and Outside Surfaces 2-5
Figure 2-5 Sizing Error Surface Model 2-6
Figure 2-6 Plan View of Sizing Error Surface Model 2-7
Figure 2-7 Probability of Correct Sizing for Passed Candidates, Appendix VIII Supplement 4. Reporting Threshold A' = 0.15 inch 2-10
Figure 2-8 Probability of Correct Rejection/Reporting (PCR) Considering Passed Plus Failed Candidates, Appendix VIII from the Outside Surface. Reporting Criterion A' = 0.15 inch 2-10
Figure 2-9 Probability of Correct Rejection/Reporting (PCR) Considering Only Passed Candidates, Appendix VIII from the Outside Surface. Reporting Criterion A' = 0.15 inch 2-11
Figure 2-10 Comparison of Sizing Accuracy Demonstrated by Appendix VIII Qualified Individuals and the Best PISC II Techniques 2-11
Figure 3-1 Typical BWR RPV 3-3
Figure 4-1 Nodal Stress Path 4-2
Figure 4-2 Nozzle Orientation 4-2
Figure 4-3 RPV Nozzle Parameters 4-4
Figure 4-4 Core Spray Mesh 4-4
Figure 4-5 Main Steam Mesh 4-5
Figure 4-6 Recirculation Inlet Mesh 4-5
Figure 4-7 Recirculation Outlet Mesh 4-6
Figure 4-8 Nozzle Pressure Load 4-9
Figure 4-9 Nozzle Unit Axial Load 4-10
Figure 4-10 Nozzle In-Plane Bending Moment Load 4-10
Figure 4-11 Nozzle Out-of-Plane Bending Moment Load 4-11

Figure 4-12 Core Spray Nozzle Thermal Load Case 1-Heat Up 4-12
Figure 4-13 Core Spray Nozzle Thermal Load Case 2-Emergency Cooldown 4-12
Figure 4-14 Main Steam Nozzle Thermal Load Case 1-Heat Up 4-13
Figure 4-15 Main Steam Line Nozzle Thermal Load Case 2-Cooldown 4-13
Figure 4-16 Recirculation Inlet Nozzle Thermal Load Case 1-Heat Up 4-14
Figure 4-17 Recirculation Inlet Nozzle Thermal Load Case 2-Sudden Pump Start of Cold Recirculation Loop 4-14
Figure 4-18 Recirculation Outlet Nozzle Thermal Load Case 1-Heat Up 4-15
Figure 4-19 Recirculation Outlet Nozzle Thermal Load Case 2-SRV Blow Down 4-15
Figure 4-20 Recirculation Outlet Nozzle Thermal Load Case 3-Loss of Feedwater Pumps 4-16
Figure 4-21 Nozzle Boundary Conditions 4-16
Figure 4-22 Core Spray Nozzle Pressure Stress Intensity 4-17
Figure 4-23 Core Spray Nozzle Thermal Stress Intensity 4-18
Figure 4-24 Main Steam Nozzle Pressure Stress Intensity 4-19
Figure 4-25 Main Steam Nozzle Thermal Stress Intensity 4-20
Figure 4-26 Recirculation Inlet Nozzle Pressure Stress Intensity 4-21
Figure 4-27 Recirculation Inlet Nozzle Thermal Stress Intensity 4-22
Figure 4-28 Recirculation Outlet Nozzle Pressure Stress Intensity 4-23
Figure 4-29 Recirculation Outlet Nozzle Thermal Stress Intensity 4-24
Figure 4-30 Core Spray Nozzle Blend Radius Stress Profile 4-25
Figure 4-31 Main Steam Line Nozzle Blend Radius Stress Profile 4-26
Figure 4-32 Recirculation Inlet Nozzle Blend Radius Stress Profile 4-27
Figure 4-33 Recirculation Outlet Nozzle Blend Radius Stress Profile 4-28
Figure 4-34 Core Spray Nozzle-to-Shell Weld Stress Profile 4-29
Figure 4-35 Main Steam Line Nozzle-to-Shell Weld Stress Profile 4-30
Figure 4-36 Recirculation Inlet Nozzle-to-Shell Weld Stress Profile 4-31
Figure 4-37 Recirculation Outlet Nozzle-to-Shell Weld Stress Profile 4-32
Figure 5-1 Fatigue Crack Growth Data 5-5
Figure 5-2 Curve Fit of the Fatigue Crack Growth Data 5-6
Figure 5-3 Residual Plot of Fatigue Crack Growth Data 5-7
Figure 5-4 PVRUF Flaw Size Distribution 5-11

LIST OF TABLES

Table 2-1 Number of Measurements 2-5
Table 3-1 U.S. BWR RPVs 3-1
Table 3-2 Typical BWR Nozzle Materials 3-5
Table 3-3 Summary of Nozzles for BWR Product Lines 3-6
Table 4-1 RPV Nozzle Dimensions (Inches) 4-3
Table 4-2 Material Properties 4-7
Table 5-1 Random Parameters Summary 5-2
Table 5-2 Nozzle Thermal Cycles 5-9
Table 5-3 Probability of Failure Results Summary for 0% Inspection Sampling 5-12
Table 5-4 Probability of Failure Results Summary for 25% Inspection Sampling, 10 Year Interval 5-12
Table 5-5 Probability of Failure Results Summary for 90% Inspection Sampling, 10 Years Interval 5-13
Table 6-1 Nozzle Blend Deterministic Fracture Mechanics Analysis Results 6-2
Table 6-2 Nozzle-to-Shell Weld Deterministic Fracture Mechanics Analysis Results 6-2

1
BACKGROUND

1.1 Introduction

The report presents the technical basis to reduce inspection requirements of Boiling Water Reactor (BWR) Reactor Pressure Vessel (RPV) nozzle-to-shell welds and nozzle blend radii. Currently, BWR RPV welds are inspected per American Society of Mechanical Engineers (ASME) Boiler and Pressure Vessel (B&PV) Code, Section XI requirements, which requires 100% inspection each 10-year interval. The goal of this project is to provide the technical basis for the reduction of the nozzle-to-shell welds and nozzle blend radii to 25% of the nozzles every 10 years. The 25% coverage refers to 25% of the nozzles for each nozzle type, e.g., 1 of 4 main steam nozzles would be inspected.

The 25% inspection sampling size was selected by considering various aspects of this issue. These considerations were:

1. Inspection sampling size had to be sufficient to effectively identify aging degradation,
2. Inspection sampling size should be consistent with current industry and regulatory practice/requirements,
3. Inspection sampling size reduction should be sufficient to result in significant cost savings and dose reduction.

The 25% inspection sampling level was selected in part because it was considered to be sufficient to effectively identify aging degradation in the nozzle-to-shell welds and nozzle blend radii. The determination of whether the 25% inspection sampling is sufficient is the object of the PFM evaluation. If the results of the PFM evaluation show very low probability of failure, then the 25% inspection sampling is considered sufficient to identify aging degradation.

The 25% sampling level is similar to industry practice and in some cases exceeds current practice. The following examples demonstrate the consistency of the selected 25% sampling level with current industry practice.

1. ASME Code Section XI, IWB-2500 requires 25% of Category B-J (Item No. B9.11) circumferential welds be inspected each interval.
2. ASME Code Case N-560 (risk informed inspection) requires inspection of 10% of higher risk Class I Category B-J piping welds.
3. ASME Code Case N-578 (risk informed inspection) requires inspection of at least 25% of the highest risk (Risk Category 1, 2 and 3) and at least 10% of the next highest risk (Risk Category 4 or 5) Class I piping welds.

4. ASME Code Section XI, IWC-2500 (Class II piping) Categories C-F-1 and C-F-2 requires inspection of 7.5% of welds.
5. Generic Letter 88-01 requires 25% inspection of Category A piping welds.

The 25% sampling level also provides a significant cost savings and reduces worker dose exposure. Several utilities have estimated that the proposed reduction of inspection requirements would result in a savings of up to $750,000 per 10-year interval not including exposure considerations. The dose exposure has been estimated to be approximately 75% of the current exposure.

In order to address the potential impact of the proposed reduced inspection on RPV reliability, the evaluation documented in this report included available field inspection data, a survey of BWR nozzles and selection of representative nozzles for evaluation, and calculations to determine the reliability of the proposed nozzle inspections. The calculations were performed using probabilistic fracture mechanics (PFM) and deterministic fracture mechanics (DFM) methods.

Field experience has shown that very few indications have been discovered at the nozzle-to-shell weld. In addition, excluding the feedwater and control rod drive return lines (CRDRL) nozzles, very few indications have been seen at nozzle blend radius locations. Thus, field inspection results support the reduction of inspection requirements of the nozzle-to-shell weld and blend radius locations.

The BWR Vessel and Internals Project (BWRVIP) completed a successful project to eliminate the requirement for inspection of RPV circumferential welds [1]. The results of a PFM evaluation contributed significantly to the technical justification for elimination of circumferential weld inspections. The nozzle-to-shell weld evaluation proposed herein takes advantage of the same methodology. The VIPER computer program, which was developed by Structural Integrity Associates (SI) as part of the BWRVIP RPV circumferential weld effort, was modified to evaluate the nozzle-to-shell welds and nozzle blend radii. The VIPER program uses Monte Carlo methods to assess the reliability of a BWR RPV given flaw distributions, material properties, fluence distributions, and several other parameters, which are assumed to be randomly distributed.

A DFM evaluation can also demonstrate that expected flaws, based on field experience, will not jeopardize the structural integrity of the vessel. A flaw is selected that bounds any expected flaws based on inspection results to date. Using appropriate material properties, a deterministic linear elastic fracture mechanics evaluation is performed to demonstrate that failure is not expected. However, the PFM evaluation provides added insight into the reliability of the RPV by including consideration for the random nature of key parameters.

The combination of PFM and DFM methods along with favorable inspection results can provide a solid justification for reduction of current inspection requirements.

2
INSPECTION HISTORY AND EXAMINATION EFFECTIVENESS BASED ON PERFORMANCE DEMONSTRATIONS

This section reviews the effectiveness of examinations performed from the outside surface of BWR Reactor Pressure Vessels (RPV). The examination effectiveness is estimated based on the results of performance demonstrations. The inspection history of BWR inner-radius and nozzle to shell welds is also described.

2.1 Examination Effectiveness

Performance demonstrations on full-scale vessel mockups, containing realistic defects, have been performed since 1994. The Performance Demonstration Initiative (PDI) carries out these demonstrations. PDI is a utility consortium that was formed in 1991 to aid utilities' implementation of the qualification requirements found in the ASME Code, Section XI, Appendix VIII [2]. All U.S. utilities and two international utilities comprise the membership. An array of ultrasonic performance data, including detection, length sizing and depth sizing, has been generated as a result of the PDI Program. Analysis of the PDI database provides valuable insights relative to the effectiveness of ultrasonic examinations currently being performed on commercial nuclear power plants. Specifically this section analyzes examinations performed from the outside surface for flaws located at the inside surface and the clad-to-base metal interface.

The analysis of examination effectiveness considers three phases:

- Detection, the probability of detection (POD)
- The sizing accuracy
- Flaw Acceptability in light of examination uncertainties

2.1.1 Detection

The first step in the examination process is the detection of flaws. The POD is defined as the conditional probability that a flaw will be detected if present. POD is often expressed as a function of relevant flaw parameters such as size, shape, location, and orientation. This section treats POD as a function of one parameter, the through-wall depth of the flaw. POD curves were estimated by performing a logistic regression [3] on detection scores using the model:

$$POD(s) = logistic(\beta_1 + \beta_2 * s_i) \qquad \textbf{Equation 2-1}$$

Where s represents the through-wall depth of the inspected flaw, logistic (z) represents the logistic function, as defined by:

$$logistic(z) = (1 + \exp(-z))^{-1} \qquad \textbf{Equation 2-2}$$

and the two parameters β_1 and β_2 are estimated by the fitting procedure to determine the POD curve. To estimate the parameters, the model is fitted to detection data using general least squares (equivalent to maximum likelihood). The regression uses the detection/sizing data pairs (Y_i, s_i), where the index identifies a unique flaw/inspection observation in the PDI database, and Y_i represents the detection outcome ($Y_i = 1$ represents a detection, while $Y_i = 0$ represents a miss no other values of Y are permitted). The POD curve is therefore determined from a regression equation that can be expressed as:

$$Y_i = logistic(\beta_1 + \beta_2 * s_i) + \varepsilon_i \qquad \textbf{Equation 2-3}$$

with the regression algorithm choosing β_1 and β_2 so that the weighted sum of squares errors is minimized. The term ε_i, an error term, is assumed to be normally distributed with a variance of σ_ε^2.

The POD estimates provided here are based on performance demonstration data defined by the following conditions:

- Examination from the outside surface
- Manual and automated procedures are considered
- Flaws of interest are located at the clad-to-base-metal interface
- Dual side access, (two directions perpendicular to the flaw)
- Results from passed and passed plus failed candidates are included
- Results from failed candidates with more than two missed detections or false calls are not included in the data
- POD curves are not applicable for flaws less than 0.1 inch

Candidates may fail to meet the Appendix VIII acceptance criteria by either missing flaws or by excessive false calls (false positive). One missed detection is allowed for examinations that contain 12 or more flaws. No missed detections are allowed for examinations of less than 12 flaws. The average number of flaws in a test normally ranges between 7 and 10. Candidates may fail for a variety of reasons. These range from lack of skill/knowledge, testing protocol, test taking anxiety and others. We do not have specific tools to determine the causes of failure. However, we have observed that they are divided into two groups. The first group will normally pass on a second attempt. The second group will need additional experience and training to successfully complete this demonstration. For the purpose of this study, failure occurs when there are two misses or false calls.

The inclusion of candidates that failed in their first attempt is provided for information. Inclusion of passed candidates only may be overly optimistic, as the large majority of candidates were required to detect 100% of the flaws in order to pass. Inclusion of Pass Plus Failed candidates provides a lower bound estimate of expected performance. The POD estimates for passed and passed plus failed candidates using both automated and manual procedures are provided in Figure 2-1. The 95% confidence limits are shown as dashed lines for the Pass Plus Failed curve.

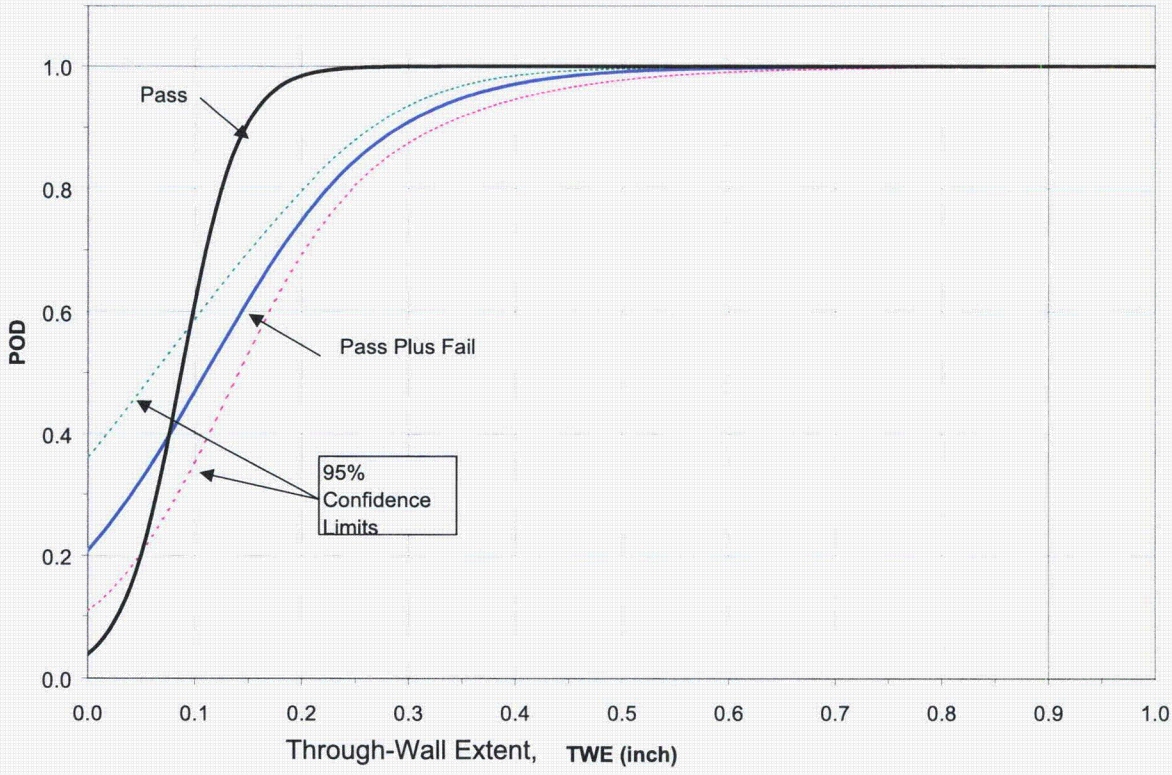

Figure 2-1
Probability of Detection Performance for Passed and Passed Plus Failed Candidates for Appendix VIII Supplement 4, from the Outside Surface. Both Automated and Manual Techniques are Included

A comparison of POD curves for automated and manual and all examination procedures are shown for passed plus failed candidates in Figure 2-2. The POD curve for the automated procedures is considerably higher than manual procedures. The comparative curves for passed candidates are shown in Figure 2-3. From Figures 2-1, 2-2 and 2-3 it can be seen that the POD for passed plus failed candidates for automated and manual techniques (shown in Figure 2-1) is conservative compared to the POD for passed candidates only.

Table 2-1 lists the number of measurements used in the POD curve fitting procedure. A measurement is the result of one candidate with one flaw. Category "all" includes both manual and automated techniques. The test result "all" includes both the passed and failed candidates.

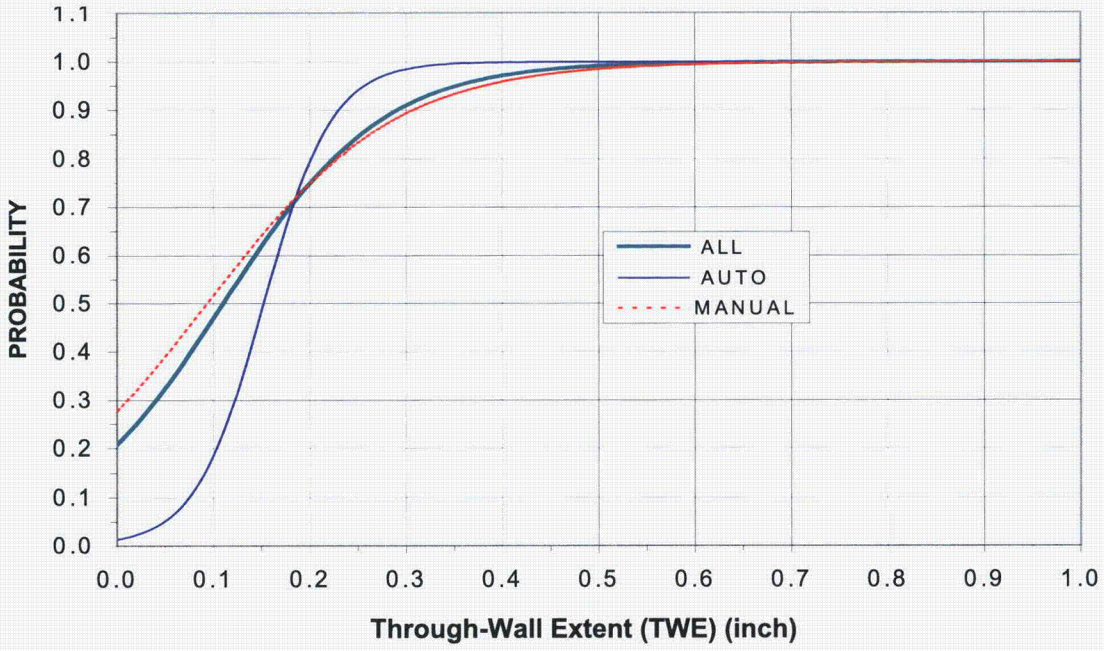

Figure 2-2
Probability of Detection for Manual, Automated and Combined (ALL), Considering All Candidates (Pass Plus Failed)

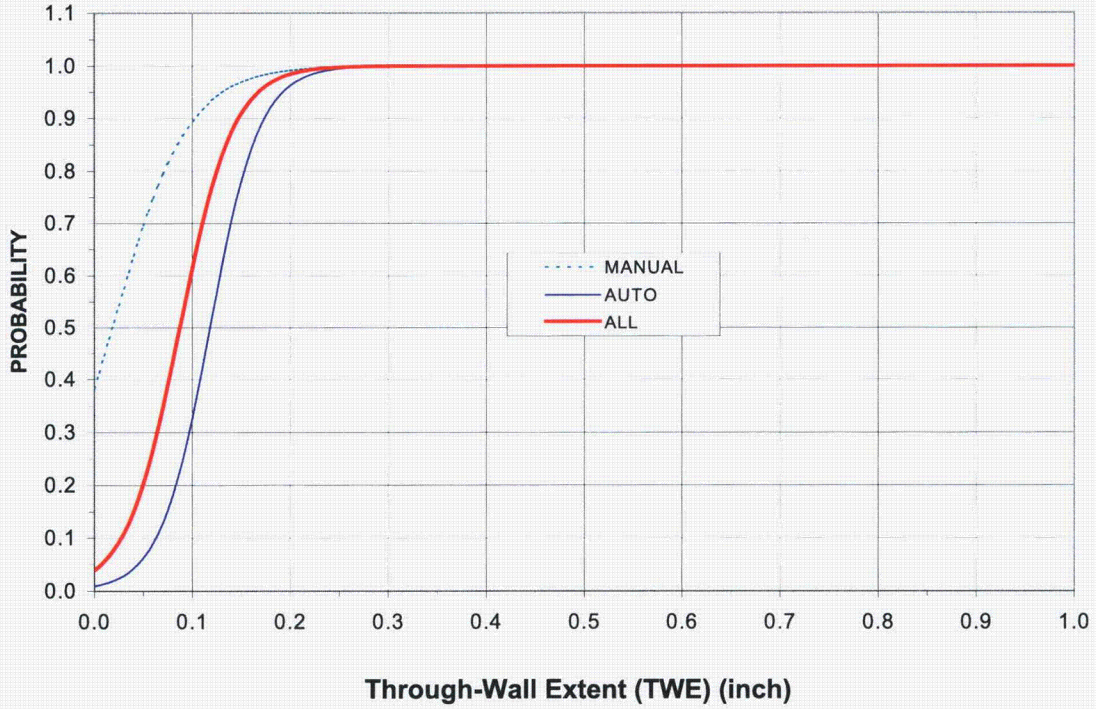

Figure 2-3
Probability of Detection for Manual, Automated, and Combined (ALL), Considering Only Passed Candidates

Table 2-1
Number of Measurements

Category	Test Results	# Measurements	Figure
ALL	ALL	741	2-1, 2-2
ALL	PASS	376	2-1, 2-3
AUTO	ALL	196	2-2
AUTO	PASS	85	2-3
MANUAL	ALL	545	2-2
MANUAL	PASS	291	2-3

2.1.2 Sizing

The second step in the examination process is sizing. Sizing performance of 41 successful Supplement 4 (clad-to-base-metal region), depth-sizing candidates, is shown in Figure 2-4. Acceptable depth-sizing performance, for Supplement 4, is 0.150 inch (3.809 mm) Root-Mean-Square-Error (RMSE) or less. The top 15% of candidates sized the required flaws with an error of 0.08 inch (2 mm) RMSE or less. These were all lead personnel who have developed the sizing procedure and are normally responsible for making the final decisions on the acceptability of flaw indications. Other team members make an initial estimate of the flaw size. Lead personnel typically evaluate any indication that is close to or exceeds the limits of acceptability.

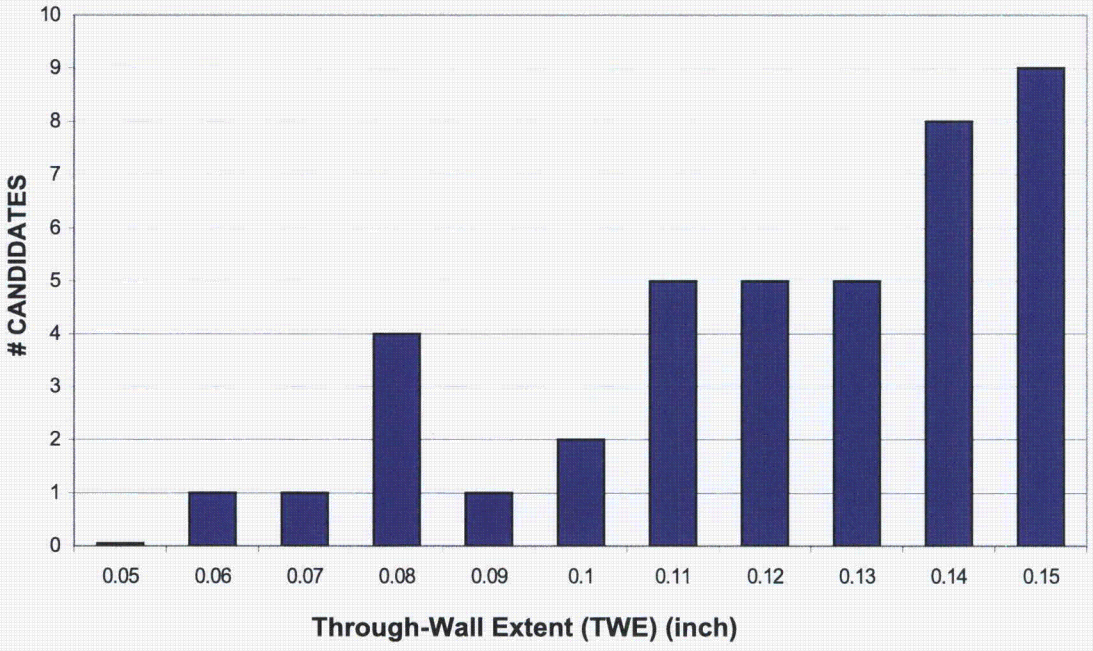

Figure 2-4
Histogram of Depth Successful Sizing Candidate Test Scores, Appendix VIII, Supplement 4. Examinations were Performed Both from the Inside and Outside Surfaces

Sizing error is equal to the measured value minus the actual flaw size. This convention yields a positive error for over sizing and a negative error for under sizing. Upon examination of the sizing errors, two trends emerge:

1. A tendency to oversize small flaw and undersize very large flaws.
2. The magnitude of errors increases with flaw size.

The distribution may be characterized by a mean error, with a negative slope. If small incremental slices of flaw sizes are evaluated, a piece-wise estimate of the standard deviation as a function of flaw depth can be obtained. A three-dimensional model of the distribution is shown in Figure 2-5. In Figure 2-5, each line parallel to the Y-axis (error) represents a normal distribution with a mean error and standard deviation that is appropriate for each flaw size on the X-axis (true size). The amplitude (Z-axis) is the amplitude of a normal distribution curve given its mean and standard deviation. It can be seen that for larger flaws, in the foreground, the maximum of the distribution is less and breadth is wider. The mean or peak of the distribution shifts from positive to negative with increasing flaw size, as shown in Figure 2-6. Figures 2-5 and 2-6 are provided for a qualitative understanding of the error distribution. These data are used in more detail in the following section to evaluate the examination uncertainties.

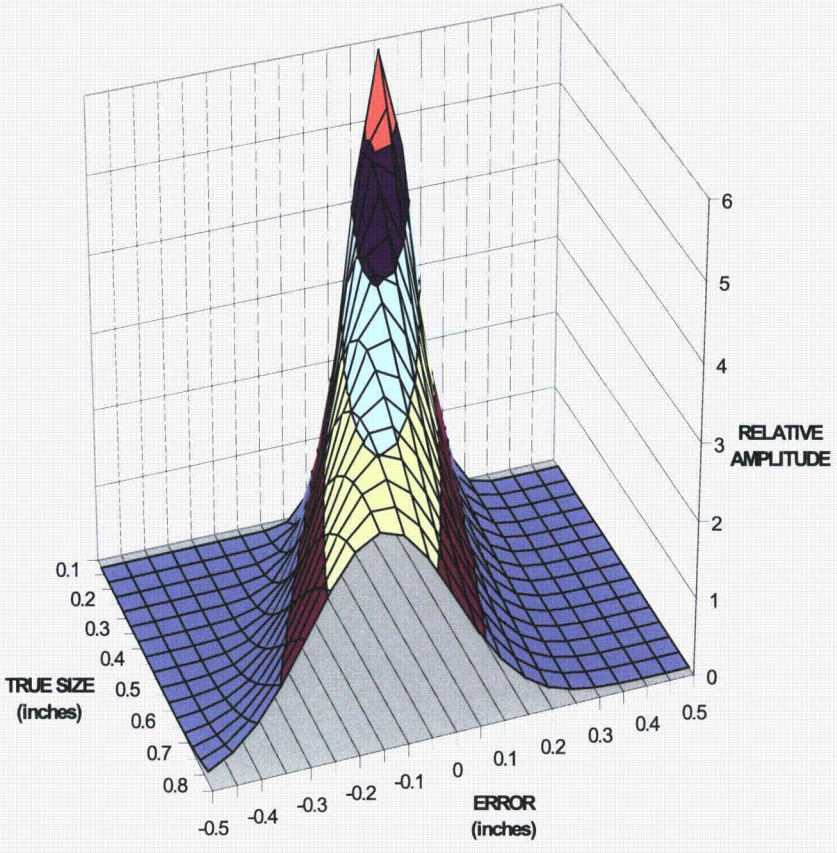

Figure 2-5
Sizing Error Surface Model

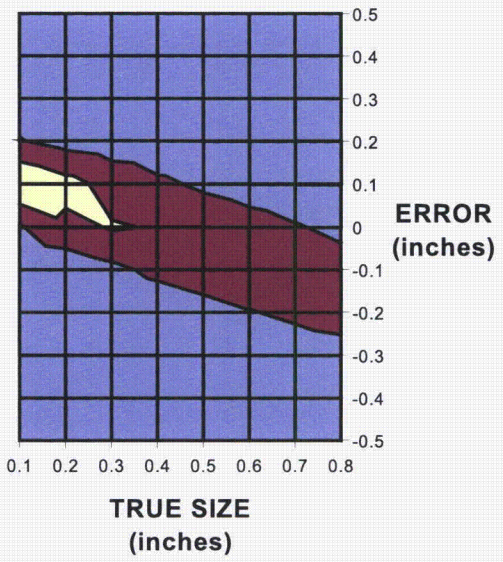

Figure 2-6
Plan View of Sizing Error Surface Model

Data used in the evaluation of sizing capability are applicable to the following conditions:

- Inside plus outside surface examination
- Flaws located at the clad-to-base metal interface
- Dual-side access, (two directions perpendicular to the flaw)
- Only passed candidates are included
- Sizing data from the inside surface was included as it is nearly identical to that from the outside surface

2.1.3 Flaw Acceptability Evaluation in Light of Examination Uncertainties

The third step in the examination process is the flaw acceptability evaluation. The conditional probability that a flaw will be reported, given that it is present, depends on the capabilities of the procedure and the individual performing the examination. This probability increases with the size of the flaw. The examination is a two-step process. First, the flaw must be detected and secondly, it must be sized correctly. Each step has an associated uncertainty. If both steps are completed successfully, the flaw is either accepted or correctly rejected depending on its size relative to the standards of acceptability. The process is described in probabilistic terms by:

$$PCR = POD \times PCS \qquad \textbf{Equation 2-4}$$

Where:

POD = the probability of detection

PCS = the probability of correct sizing and

PCR = the probability of reporting or rejecting the flaw as unacceptable

The results of the PDI program indicate that the POD, for flaws at the clad-to-base metal interface, is high. The POD curves for examination from the outside surface are shown in Figures 2-1, 2-2, and 2-3. These include manual as well as automated examination procedures.

The Probability of Correct Sizing (PCS) is defined here as the Probability that a flaw of unacceptable size will be sized to be equal to or greater than the flaw acceptance or reporting threshold. The reporting level is often lower than the absolute level of unacceptability.

Consider the hypothetical population of all candidate examiners who ever have and/or will take the performance demonstration test given by the PDI. The subject model assumes that the true relation between a randomly chosen candidate examiner's measured crack size for any actual crack size, is described by the following linear stochastic model

$$A_M = A_t + B + E \qquad \textbf{Equation 2-5}$$

Where:

A_M = measured crack size (depth)

A_t = actual crack size

B = is the Bias or mean measurement error as a function of true flaw size

E = Stochastic disturbance term and is normally distributed with mean of zero and variance of σ^2 (σ = standard deviation).

Any given measured crack size will have an expected error and can be viewed as being drawn from a normal distribution with mean and variance of:

Expectation (i.e., mean) of $A_t + B$ **Equation 2-6**

Variance of AM = Var (E) = σ^2 **Equation 2-7**

For any given flaw size, A_t, there is a normal probability distribution with mean B and standard deviation of σ describing the sizing measurement error that will be produced by any randomly chosen examiner. Given values for B and σ and the tabulated values for the cumulative standardized normal distribution, the following question can be asked: What is the probability, PCS, that a randomly chosen examiner will report a crack (given that the crack has been detected) as equal to or greater than the acceptance or screening criteria A'?

PCS = 1- CN **Equation 2-8**

Where:

CN is the cumulative form of the normal distribution and is a function of A', B, and σ,

A' is the acceptance, reporting or screening criteria

A_t is the true size of the flaw

B is calculated according to (2-6) and

σ is the standard deviation of the sizing error distribution according to (2-7).

Equation (2-5) assumes that E is constant over the range of flaw sizes A_t. The range of measurement error actually increases with flaw size and is not unexpected. Errors for small flaws are constrained by zero flaw size, and large flaws provide an opportunity for larger errors. Therefore, both E and B are a function of A_t. The mean error as a function of true flaw size is estimated from the measurement database by a linear regression of the form $B = a + b A_t$. The stochastic term E is estimated by calculating a standard deviation for each value of At, in increments of 0.1 inch (2.54 mm) and fitting these calculations using a linear regression model.

Given the values of B, E, and a reporting criteria A', the PCS may be calculated for each value of A_t, according to Equation 2-8. Selecting an A' of 0.15 inch (3.80 mm) yields the PCS shown in Figure 2-7. PCS is that portion of the curve that is equal to or greater than 0.15 inch (3.80 mm). The portion of the curve that is to the left of the threshold is actually incorrectly reported. In this example, if the true flaw size were 0.25 inch (6.35 mm) deep, it would be expected to be equal to or greater than the threshold value 96% of the time.

The reporting criterion of 0.15 inch (3.80 mm) is used here as an example. An A' of 0.15 inch represents 2% of a 7.5 inch plate thickness. The acceptance criteria contained in the ASME Code Section XI, Division 1, IWB-3500 is based on the thickness of the pressure vessel and may be larger than 0.15 inch (3.80 mm).

The Probability of Correct Rejection (PCR) is the product of POD and PCS as in Equation (2-4). The detection capability (POD) is described in Figures 2-1, 2-2,and 2-3 and the PCS is shown in Figure 2-7. The product or PCR is shown in Figure 2-8 and 2-9. Correct rejection is actually that portion of the curve to the right of the screening criteria A', in this case 0.15 inch (3.80 mm).

The probability of correct rejection considering both passed and failed candidates is shown in Figure 2-8. The probabilities for all, automated and manual techniques are shown. The probability of correct rejection considering only passed candidates is shown in Figure 2-9. For the purpose of calculating structural reliability the "ALL" curve of Figure 2-9 is most appropriate for examinations performed since 1995 as well as future examinations.

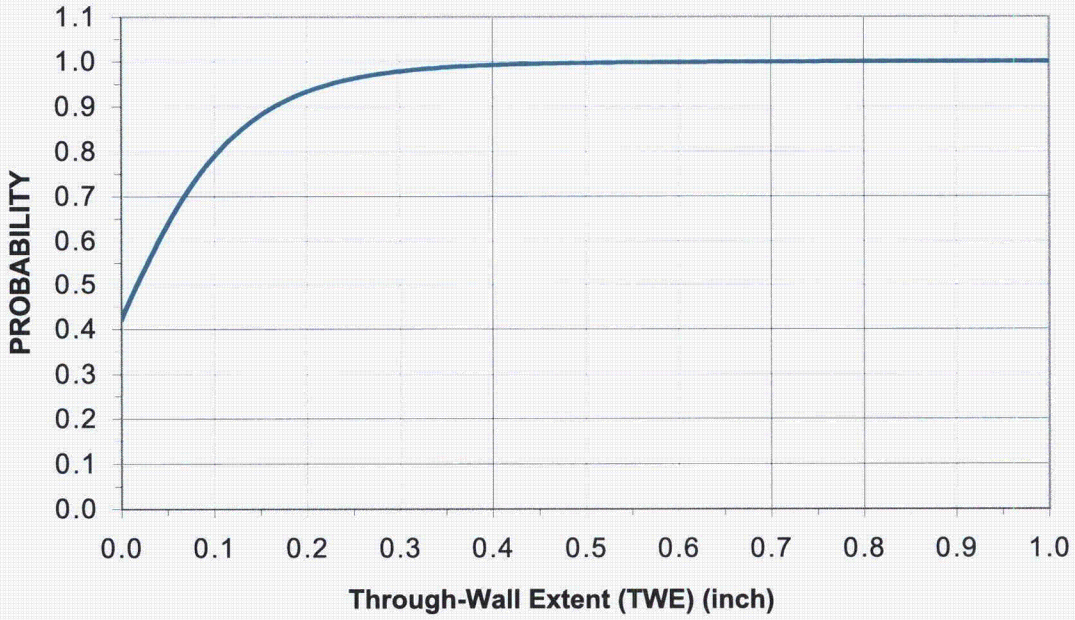

Figure 2-7
Probability of Correct Sizing for Passed Candidates, Appendix VIII Supplement 4. Reporting Threshold A' = 0.15 inch

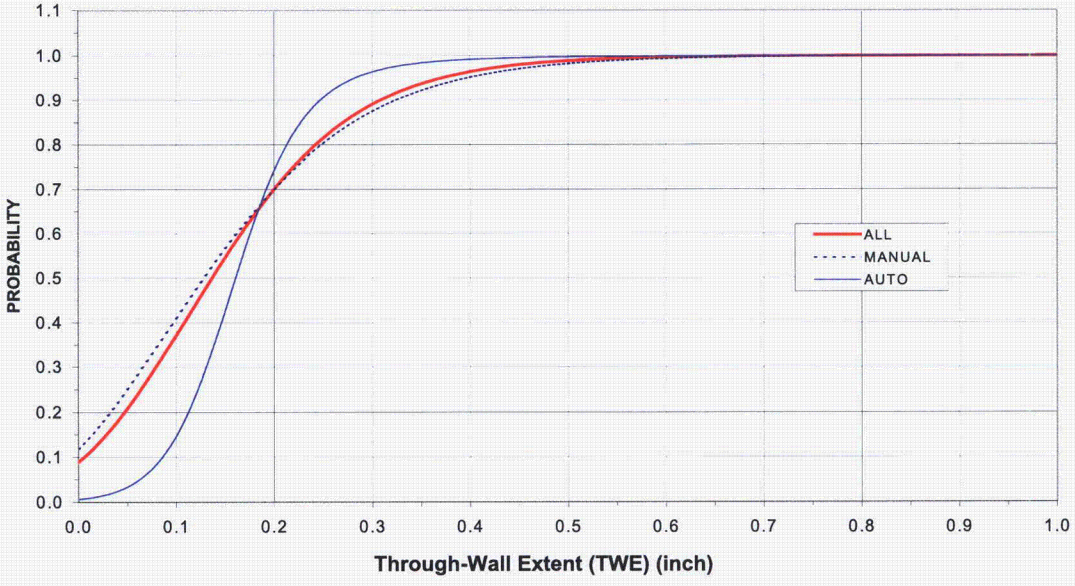

Figure 2-8
Probability of Correct Rejection/Reporting (PCR) Considering Passed Plus Failed Candidates, Appendix VIII from the Outside Surface. Reporting Criterion A' = 0.15 inch

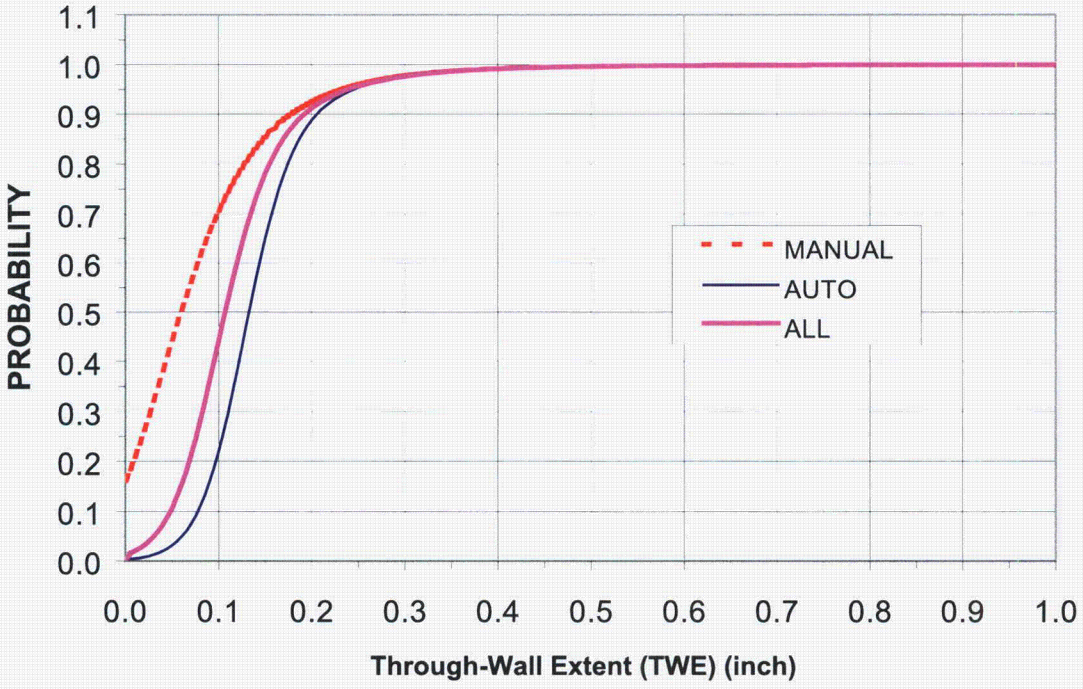

Figure 2-9
Probability of Correct Rejection/Reporting (PCR) Considering Only Passed Candidates, Appendix VIII from the Outside Surface. Reporting Criterion A' = 0.15 inch

Examinations performed prior to 1985 can be compared to the PISC II Study [4]. The most significant improvements were in the area of sizing. Figure 2-10 compares the current demonstrated sizing capabilities with that of the best techniques demonstrated by PISC II. Sizing techniques have consistently improved since the PISC II Study.

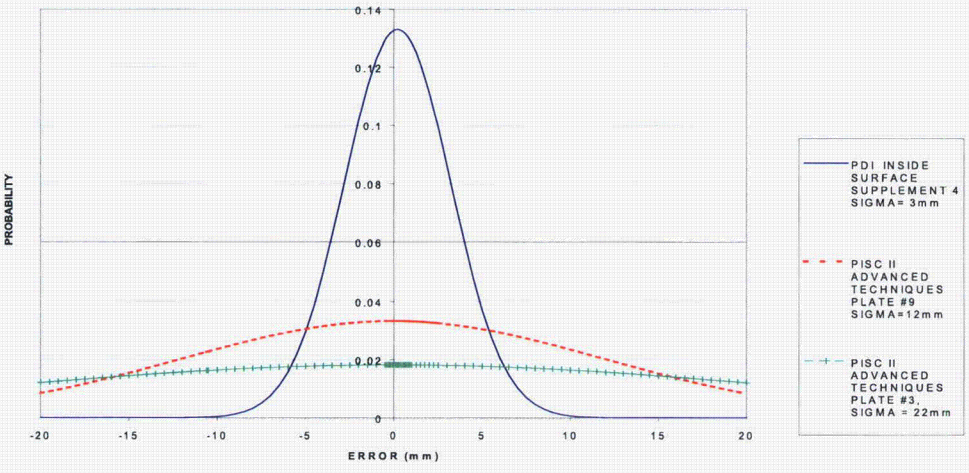

Figure 2-10
Comparison of Sizing Accuracy Demonstrated by Appendix VIII Qualified Individuals and the Best PISC II Techniques

2.2 Inspection History

2.2.1 Manufacturing and Preservice Inspection

The nozzle inner radius regions and the nozzle-to-shell are subjected to a surface examination both before and after the weld deposition of the stainless steel cladding. The inspection before cladding also includes a 100 percent volumetric exam of the nozzle forging. The inspection after cladding includes a surface exam performed before the hydrotest and a radiographic exam of the nozzle-to-shell weld for acceptance to ASME Section III requirements. The BWR/6 nozzles and some earlier models were manufactured without cladding on the nozzle inner-radius and the nozzle-to-shell weld. The absence of cladding in these areas greatly enhances inspection capability. The Section III acceptance is followed by the preservice baseline using ultrasonic examination in accordance with Section XI requirements.

2.2.2 Nozzle Inner-Radius Inservice Examinations

The nozzle inner radius, volume defined by IWB 2500-7 is normally examined from the outside surface for BWR reactor pressure vessels using manual or automated examination systems. Cracking in the inner radius of BWR feedwater nozzles in the early 1970s stimulated extensive NDE development and modeling techniques to detect and characterize these conditions. Demonstrations, using full-scale mockups, were performed to provide assurance that these examinations were adequate to address the potential cracking conditions in the feedwater and CRDM return nozzles. The same technology was extended to other BWR nozzles in the 1980s and early 1990s. It soon became apparent that the use of full-scale mockups for every configuration, was not a practical solution for the wide range of nozzle applications present in BWR vessels. Geometric modeling, as described in Code Case N-552 [5] was developed to provide a more uniformly effective approach for qualifying the examination of the nozzle inner-radius area. This is not to say that previous examinations were not effective. Most were very capable of detecting the flaws of interest.

The capabilities of this technology have been extensively demonstrated to the NRC in response to NUREG-0619, [6]. These techniques have included both automated and manual applications. The EPRI NDE Center and inspection vendors have developed and demonstrated capabilities for modeling and examining a wide range of nozzle configurations for BWR applications. These approaches provide a uniform method of assuring coverage of the required volume in the "spirit of Code Case N-552."

2.2.3 Inservice Inspection of Nozzle-to-Vessel Welds

Inservice inspection of 100% of the nozzle-to-shell welds currently is required every 10 years. These inspections are normally performed at the same time as the inner-radius examinations. In many cases, the feedwater and CRDM return nozzle inner-radius examinations are performed more frequently. The techniques used to detect flaws parallel to the weld are the same as those used for the RPV shell welds. The effectiveness of these examinations is described in Section 2.1. The effectiveness of techniques designed to detect flaws that are transverse to the weld axis are the same as those described in 2.2.2 above.

2.2.4 Inspection History

All BWR RPV feedwater nozzles in the entire fleet have been examined at least once, many twice, with modern techniques of demonstrated effectiveness, as required by NUREG-0619. The remainder of the nozzles in the RPV that were examined using automated systems were performed using the same approach as that used for the feedwater nozzles. This list includes at least 6 units that have been operational for more than 20 years and at least 1 that has been operational for more than 30 years.

The EPRI NDE Center has participated in the NUREG-0619 demonstrations performed for Brunswick, Perry and Duane Arnold. From these demonstrations the NDE Center has concluded that this examination vendor has developed a modeling capability and procedures that are effective on a wide range of nozzles. General Electric, using the Geris and Geris 2000 systems, has examined more than 514 nozzles since 1992 [7]. Both systems are capable of reliably detecting flaws greater than 0.25 inch penetration into the base metal. These 514 examinations found no indications of inservice degradation.

Demonstrations for NUREG-0619 compliance were performed for Grand Gulf and River Bend using manual examination techniques. These procedures were found to be effective and were accepted by the NRC. This utility has extended this procedure to the remainder of the nozzles. Approximately 50% of the nozzles at Grand Gulf have been examined without findings of degradation.

Based on available information, no significant flaws have been detected in the nozzle-to-shell welds and the nozzle inner-radius, other than early cracking on BWR feedwater and CRDM nozzles. A significant number of effective examinations have been performed on BWR units that have been operational for periods up to 30 years using modern examination techniques. It is concluded that a large number of examinations have been performed with techniques capable of detecting significant cracking if it were present and no degradation or failure mechanism has become apparent.

2.3 Conclusions

Performance capabilities of ultrasonic techniques for examination of the reactor pressure vessel shell nozzles and shell welds have improved substantially since 1985. Analysis of the PDI database has provided valuable insight into the effectiveness of these ultrasonic examinations. Evaluations presented herein demonstrate that the probability of detecting and sizing flaws equal to and greater than 0.25 inches in depth, located at the inside surface and the clad-to-base metal interface, is excellent.

3
SURVEY OF BWR NOZZLES, DATA COLLECTION AND SELECTION OF REPRESENTATIVE NOZZLES FOR ANALYSIS

This section summarizes the results of a survey of BWR nozzles and discusses the selection of the representative nozzles for the PFM and DFM analyses performed for this evaluation.

3.1 Vessel Geometry and Design Features

The BWR RPV is comprised of a shell and a removable top head (flanged and joined via the head to flange closure studs), closure studs, a bottom head which is welded to the shell, multiple nozzles and safe ends, multiple penetrations and control rod drive stub tubes, a vessel support skirt and numerous attachments welds.

Vessel inside diameters (IDs) range from 185 to 254 inches, vessel shell thickness from 4.5 to 7.1 inches, vessel heights (inside top head to inside bottom head) from 758 to 872 inches and vessel head thicknesses from 2.7 to 6.8 inches. Table 3-1 provides representative dimensions and identifies fabricators for the vessels of all U.S. BWR plants from BWR/2 through BWR/6. Figure 3-1 shows a typical RPV. RPV nozzles and locations of the various internals are denoted in Figure 3-1.

Table 3-1
U.S. BWR RPVs

BWR Plant	Product Line	Vessel Fabricator	RPV Inner Diameter (in)	RPV Shell Thickness (in)
Browns Ferry 1	4	B&W	252.8	6.152
Browns Ferry 2	4	B&W/I-H	252.8	6.152
Browns Ferry 3	4	B&W/I-H	252.8	6.152
Brunswick 1	4	CB&I	220.4	5.375
Brunswick 2	4	CB&I	220.4	5.375
Clinton 1	6	CBIN	220.6	5.59
Cooper	4	CE	220.8	5.375
Dresden 2	3	B&W	251.4	6.125
Dresden 3	3	B&W	251.4	6.125

Table 3-1
U.S. BWR RPVs (Continued)

BWR Plant	Product Line	Vessel Fabricator	RPV Inner Diameter (in)	RPV Shell Thickness (in)
Duane Arnold	4	CB&I	185.0	4.47
Fermi 2	4	CE	254.0	6.125
Fitzpatrick	4	CE	220.2	5.375
Grand Gulf	6	CBIN	253.4	6.19
Hatch 1	4	CE	220.1	5.375
Hatch 2	4	CE	220.2	5.375
Hope Creek 1	4	Hitachi	253.0	6.1
La Salle 1	5	CE	254.0	6.125
La Salle 2	5	CBIN	253.0	6.19
Limerick 1	4	CB&I	253.4	6.19
Limerick 2	4	CB&I	253.4	6.19
Millstone 1	3	CE	226.0	5.5
Monticello	3	CB&I	206.4	5.29
Nine Mile Point 1	2	CE	213.4	7.125
Nine Mile Point 2	5	CBIN	253.4	6.19
Oyster Creek 1	2	CE	213.4	7.125
Peach Bottom 2	4	B&W/CB&I	251.0	6.125
Peach Bottom 3	4	B&W/CB&I	251.0	6.125
Perry 1	6	CBIN	240.4	6
Pilgrim	3	CE	227.4	5.531
Quad Cities 1	3	B&W	251.4	6.125
Quad Cities 2	3	B&W/RDM/ CB&I	251.4	6.125
River Bend	6	CBIN	220.4	5.41
Susquehana 1	4	CB&I	253.0	6.16
Susquehana 2	4	CB&I	253.0	6.16
Vermont Yankee	4	CB&I	206.0	5.063
WNP-2(Hanford)	5	CB&I	253.0	6.19
Average	–	–	237.0	5.9
Maximum	–	–	254	7.125
Minimum	–	–	185	4.47
Standard Deviation	–	–	19.31	0.53

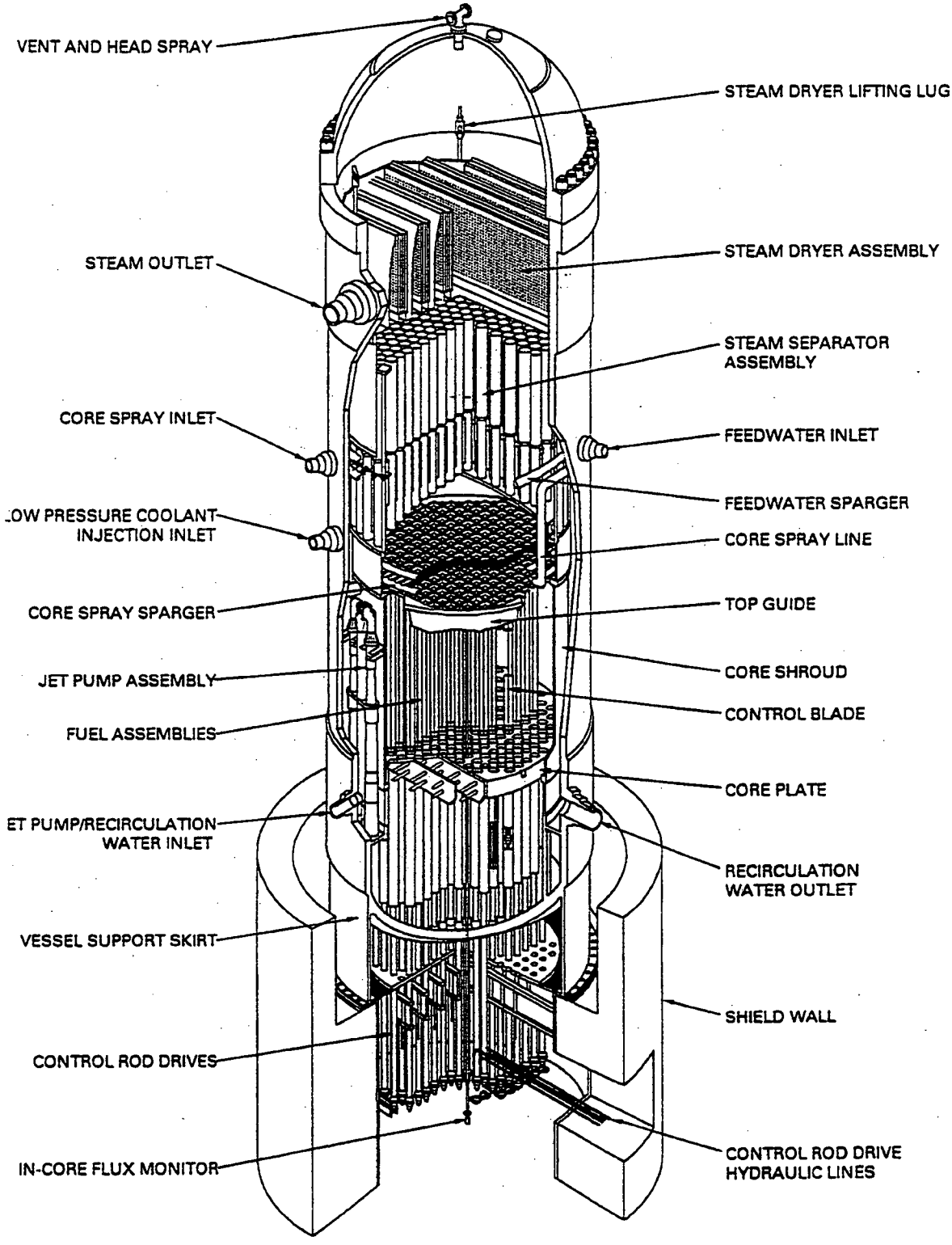

Figure 3-1
Typical BWR RPV

General Electric Company product lines BWR/2 through BWR/6 represent an evolutionary development of RPV design concepts. For example, the BWR/2 product line uses forced recirculation. Internal jet pumps were introduced with the BWR/3 product line to improve recirculation efficiency and jet pump use was continued on later product lines. BWR/4 and BWR/5 product lines increased power density and made other product improvements. Later vessels tend to have more nozzles and penetrations than do earlier ones, i.e., more emergency core cooling system (ECCS) nozzles and control rod drive (CRD) and flux monitoring penetrations. BWR/2 through BWR/5 vessels have stub tube and CRD housing designs for the bottom head CRD penetrations. BWR/6 vessels use a straight through design with CRD housings welded directly to the bottom head.

Plant operating pressure is typically 1000 to 1050 psi, the vessel design pressure is 1250 psi, and the usual hydrotest pressure is 1563 psi. Vessel design temperature is typically 575°F. Operating temperatures range from 540 to 550°F. Transients at the various nozzles can vary significantly. This is one of the criteria for selection of the four nozzles for use in this evaluation.

3.2 Vessel/Vessel Nozzle Materials and Fabrication

The different components of BWR RPVs (nozzles, shells, flanges, studs, etc.) are fabricated from different materials. In addition, the choice of the construction materials changed as the BWR product line evolved. For example, shell plates changed from American Society for Testing and Materials (ASTM) A-302, Grade B, to ASME SA-533, Grade B, Class 1. Table 3-2 shows the various materials used in BWR RPV construction. Material properties, such as chemistry and toughness, are specific for each heat of material in each RPV.

The RPV shell and heads are fabricated from rolled plate segments joined by full penetration welds. The vessel shell is fabricated from four or five shell courses joined by circumferential full penetration welds; individual shell courses are fabricated from two or more rolled plates joined by full penetration longitudinal welds. Weld seams are located to avoid intersection with a nozzle penetration weld and welds within the beltline region are minimized. Portions of longitudinal shell course welds are within the beltline region and at least one circumferential weld is near or marginally within the beltline region.

The shell courses and the bottom heads are clad, but on later RPVs the top head was left unclad because the interior surface is in contact with dry steam during normal operation. Carbon and low alloy steel vessel nozzles are normally clad if located below the water line. Recent construction practice uses unclad feedwater nozzles, and cladding has been removed from the feedwater nozzles of many operating plants. On BWR/6 RPVs, all nozzles except recirculation nozzles are unclad to improve the capability for inspection of the nozzle-to-shell welds by ultrasonic testing (UT). On BWR/6 RPVs, all nozzles are unclad because corrosion studies showed minimal oxide buildup on exposed low alloy steel surfaces.

Table 3-2
Typical BWR Nozzle Materials

Component	Typical Materials
Attachment Welds	Stainless Steel or Alloy 182
Closure Studs	SA-193 or SA-540
Nozzles (Forgings) BWR/5 LPCI Feedwater BWR/2 CRDRL Core Spray Recirculation Inlet Recirculation Outlet	 SA-508, Class 2 SA-508, Class 2 SA-508, Class 2 SA-508, Class 2 SA-508, Class 2 SA-508, Class 2
Safe Ends BWR/5 LPCI Feedwater BWR/2 CRDRL Core Spray Recirculation Inlet Recirculation Outlet	 Stainless Steel or SB-166 (Ni-Cr-Fe Alloy) Carbon Steel or SB-166 Carbon Steel or SB-166 Carbon Steel or SB-166 Carbon Steel or SB-166 Carbon Steel or SB-166
Penetrations CRD stub tubes All others (instrumentation, etc.)	 Stainless Steel or SB-167 (Ni-Cr-Fe Alloy) SB-167
Vessel Shell Shell Beltline Weldments	 A-302 Grade B or SA-533, Grade B, Class 1 Low Alloy Steel Weldment
Vessel Support Skirt	SA-533, Grade B, Class 1
Vessel Flanges	SA-336 or SA-508, Class 2
Top & Bottom Heads	SA-302, Grade B or SA-533, Grade B, Class 1

3.3 Nozzles and Penetration Design Features

RPVs have many penetrations for piping and equipment. Vent, instrumentation, and head spray nozzles are located in the top head. CRD penetrations, flux monitoring instrument penetrations, core pressure drop, standby liquid control, and drain nozzles are in the RPV bottom head. The

remaining nozzles are in the cylindrical shell. Recirculation system nozzles and the jet pump sensing line penetrations are located in the shell course below the core. Recirculation system nozzles for the BWR/3 through BWR/6 product lines are in the lower shell course; BWR/2 recirculation system nozzles are in the lower shell and bottom head. The beltline region shell course has no nozzle penetrations. The upper shell course has steam nozzles and some instrumentation nozzles. The remaining nozzles, which include feedwater, high pressure core spray, low pressure core spray, control rod drive (CRD) hydraulic return line instrumentation and low pressure coolant injection (LPCI) are typically located in the shell course just above the core region. Of these, the LPCI nozzles are located nearest to the beltline region. Some plants do not have all these nozzles. Table 3-3 lists a typical GE BWR plant configuration showing the number of nozzles found on vessels of each product line.

Table 3-3
Summary of Nozzles for BWR Product Lines

Quantity of Nozzles by BWR Product Type					
Nozzle or Penetration	BWR/2	BWR/3	BWR/4	BWR/5	BWR/6
Recirculation Outlet	5	2	2	2	2
Recirculation Inlet	5	10	10	10	10
Steam Outlet	2	4	4	4	4
Feedwater	4	4	4 or 6	6	4 or 6
Core Spray	2	2	2	2	2
Jet Pump Instrumentation	–	2	2	2	2
Low Pressure Coolant Injection	–	–	3	3	3
Drain	1	1	1	1	1
CRD Return	1	1	1	1	1
Head Spray	-	1	1	1	1
Core Pressure Drop	1	1	1	1	1
Isolation Condenser	2	0 or 2	–	–	–
Vent	1	1	1	1	1
Instrumentation	14-29	4-6	6-10	10	12
CRD	129-137	121-177	89-185	185	145-193
In-Core	64-69	40-53	30-55	55	45-58

3.4 Selection of Nozzles for Evaluation

This section describes the selection of the nozzles used in the specific probabilistic and deterministic fracture mechanics evaluations. Selection of the four representative nozzles considered the following items:

- Stress
- Loadings (thermal loadings)
- Materials
- Field experience
- Applicability to BWR fleet
- Quantity of Nozzles

The nozzles being considered in this evaluation are those that are joined with full penetration welds. Thus, any penetrations with partial penetration welds are not included. Table 3-3 shows several nozzles that are present in very few quantities, are very small diameter, partial penetration welds and/or applicable to only a few of the BWR product lines. For these reasons, the following nozzles are eliminated from consideration in this evaluation:

- Jet Pump Instrumentation
- Low Pressure Coolant Injection
- Drain
- CRD Return
- Head Spray
- Core Pressure Drop
- Isolation Condenser
- Vent

The instrumentation, CRD and in-core nozzles are also eliminated from consideration since they are not full penetration welds.

The feedwater nozzle is not included in the analysis since it has been addressed separately by the BWR industry and specific inspection requirements have been established to manage thermal fatigue induced cracking observed at the nozzle blend radius.

Thus, the four nozzles selected for detailed evaluation are the following:

- Recirculation Outlet
- Recirculation Inlet
- Steam Outlet
- Core Spray

Selection of these four nozzles is supported by the fact that they are typically larger in size, which increases the probability of flaws being present due to the larger weld volume. These nozzles also are subjected to significant stresses during various thermal loadings and normal startup shutdown operation.

4
NOZZLE STRESS ANALYSIS

A key input in evaluating the RPV reliability is the applied stress at the nozzle-to-vessel weld and nozzle blend radii. Due to the complex behavior of the stress distribution near the nozzle blend radii, finite element analyses were performed for the four nozzles of interest selected in Section 3. As can be seen in Table 3-1, there are many variations in RPV size and product line. Thus, it is difficult to select bounding nozzles for these evaluations. Due to the complexity and resources required to develop these finite element models, currently available finite element models were used. For this evaluation, the following nozzles were selected for the detailed evaluations described in this section.

Nozzle	Plant
Core Spray	Oyster Creek
Recirculation Inlet	Brunswick
Recirculation Outlet	Pilgrim
Steam Outlet	Oyster Creek

A three dimensional, finite element model was constructed for each of the reactor vessel nozzles to be evaluated. The finite element models included the nozzle-to-vessel and nozzle-to-pipe welds. The applicable loadings for the nozzles, such as heat-up and other significant thermal transients, were applied to determine the through-wall stress distribution in the nozzles at the locations of interest.

Figure 4-1 shows the typical paths for which stress distributions were extracted from the finite element analysis. Path C corresponds to the approximate center of the nozzle-to-vessel welds.

Stress distributions were also evaluated at different azimuthal locations for each nozzle. Figure 4-2 shows the azimuthal location for which stresses were extracted (0°, 90°, 180°, 270°). The 0° to 180° axis defines the horizontal plane.

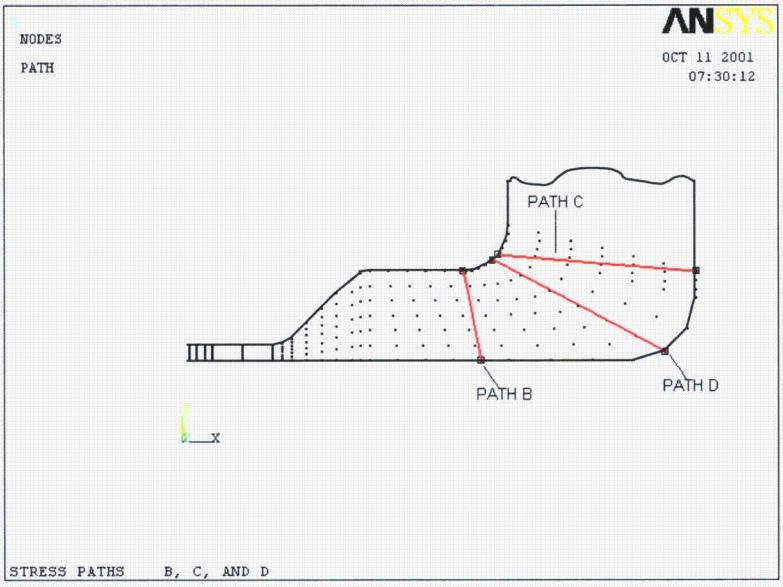

Figure 4-1
Nodal Stress Path

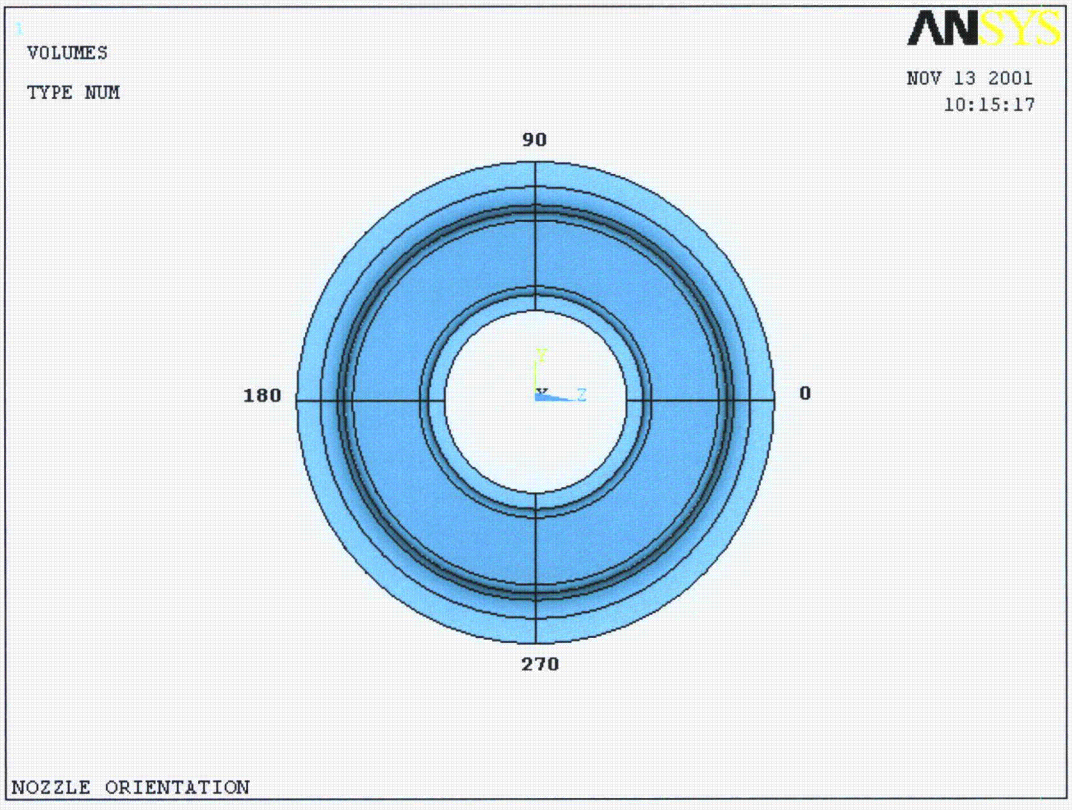

Figure 4-2
Nozzle Orientation

4.1 Analysis

4.1.1 Finite Element Models

A three-dimensional finite element model was developed for each nozzle using the ANSYS finite element software package [8]. The dimensions used for the core spray nozzle and local RPV shell was provided by Reference [9]. The dimensions used for the main steam nozzle and local RPV shell was provided by Reference [10]. The dimensions for the recirculation inlet nozzle and local RPV shell are found in References [11] and [12]. The dimensions for the recirculation outlet nozzle and local RPV shell are found in References [13] and [14]. These dimensions are summarized in Table 4-1 and the parameters are illustrated in Figure 4-3.

Table 4-1
RPV Nozzle Dimensions (Inches)

	Parameters	Core Spray	Main Steam	Recirculation Inlet	Recirculation Outlet
Vessel	Tvsl	7.125	7.125	5.69	7.00
	Rad_I	106.7188	106.7188	110.00	113.200
	Rad_O	113.8438	113.8438	115.69	120.20
Blend Radius	R1	1.75	4.00	3.63	7.00
	R2	2.375	7.125	2.50	7.00
	R3	1.00	1.00	1.00	1.00*
	R4	1.00	1.00	4.63	1.00*
Safe-End	RoSE	3.6875	12.0313	7.75	14.67
	RiSE	3.1330	10.75	6.875	12.78
Nozzle	RoN	6.5625	16.00	13.988	22.31
	Tnzl	3.4295	5.25	7.113	9.53
Lengths	L1	1.1875	1.00	1.00*	1.00*
	ΔL2	2.25	5.2813	3.5170	7.85
	ΔL3	5.5625	9.6875	10.63	15.63
	L6	126.2813	142.3125	132.38	145.513

* assumed value.

Each of the models included a full 360° representation of the nozzle and a section of the safe-end. A portion of the RPV shell was included in the finite element model for each nozzle. The length of the RPV shell included in the model was sufficient to avoid end effects at the nozzle penetration.

The finite element models for the core spray, main steam, recirculation inlet and recirculation outlet are shown in Figures 4-4, 4-5, 4-6 and 4-7, respectively.

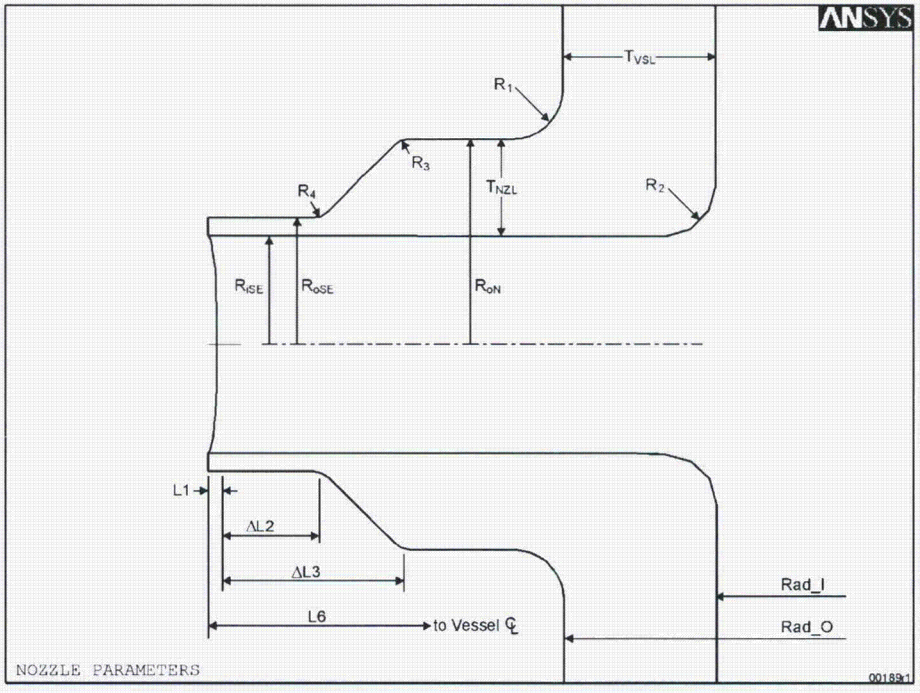

Figure 4-3
RPV Nozzle Parameters

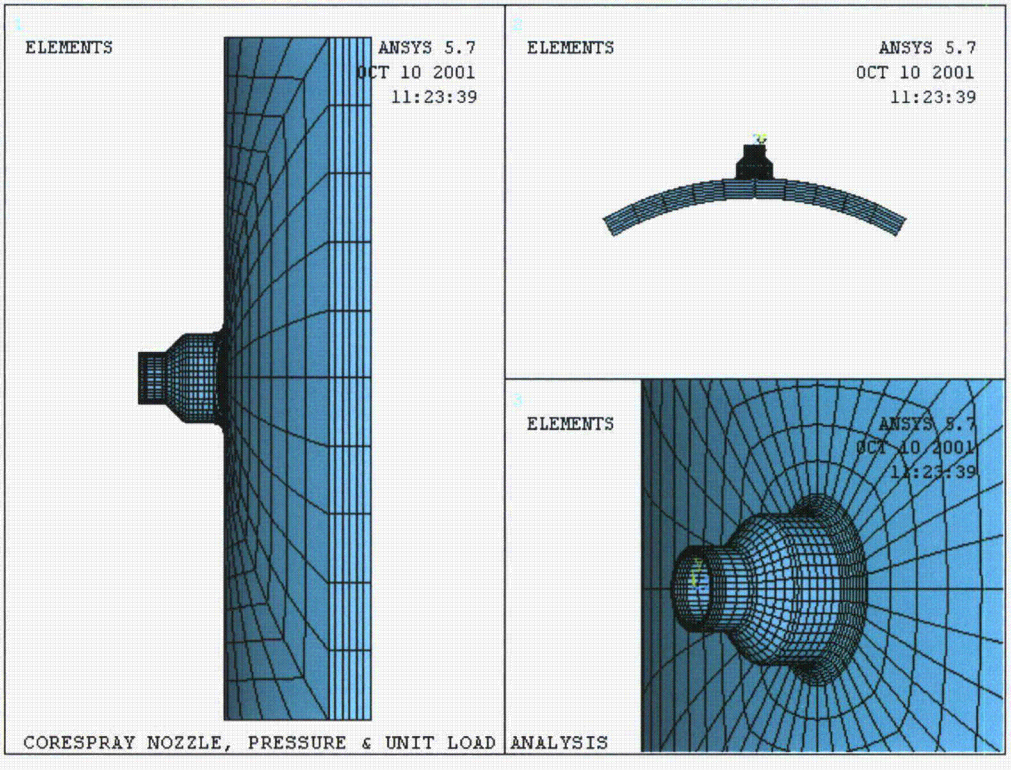

Figure 4-4
Core Spray Mesh

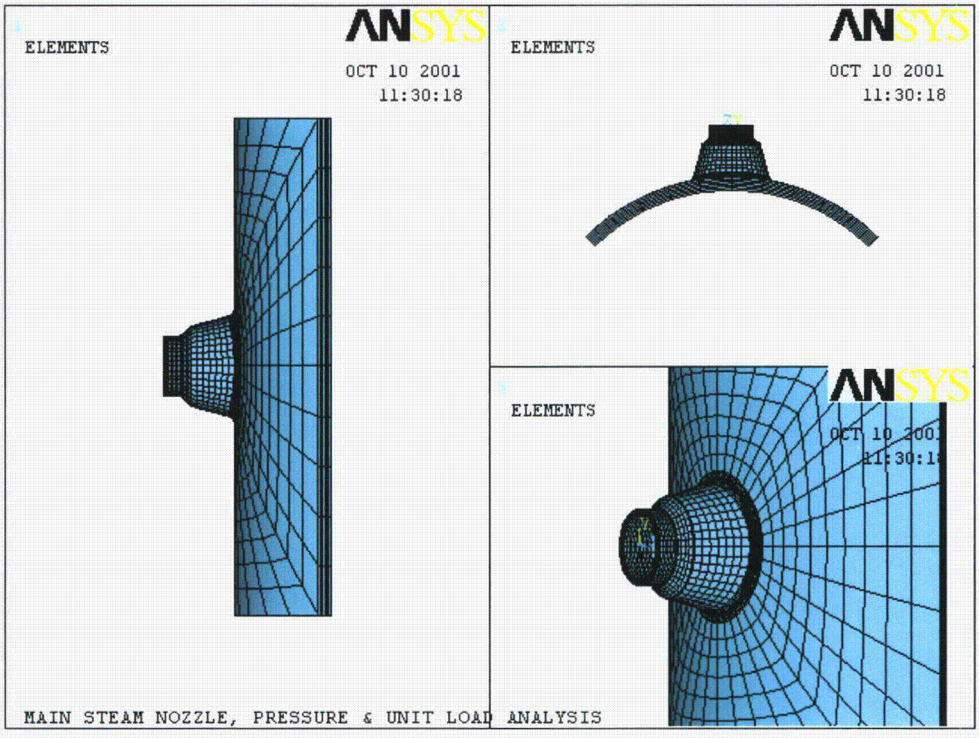

Figure 4-5
Main Steam Mesh

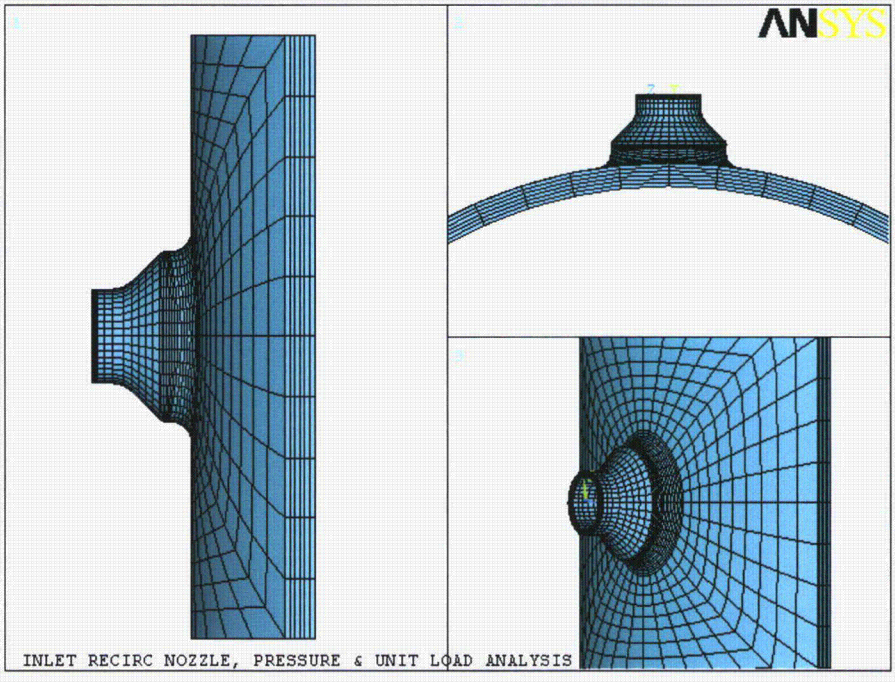

Figure 4-6
Recirculation Inlet Mesh

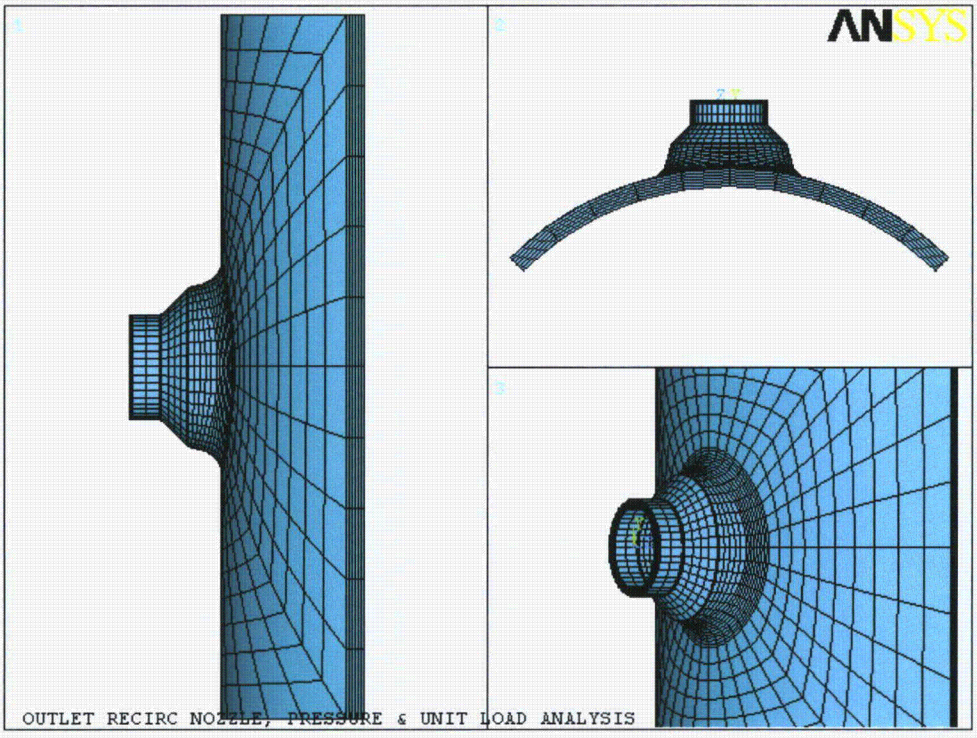

Figure 4-7
Recirculation Outlet Mesh

4.1.2 Material Properties

The RPV stress report [15] used for the core spray and main steam nozzles was performed in accordance with the requirements of the 1959 ASME B&PV Code, Section I, with Addenda through Summer 1963, and the 1963 ASME B&PV Code, Section III. Per References [10] and [11], the RPV shell is made of SA-302, Grade B, modified material and the nozzles are made of SA-336 forging material modified with Code Case 1236. For the evaluation described in this report, SA-302, Grade B, modified material is assumed to be equivalent to SA-533 Grade B, Class 1, for the vessel and the modified SA-336 is assumed to be equivalent to SA-508, Class 2 for the nozzles.

The design report [16] used for the recirculation inlet nozzle and safe end was performed in accordance with the requirements of the ASME B&PV Code, Section III, 1986 Edition. The nozzle is made of SA-508, Class 2 [16]. The report [16] did not specify the vessel material, but for this analysis the material will be assumed to be SA-533 Grade B, Class 1.

The RPV stress report [13] used for the recirculation outlet nozzle was performed in accordance with the requirements of the ASME B&PV Code, Section III, 1989 Edition, Class I Components. The nozzle is made of SA-508, Class 2 [13] and the vessel is made of SA-533, Grade B, Class 1 [13]. However, the 1995 edition of the ASME B&PV [17] was used in this evaluation in order to take advantage of updated material properties as allowed by NCA-1140 of the ASME B&PV Code. The temperature dependent material properties used in the finite element analyses are given in Table 4-2.

Table 4-2
Material Properties

SA-533, Grade B, Class 1 (Vessel)

Property	Temperature (°F)											
	70	100	150	200	250	300	350	400	450	500	550	600
Modulus of Elasticity (E) (10^6 psi)	29.2	29.0	28.8	28.5	28.3	28.0	27.7	27.4	27.2	27.0	26.7	26.4
Coefficient of Thermal Expansion (α) (10^{-6} in/in/°F)	7.02	7.13	7.29	7.45	7.60	7.74	7.88	8.01	8.13	8.25	8.36	8.46
Thermal Conductivity (K) (10^{-4} BTU/in-s-°F)	5.16	5.23	5.35	5.42	5.49	5.51	5.51	5.51	5.49	5.44	5.37	5.32
Specific Heat (c) (Btu/lb-°F)	0.106	0.108	0.111	0.114	0.117	0.119	0.122	0.125	0.128	0.131	0.134	0.138

SA-508, Class 2 (Nozzle)

Property	Temperature (°F)											
	70	100	150	200	250	300	350	400	450	500	550	600
Modulus of Elasticity (E) (10^6 psi)	29.2	29.0	28.8	28.5	28.3	28.0	27.7	27.4	27.2	27.0	26.7	26.4
Coefficient of Thermal Expansion (α) (10^{-6} in/in/°F)	6.50	6.50	6.57	6.67	6.77	6.87	6.98	7.07	7.15	7.25	7.34	7.52
Thermal Conductivity (K) (10^{-4} BTU/in-s-°F)	5.46	5.49	5.53	5.56	5.56	5.53	5.49	5.46	5.39	5.35	5.25	5.19
Specific Heat (c) (Btu/lb-°F)	0.106	0.108	0.112	0.115	0.118	0.120	0.122	0.125	0.127	0.130	0.133	0.135

4.1.3 Loads and Boundary Conditions

The steady state and transient operating conditions of the reactor vessel assembly are specified in the original stress reports [13, 15, and 16]. Attached piping loads are considered in this evaluation, even though they were not included in the original stress report. Thus, the following loads are used for the evaluation of the nozzles:

Mechanical and Pressure Load Cases

Load Case 1: A constant pressure of 1000 psi at 70°F is applied to the entire inside surface of the vessel and nozzle as shown below in Figure 4-8. A cap load is applied to the free end of the vessel, which is calculated as:

$$P_{vsl} = \frac{P * R_i^{\,2}}{R_o^{\,2} - R_i^{\,2}}$$ **Equation 4-1**

where,

P_{vsl} is the end cap pressure on the vessel.

P is the applied constant pressure.

R_i is the inside radii of the vessel.

R_o is the outside radii of the vessel.

An end cap load is also applied to the nozzle wall top surface. It is calculated as:

$$P_{nozz} = \frac{P * r_i^{\,2}}{r_o^{\,2} - r_i^{\,2}}$$ **Equation 4-2**

where,

P_{nozz} is the end cap pressure on the nozzle.

r_i is the inside radii of the nozzle.

r_o is the outside radii of the nozzle.

Load Case 2: A constant, uniform axial load of 1 kip at 70°F is applied to the safe end of the nozzle. Figure 4-9 shows the axial load.

Load Case 3: The in-plane bending moment at 70°F about the z-axis (perpendicular to RPV centerline) is applied in the form of sinusoidal varying forces on the mean radius nodes at the end of safe-end model. Figure 4-10 shows the load application. The forces are calculated using the force equation:

$$F = \frac{M_{RES} * cos\left(\frac{\theta\pi}{180}\right)}{\Sigma cos^2\left(\frac{\theta\pi}{180}\right) * R_{mid}}$$ **Equation 4-3**

where,

F is the applied sinusoidal force.

M_{RES} is the resultant moment.

R_{mid} is the mean radius at the safe end.

Load Case 4: The out-of-plane bending moment (parallel to RPV centerline) at 70°F about the y-axis is applied in the form of sinusoidal varying forces on the mean radius nodes at the end of safe-end model. Figure 4-11 shows the load application. The forces are calculated using Equation 4-3 above, except that θ is replaced by θ+90°.

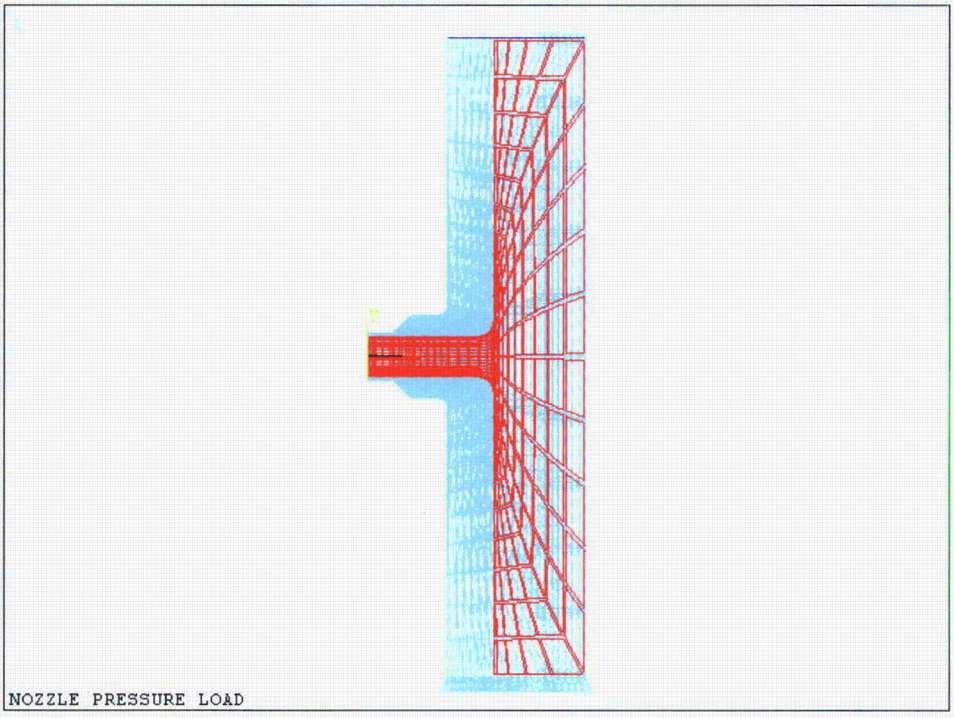

Figure 4-8
Nozzle Pressure Load

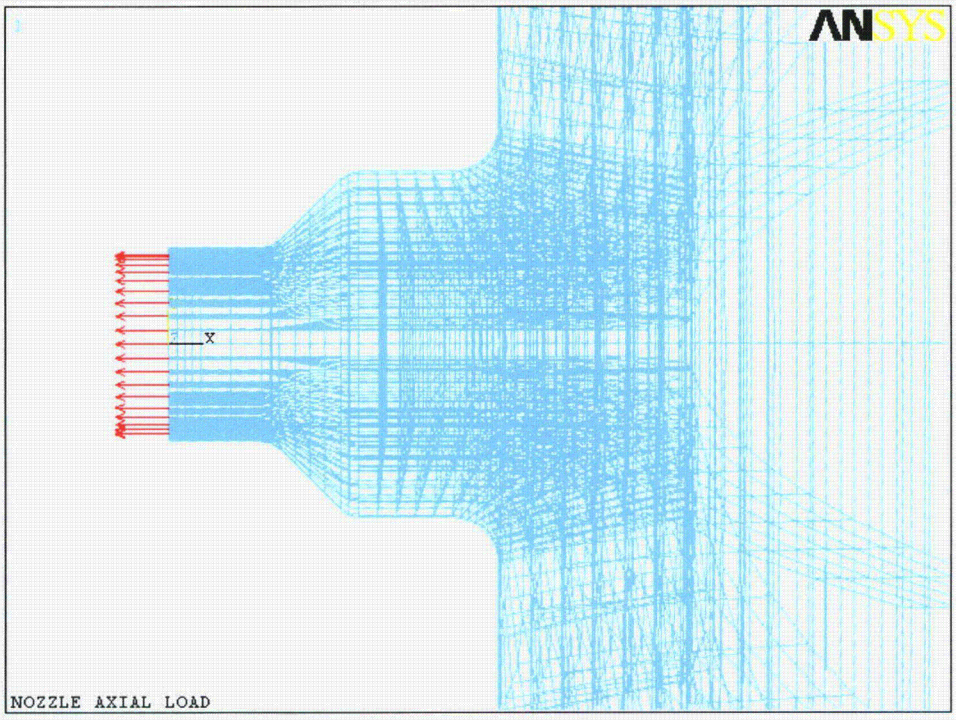

Figure 4-9
Nozzle Unit Axial Load

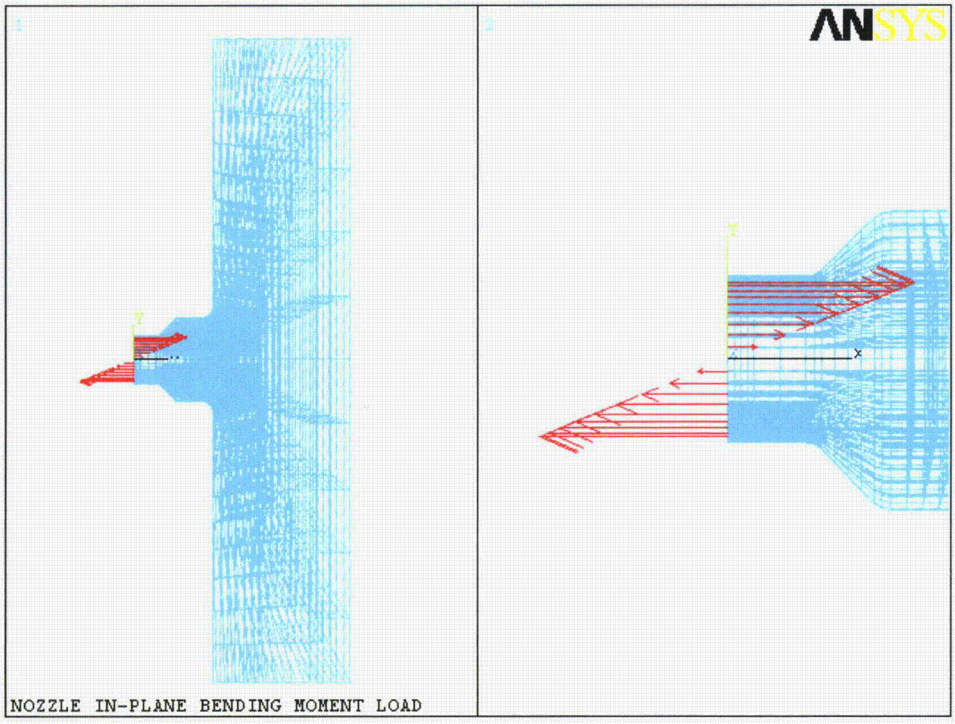

Figure 4-10
Nozzle In-Plane Bending Moment Load

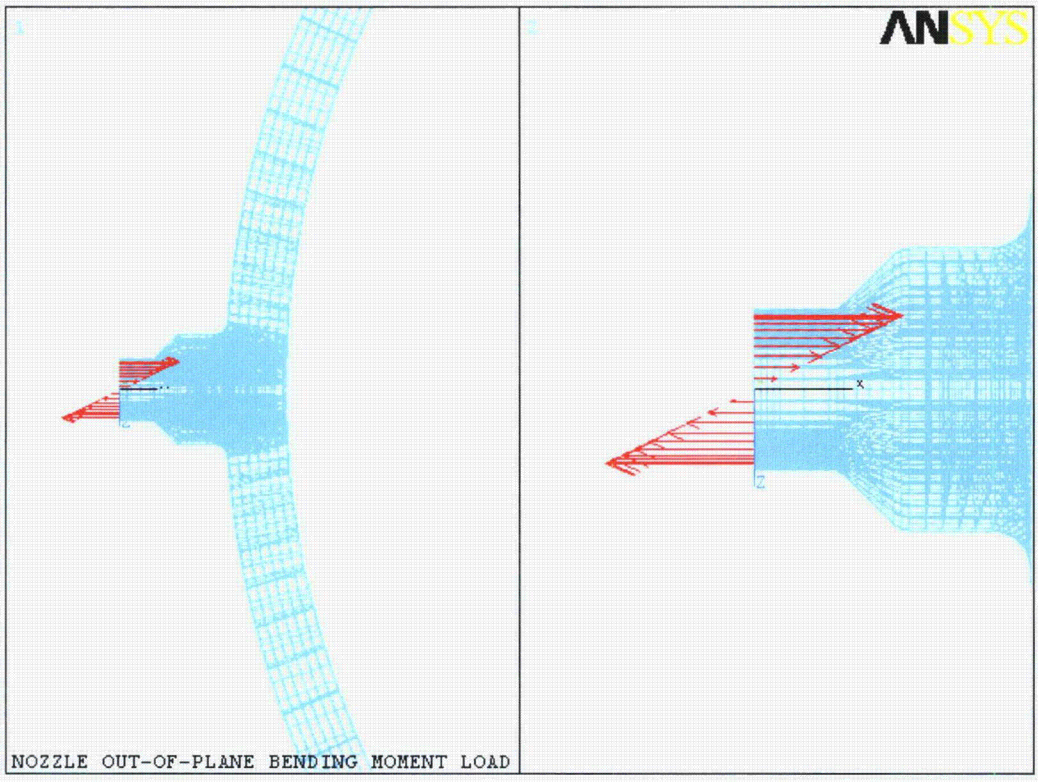

Figure 4-11
Nozzle Out-of-Plane Bending Moment Load

Thermal Load Cases

Core Spray Nozzle

Load Case 1: Heat Up [18]. This thermal transient has an initial temperature of 70°F. The temperature increases to 546°F at a rate of 100°F/hr to establish steady State at operating temperature. It reaches a steady state temperature of 546°F. Figure 4-12 shows the time history for the transient.

Load Case 2: Emergency Shutdown [19]. This thermal transient has an initial temperature of 546°F. The temperature decreases to 406°F in 10 seconds. This is followed by a step drop to 70°F. The transient then goes to a steady state condition at 70°F. Figure 4-13 shows the time history for this transient.

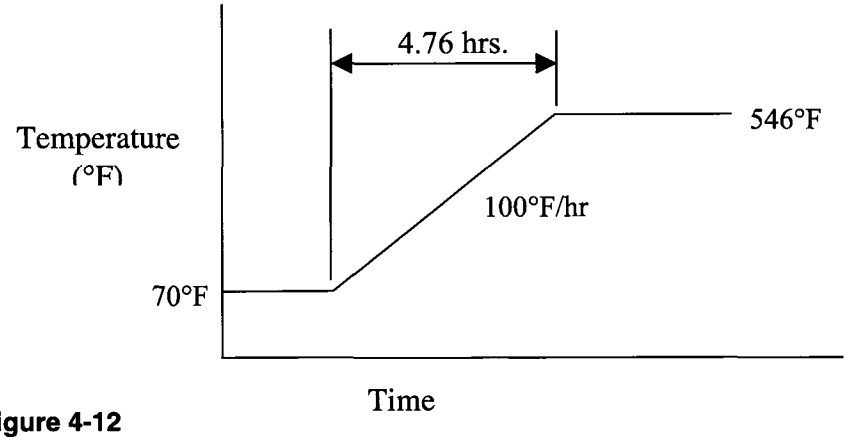

Figure 4-12
Core Spray Nozzle Thermal Load Case 1-Heat Up

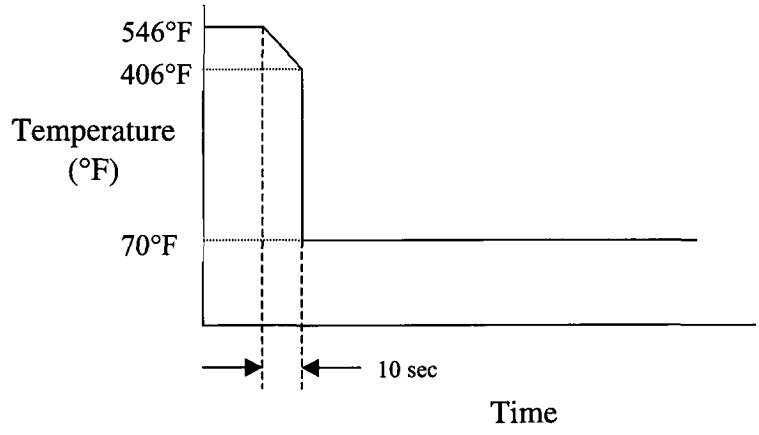

Figure 4-13
Core Spray Nozzle Thermal Load Case 2-Emergency Cooldown

Main Steam Nozzle

Load Case 1: Heat Up [18]. This thermal transient has an initial temperature of 70°F. The temperature increases to 546°F at a rate of 100°F/hr to establish steady State at operating temperature. Figure 4-14 shows the time history for this transient.

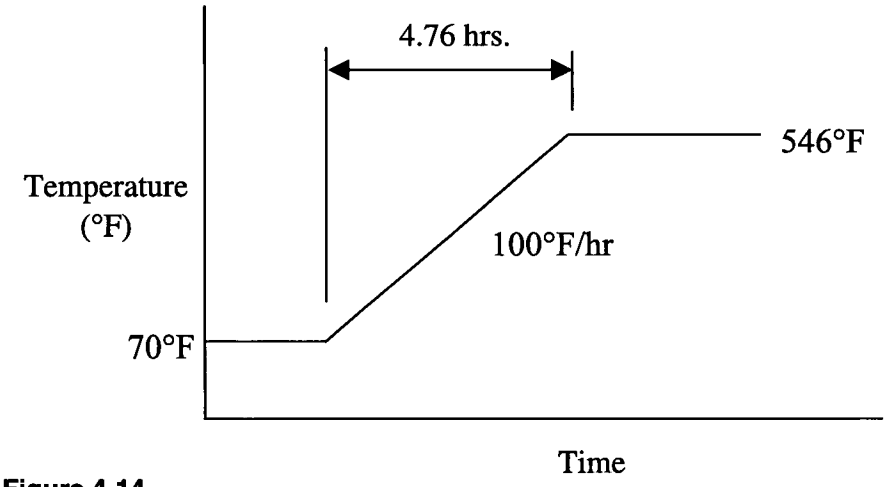

Figure 4-14
Main Steam Nozzle Thermal Load Case 1-Heat Up

Load Case 2: Cooldown Transient [18]. This thermal transient begins at an operating temperature of 546°F and the temperature decreases to 70°F at a rate of 100°F/hr. The temperature reaches a steady state temperature of 70°F. Figure 4-15 shows the time history for this transient.

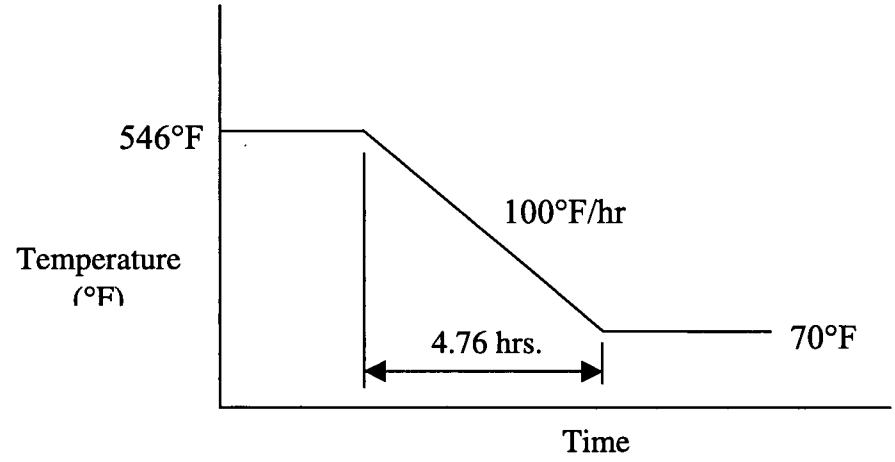

Figure 4-15
Main Steam Line Nozzle Thermal Load Case 2-Cooldown

Recirculation Inlet Nozzle

Load Case 1: Heat Up [16]. This thermal transient has an initial temperature of 70°F. The temperature increases to 546°F at a rate of 100°F/hr to establish steady state. Figure 4-16 shows the time history for this transient.

Load Case 2: Sudden Pump Start of Cold Recirculation Loop [16]. This thermal transient has an initial operating temperature of 522°F is followed by a step drop to 130°F. The temperature remains at this temperature for 34 seconds. The temperature then increases instantly to 522°F. Figure 4-17 shows the time history for this transient.

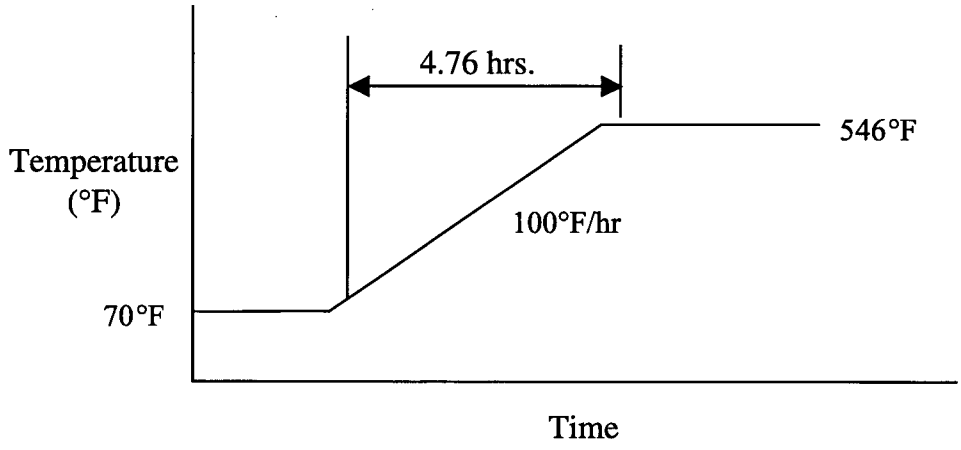

Figure 4-16
Recirculation Inlet Nozzle Thermal Load Case 1-Heat Up

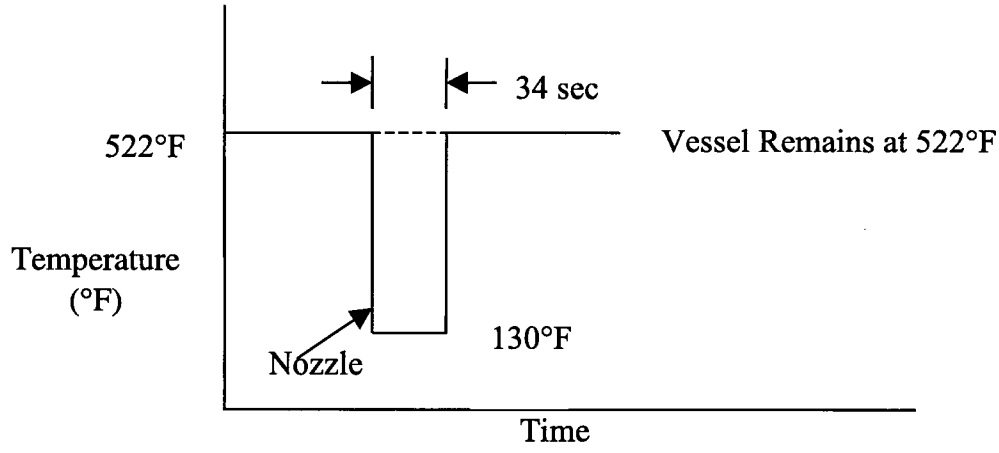

Figure 4-17
Recirculation Inlet Nozzle Thermal Load Case 2-Sudden Pump Start of Cold Recirculation Loop

Recirculation Outlet Nozzle

Load Case 1: Heat Up [13]. This thermal transient has an initial temperature of 100°F. The temperature increases to 546°F at a rate of 100°F/hr to establish the steady state operating temperature. Figure 4-18 shows the time history for this transient.

Load Case 2: Safety Relief Valve Blow Down [13]. This thermal transient has an initial temperature of 546°F. The temperature decreases to 375°F at a rate of 1024°F/hr. The temperature then decreases further to a temperature of 70°F at a rate of 94°F/hr and reaches steady state. Figure 4-19 shows the time history for this transient.

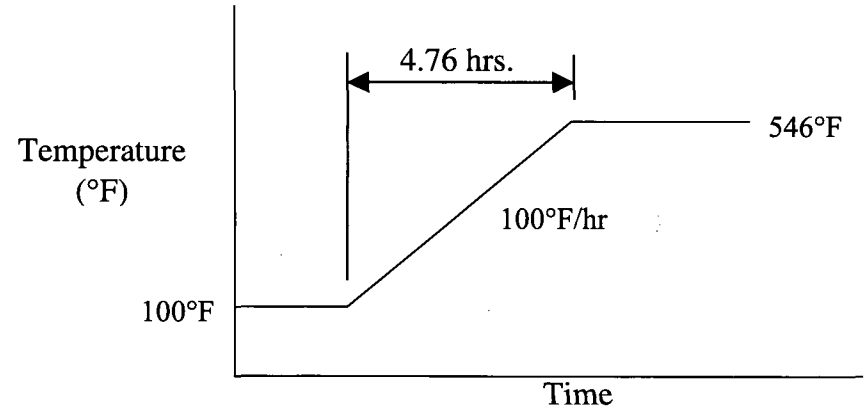

Figure 4-18
Recirculation Outlet Nozzle Thermal Load Case 1-Heat Up

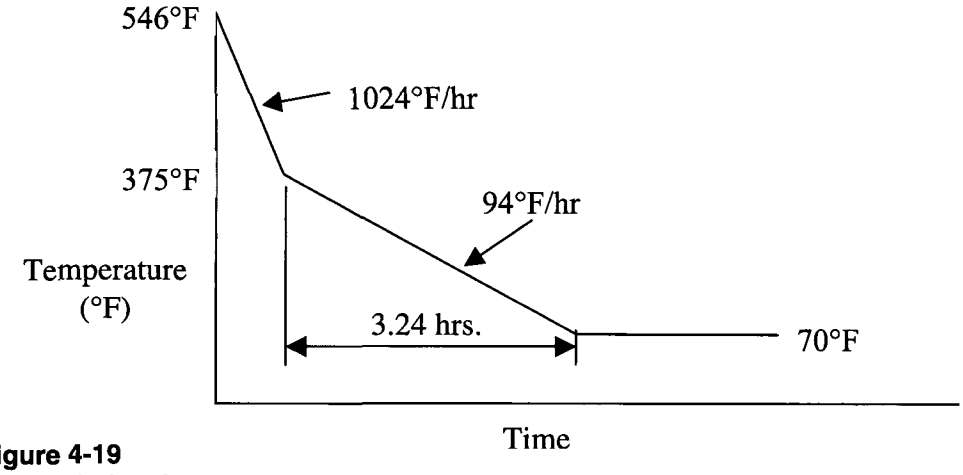

Figure 4-19
Recirculation Outlet Nozzle Thermal Load Case 2-SRV Blow Down

Load Case 3: Loss of Feedwater Pumps [13]. This thermal transient has an initial temperature of 522°F. The temperature then decreases to 300°F in 3 minutes and 40 seconds. The temperature then ramps up to 500°F in 33 minutes. The temperature decreases to 300°F in 3 minutes. This is followed by an increase to 500°F in 73 minutes and then back down to a temperature of 300°F in 7 minutes. The temperature remains at 300°F for 5 minutes until finally increasing to 546°F for steady state. See Figure 4-20 shows the time history for this transient.

Boundary Conditions

The boundary conditions applied to the finite element model are shown in Figure 4-21. The intent of these boundary conditions is to simulate the effect of the entire RPV and the interaction between the nozzle and RPV.

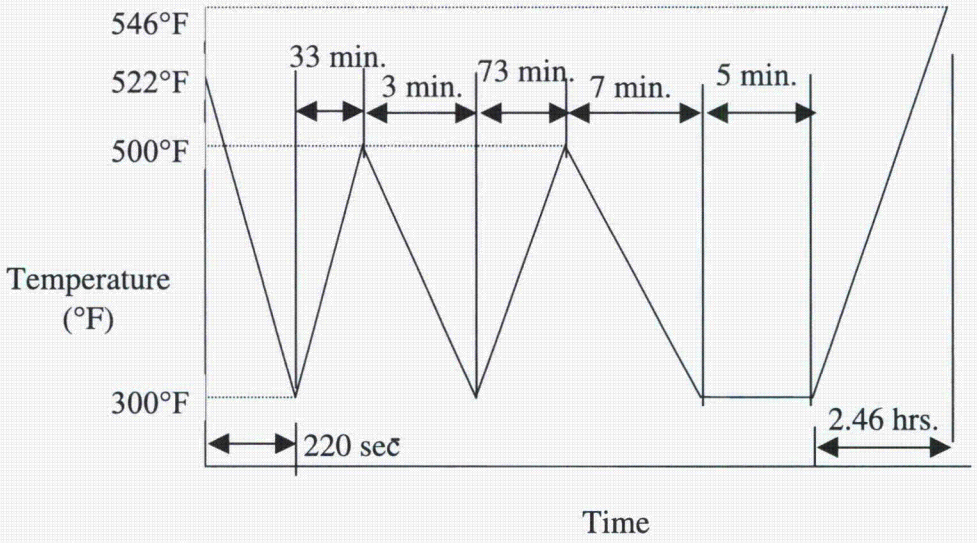

Figure 4-20
Recirculation Outlet Nozzle Thermal Load Case 3-Loss of Feedwater Pumps

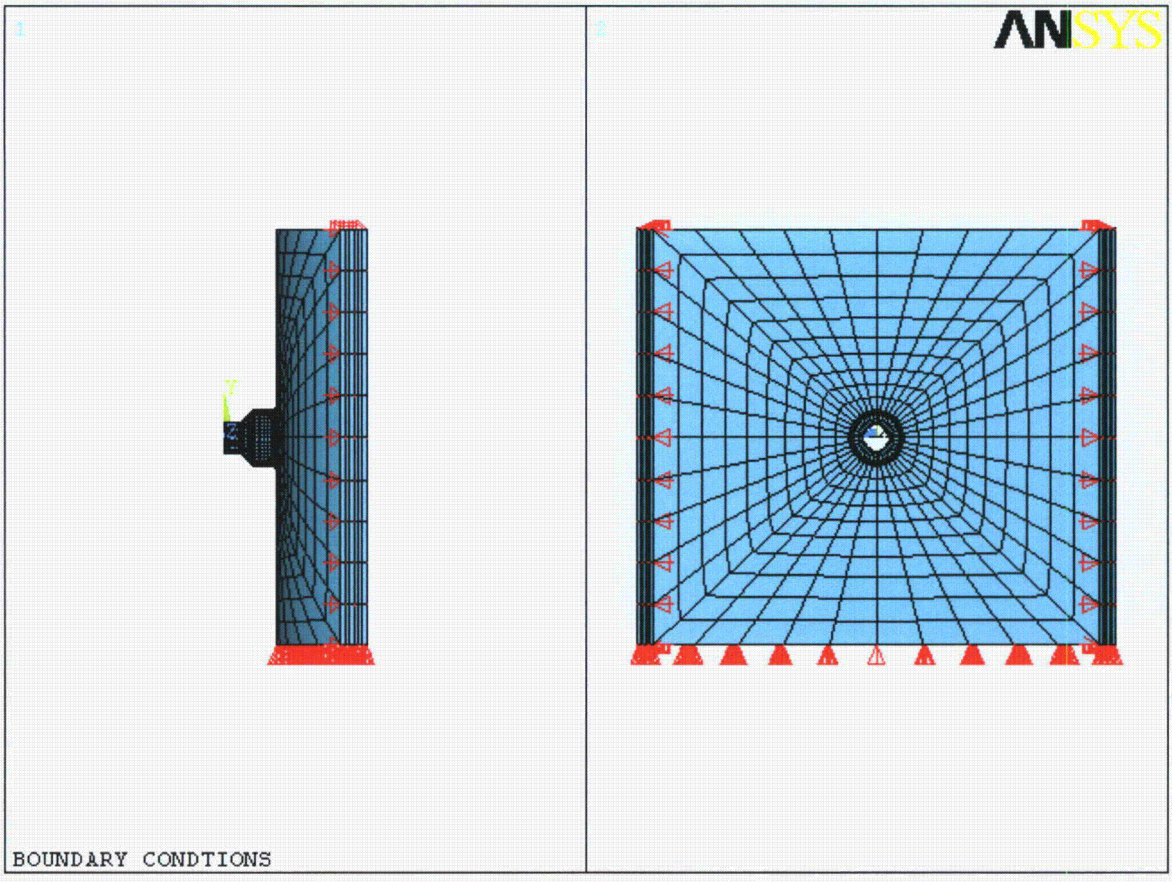

Figure 4-21
Nozzle Boundary Conditions

4.2 Results of Stress Analysis

The stresses were extracted from the transient analysis results for each nozzle. Results were obtained for each radial direction at the 0°, 90°, 180°, and 270° azimuths. These stresses are used in the PFM and DFM analyses described in Sections 5 and 6 of this report. Figures 4-22 through 4-29 show the general behavior of the stress results and the stress intensity in the general vicinity of each nozzle.

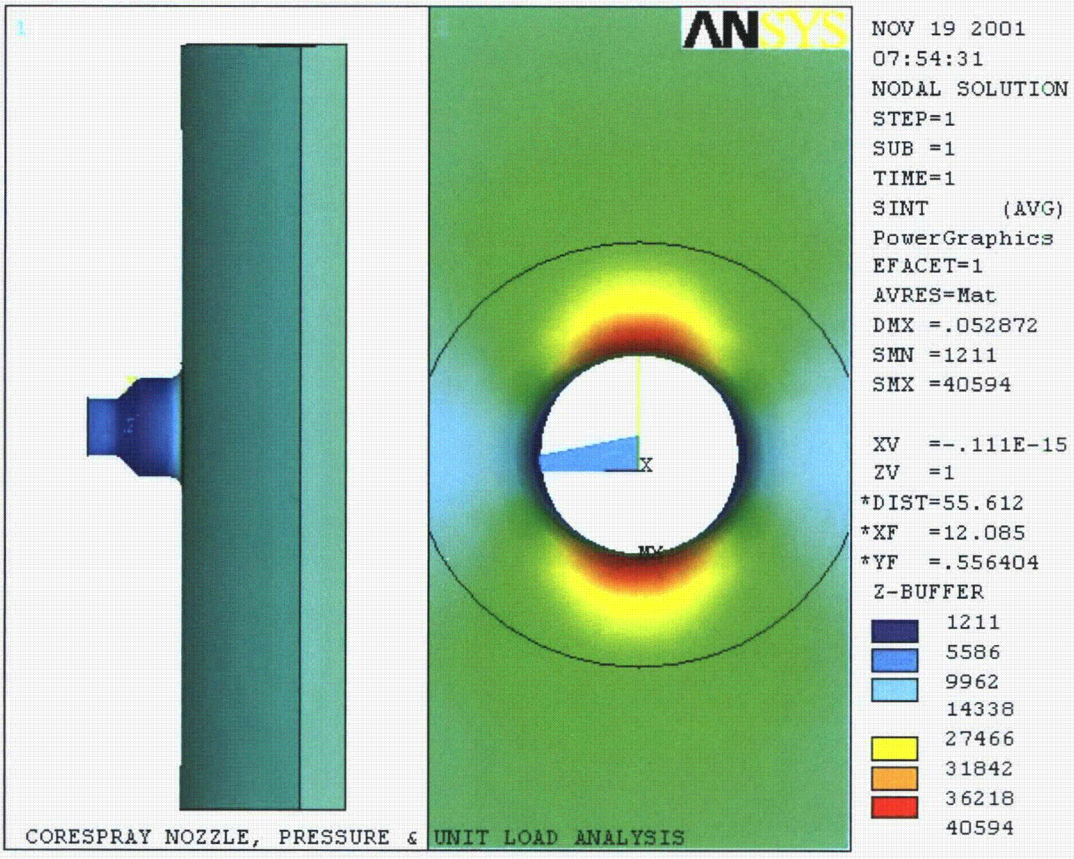

Figure 4-22
Core Spray Nozzle Pressure Stress Intensity

Figure 4-30 through 4-37 show the variation of the surface stress components around the circumference of the nozzle (with respect to the nozzle axis) for steady state. These figures show the stress components versus azimuth as defined in Figure 4-2. The 0° and 180° axis is horizontal and the 0° to 270° axis is vertical. Figures 4-30 through 4-33 show the stress components for the nozzle blend radius, and Figures 4-34 through 4-37 show the stress intensity at the nozzle-to-vessel shell weld. These figures illustrate that there is significant variation in stress depending on which azimuthal location is being considered. The pressure hoop stress peaks at +90° and -90° (90° and 270°), which is expected due to the concentration of stress due to a hole in the vessel. The axial pressure stress is 90° out of phase with the hoop pressure stress and the thermal stress is much lower in magnitude.

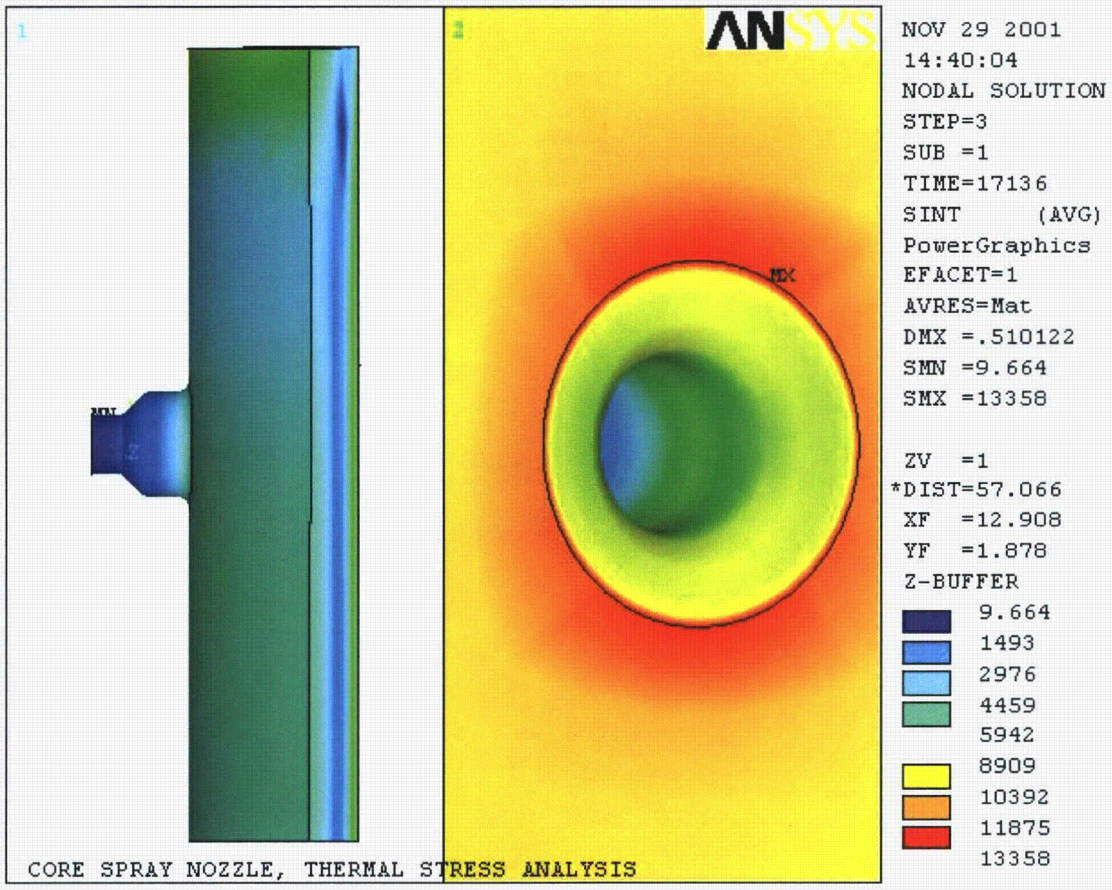

Figure 4-23
Core Spray Nozzle Thermal Stress Intensity

The fracture mechanics evaluation presented in Sections 5 and 6 considers flaws either parallel or perpendicular to the nozzle-to-shell weld location. The evaluation considers an axial flaw at the nozzle blend radii (with respect to the nozzle axis). For these orientations, the stress profile used to perform the fracture mechanics evaluation were either the hoop or axial stress. Based on the results obtained in the stress analysis and since an axial flaw (parallel to weld) is the limiting condition, the hoop stress at the 90° azimuth was selected for the fracture mechanics evaluations. Note that this is conservative since a postulated axial flaw would likely align itself with the weld orientation. As will be discussed in Section 5, it is conservatively assumed that if a flaw exists in a nozzle weld, it is postulated to exist such that it is subjected to the maximum stress anywhere around the nozzle.

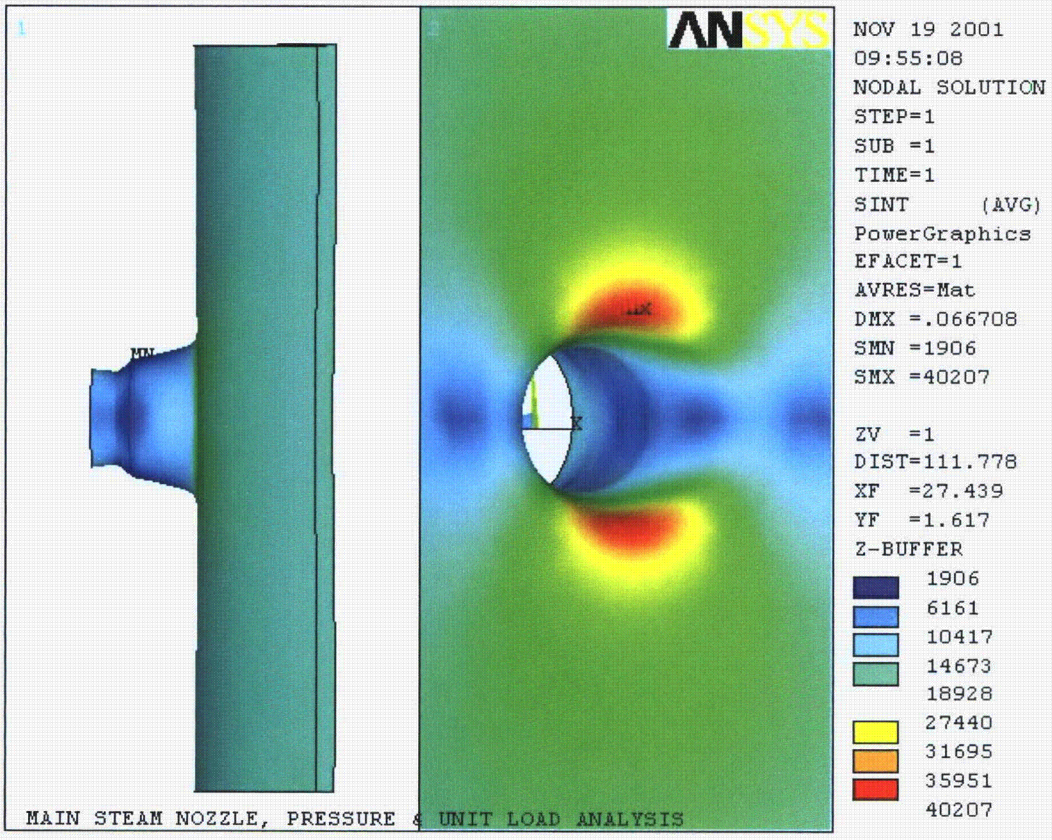

Figure 4-24
Main Steam Nozzle Pressure Stress Intensity

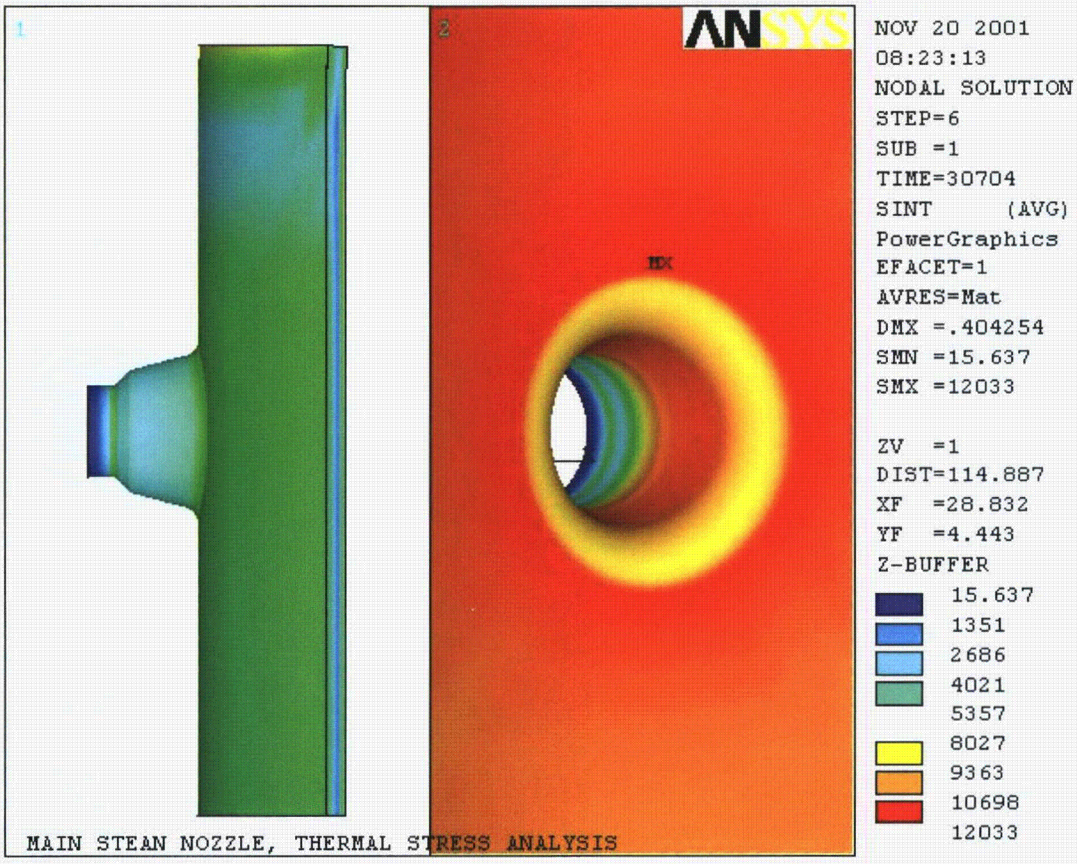

Figure 4-25
Main Steam Nozzle Thermal Stress Intensity

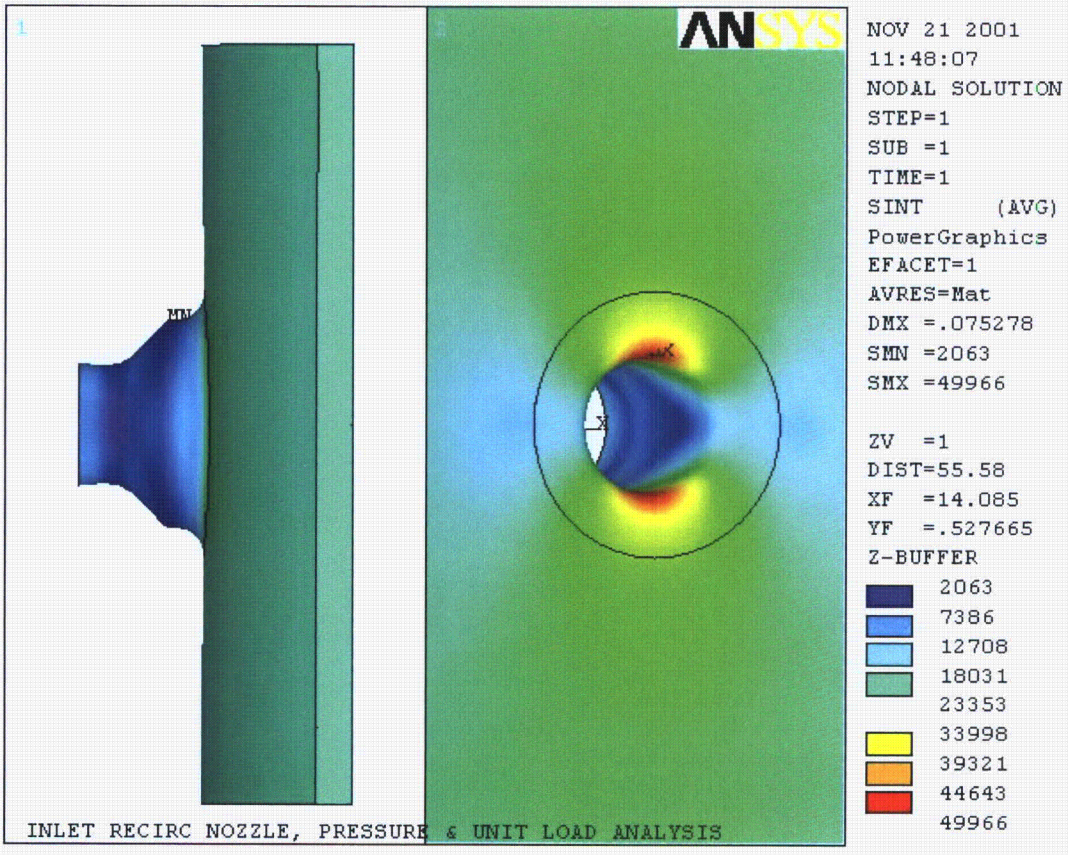

Figure 4-26
Recirculation Inlet Nozzle Pressure Stress Intensity

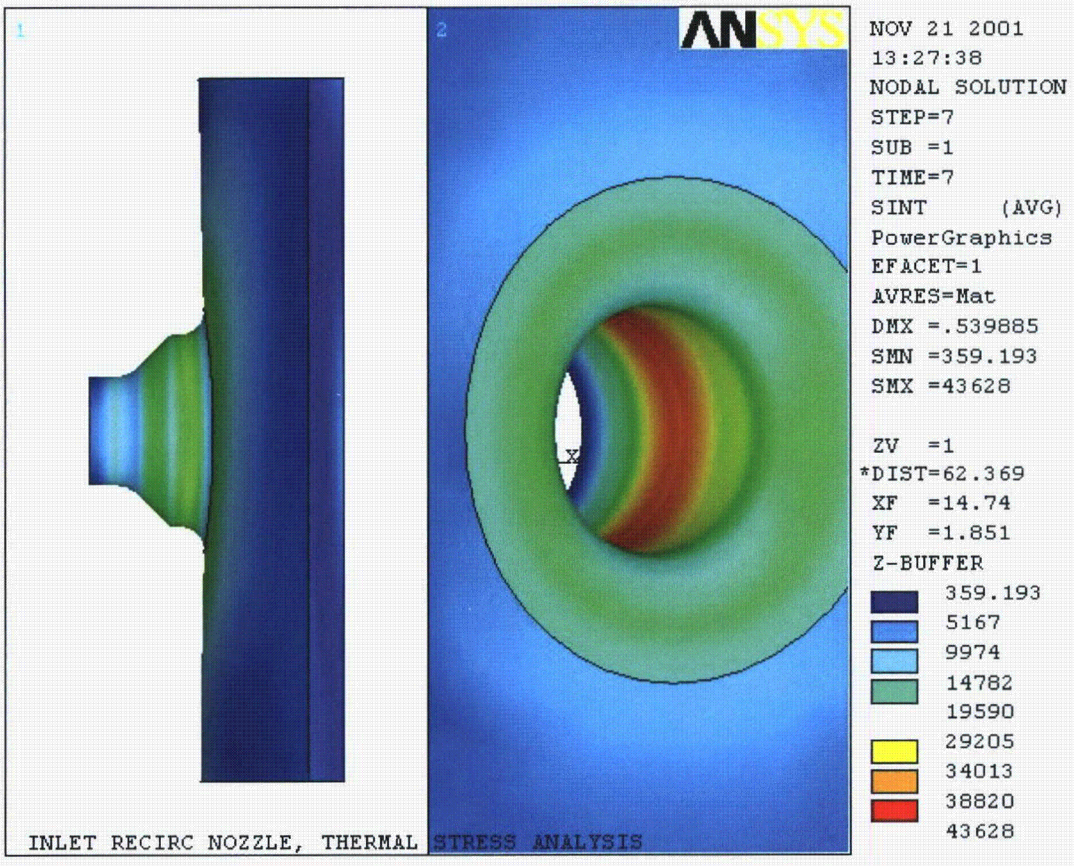

Figure 4-27
Recirculation Inlet Nozzle Thermal Stress Intensity

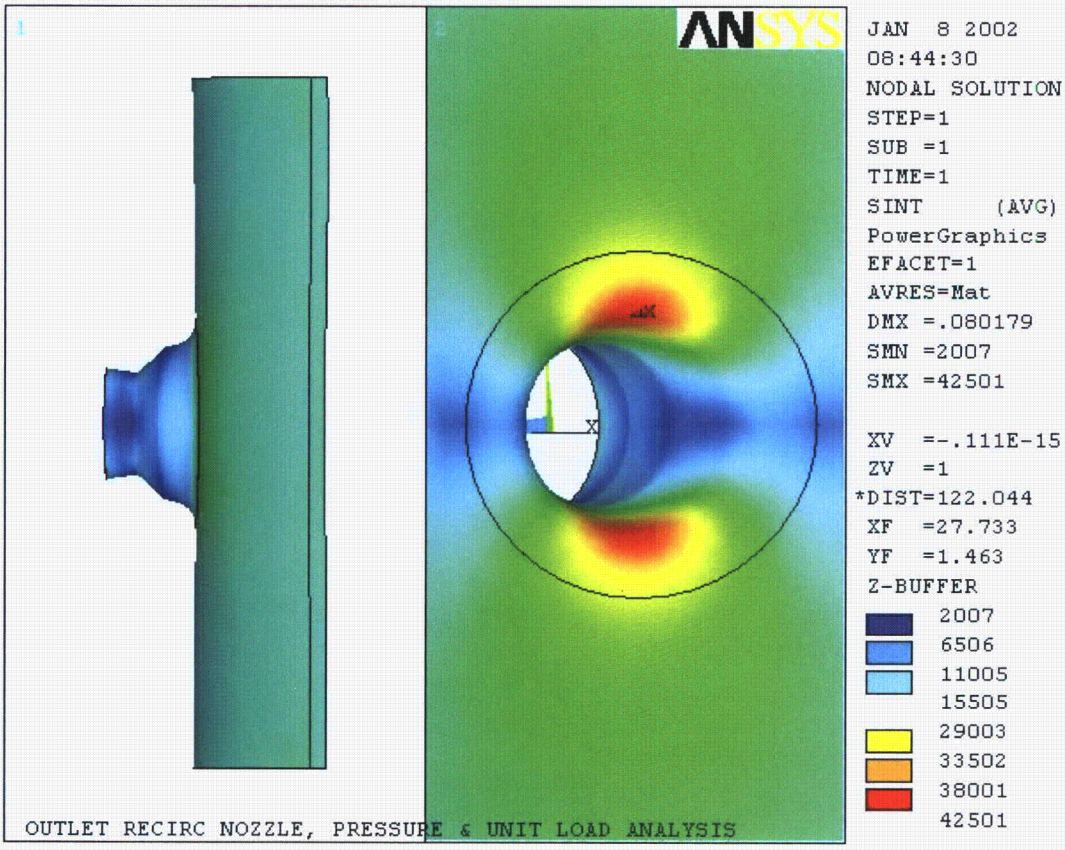

Figure 4-28
Recirculation Outlet Nozzle Pressure Stress Intensity

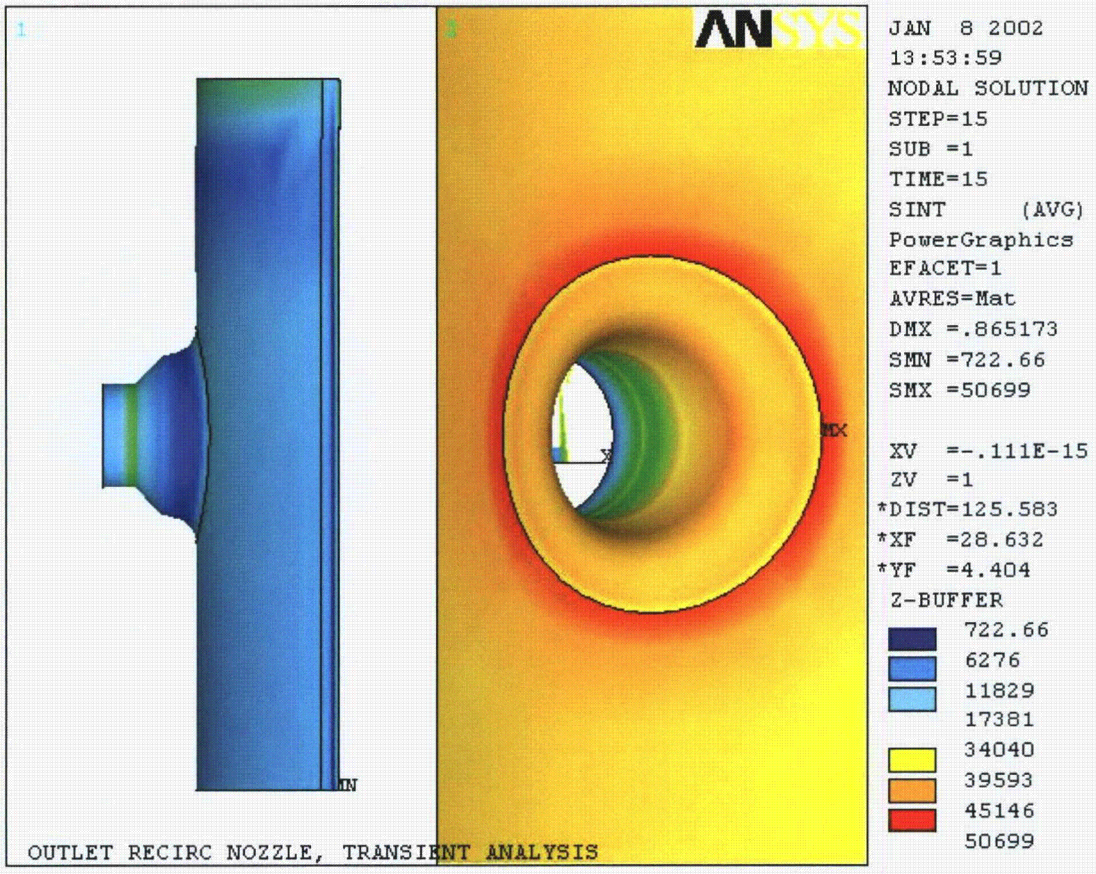

Figure 4-29
Recirculation Outlet Nozzle Thermal Stress Intensity

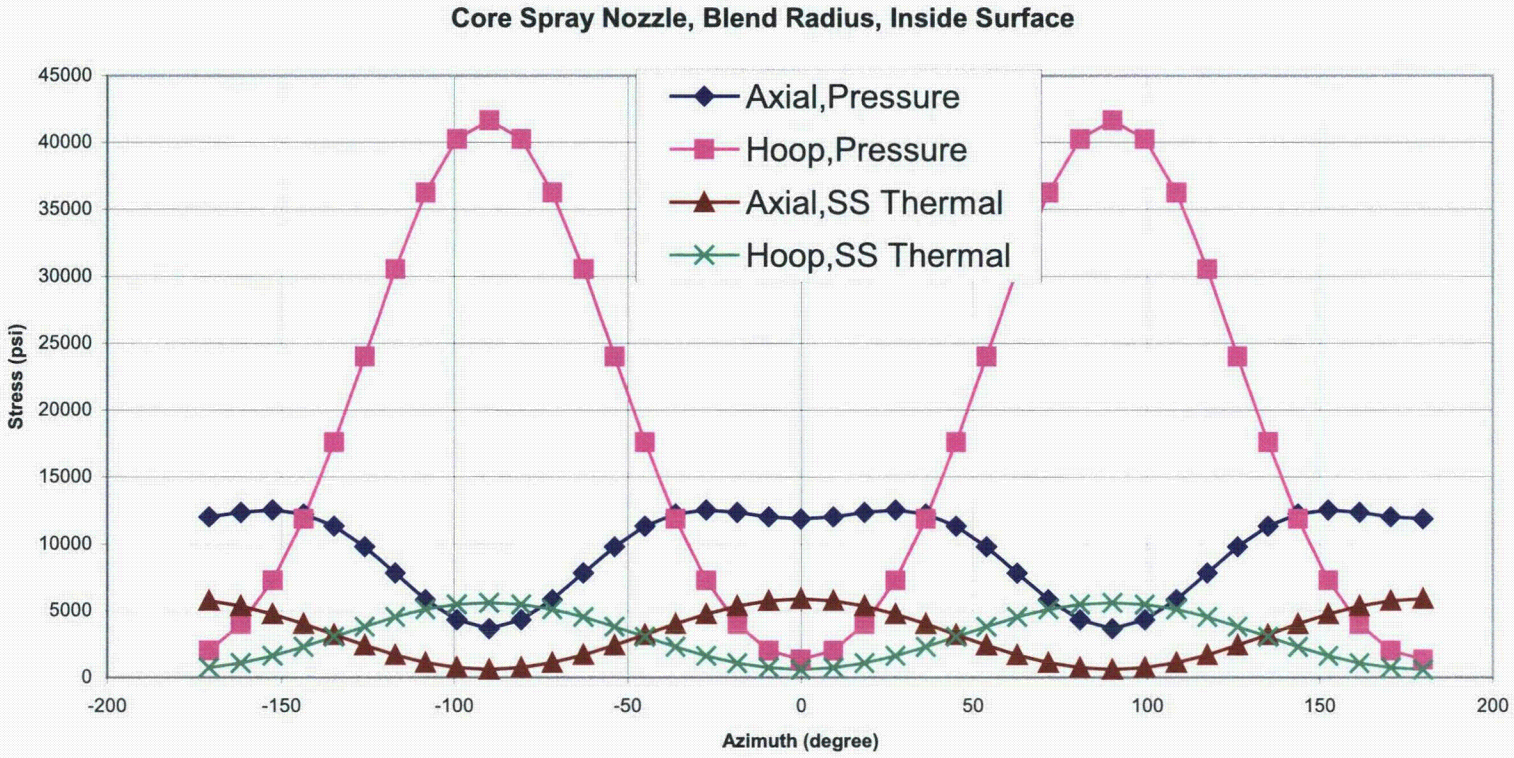

Figure 4-30
Core Spray Nozzle Blend Radius Stress Profile

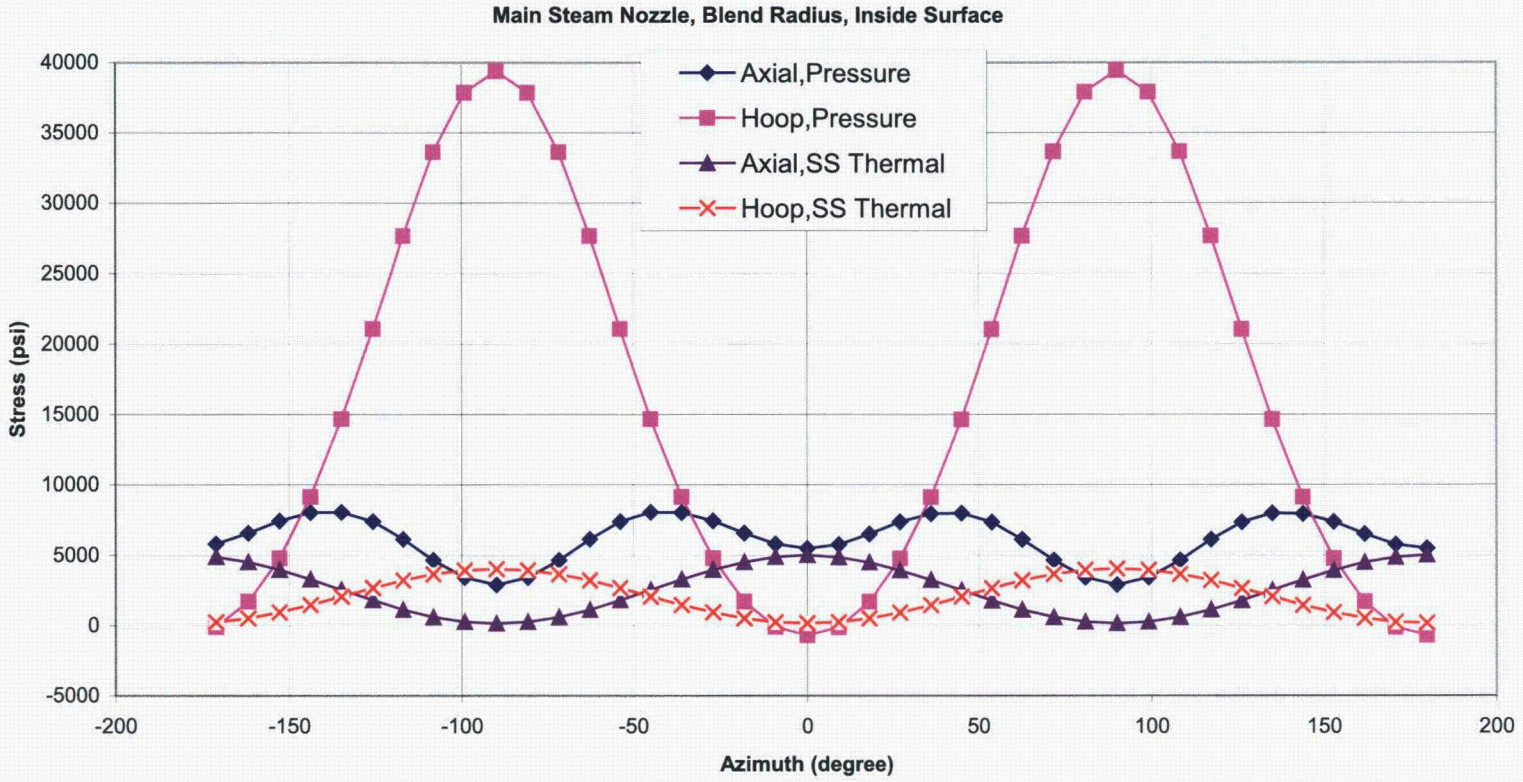

Figure 4-31
Main Steam Line Nozzle Blend Radius Stress Profile

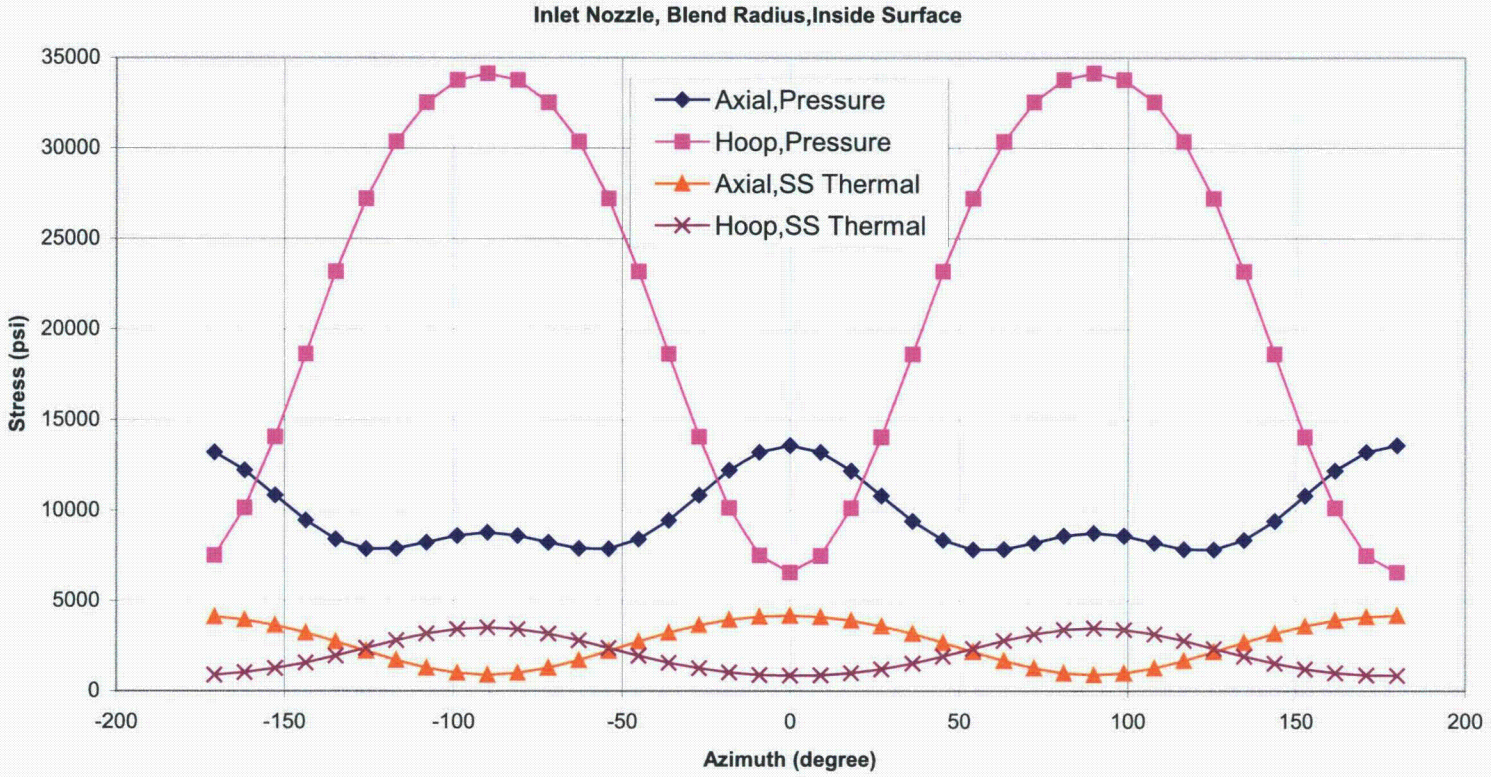

Figure 4-32
Recirculation Inlet Nozzle Blend Radius Stress Profile

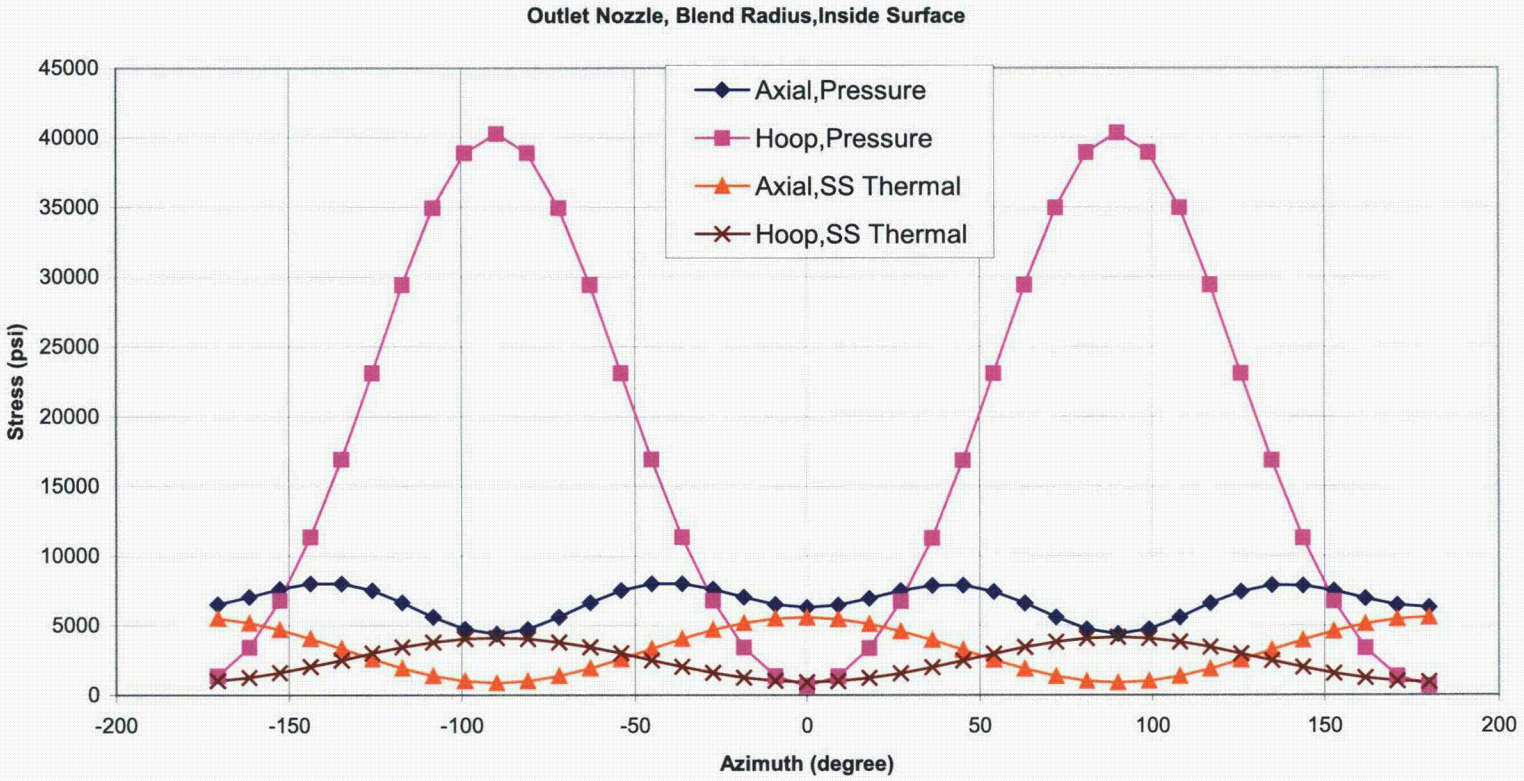

Figure 4-33
Recirculation Outlet Nozzle Blend Radius Stress Profile

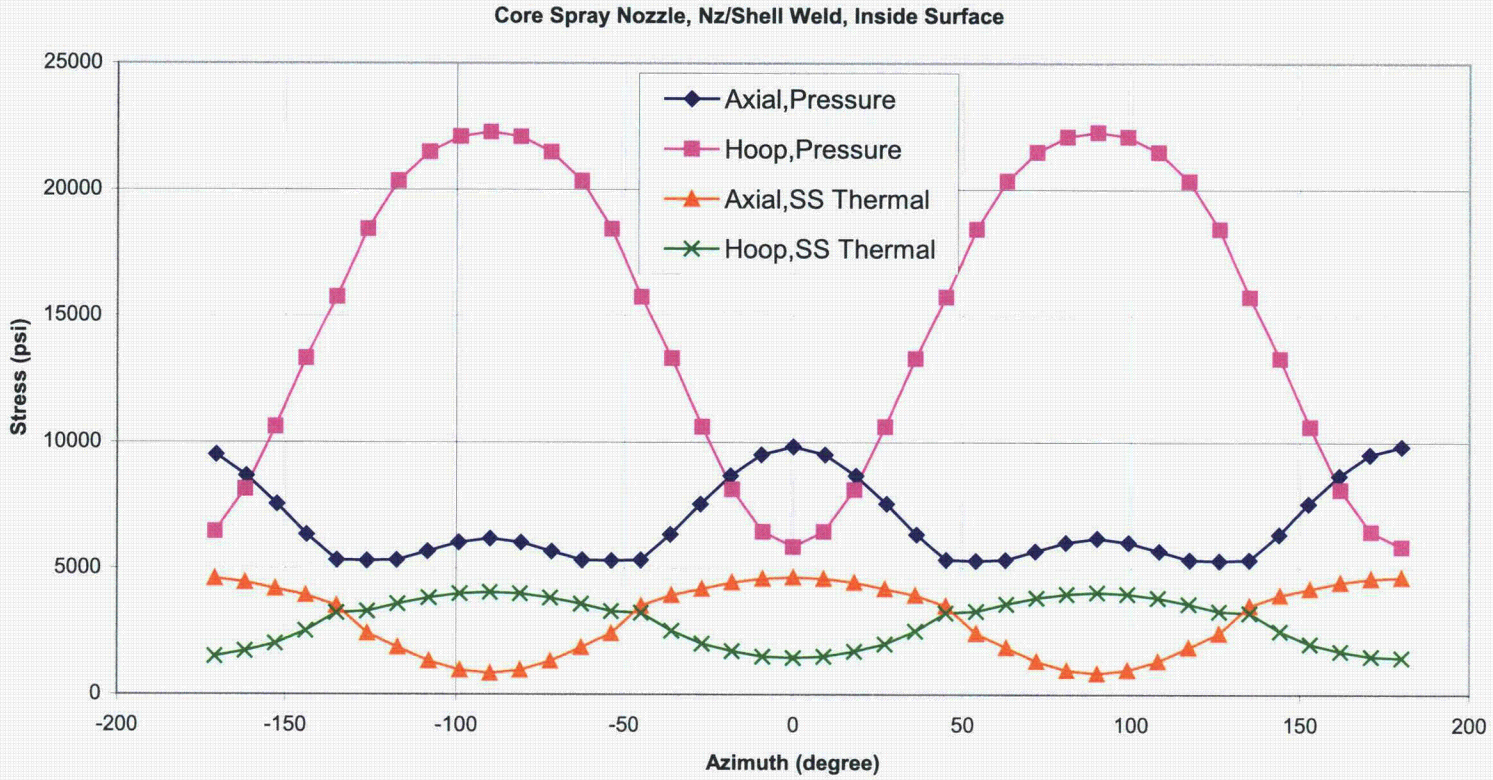

Figure 4-34
Core Spray Nozzle-to-Shell Weld Stress Profile

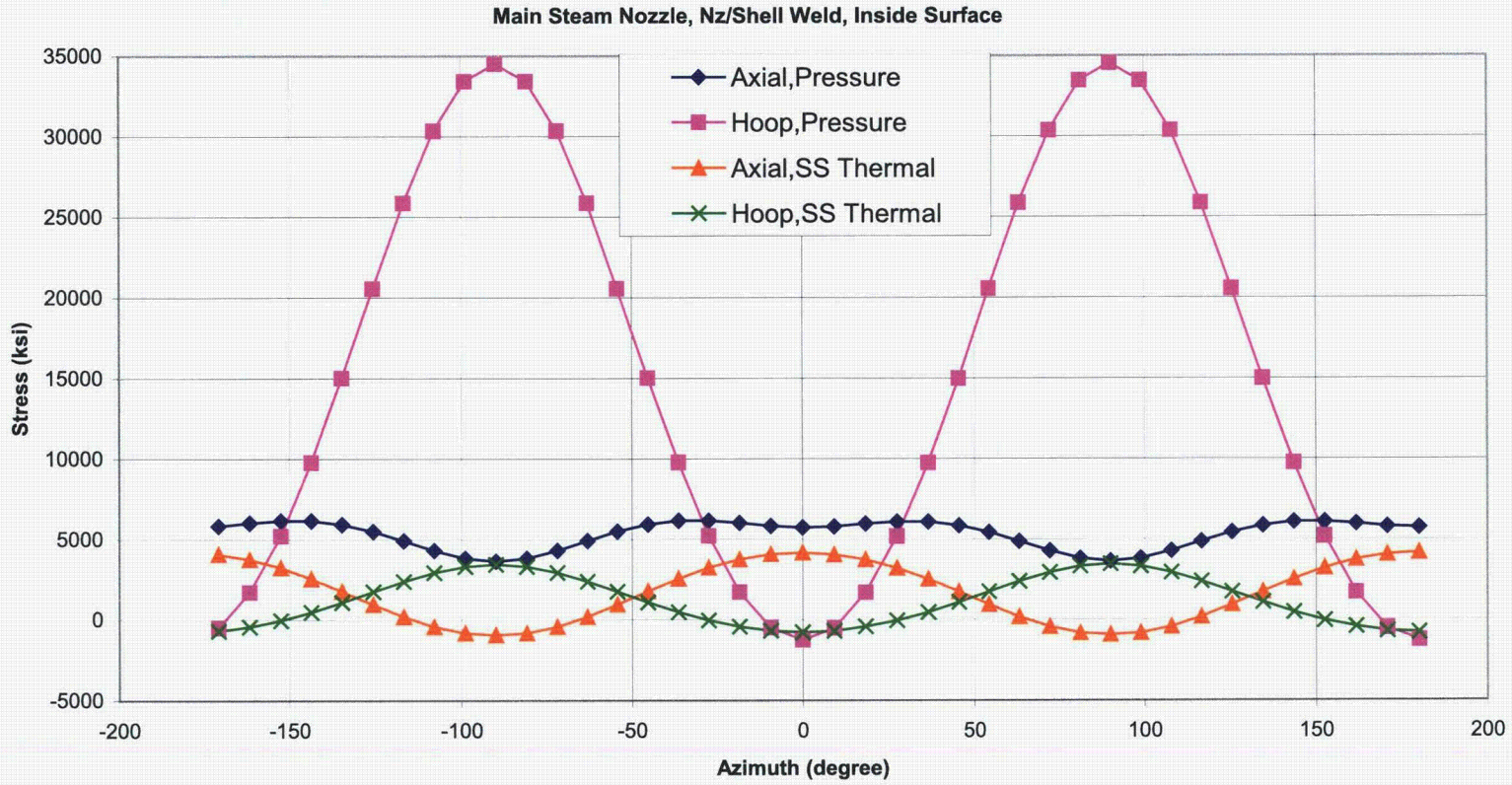

Figure 4-35
Main Steam Line Nozzle-to-Shell Weld Stress Profile

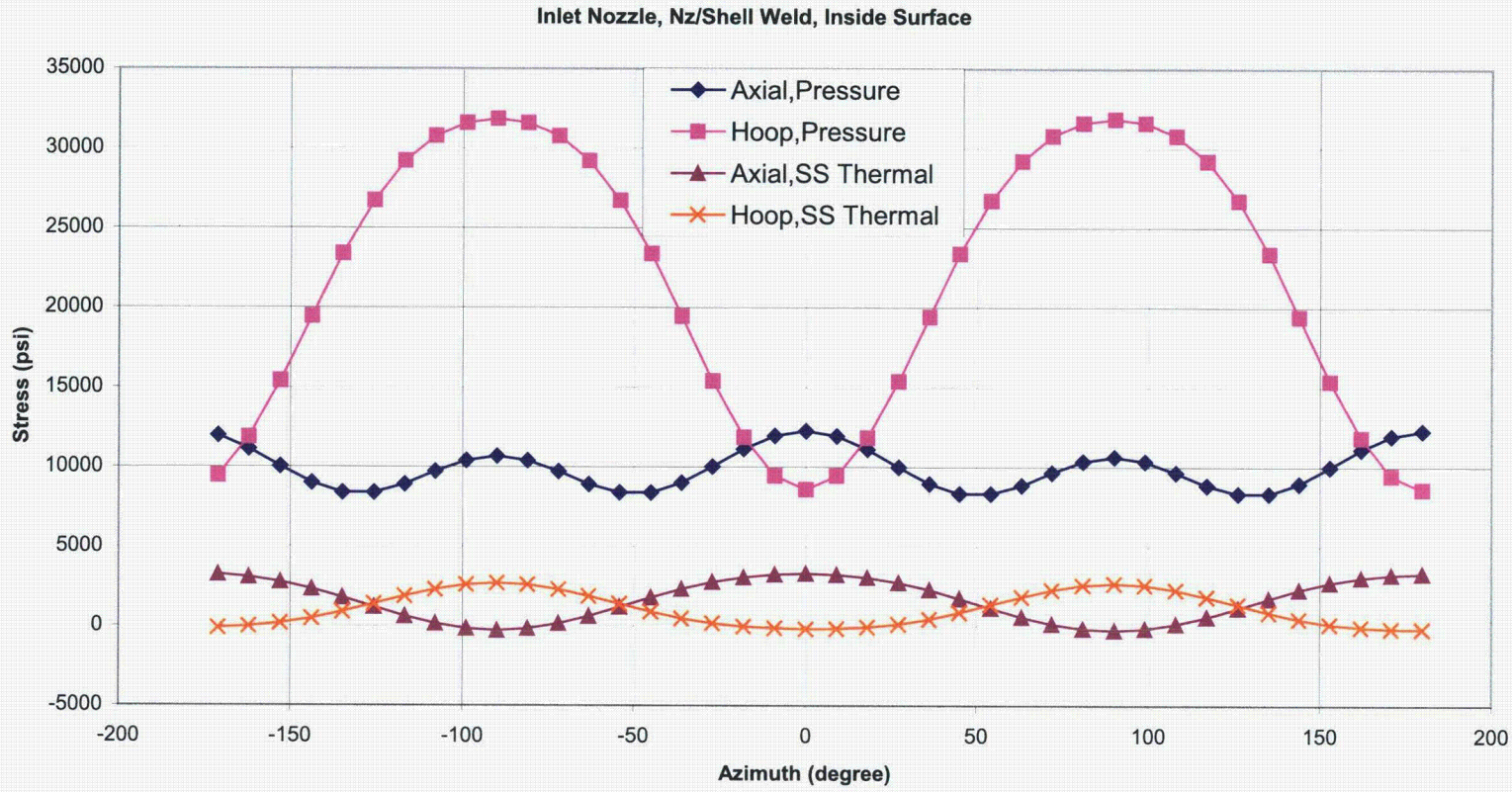

Figure 4-36
Recirculation Inlet Nozzle-to-Shell Weld Stress Profile

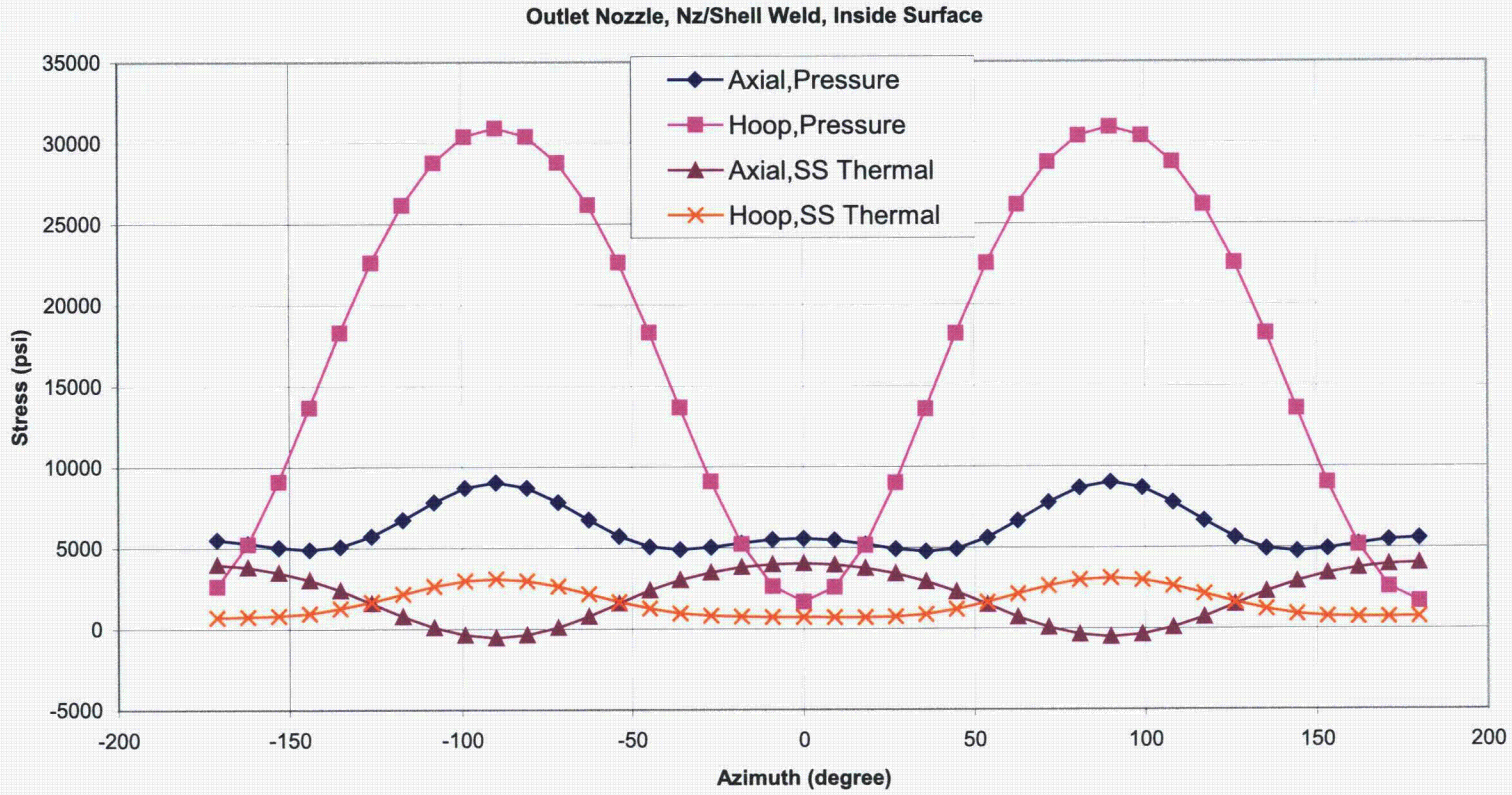

Figure 4-37
Recirculation Outlet Nozzle-to-Shell Weld Stress Profile

5
PROBABILISTIC FRACTURE MECHANICS EVALUATION

This section describes the probabilistic fracture mechanics evaluation performed to determine the probability of failure for the nozzle-to-shell weld and the nozzle blend radii. Evaluation was performed for the four nozzles of interest. The purpose of the PFM evaluation is to determine the reliability of the nozzle-to-shell weld and nozzle blend radii locations assuming various levels of inspection sampling. The key results from the PFM evaluation is the difference in reliability due to the inspection sampling level. Three cases of inservice inspection sampling level were evaluated; 0%, 25%, and 90%. The 0% case corresponds to no inspection, 25% corresponds to performing 25% of the nozzles for each nozzle type (e.g., 1 of 4 main steam nozzles), and 90% corresponds to performing 90% of the nozzles for each nozzle type.

5.1 Methodology

The approach was based on the methodology presented in Reference [1]. A Monte Carlo simulation was performed using a modified version of the VIPER program [20]. The VIPER program was developed as part of the program described in Reference [1] to support the technical justifications for eliminating RPV circumferential weld inspection. Also note that fluence is not significant at the nozzle locations.

The detailed description of the methodology incorporated in the VIPER program is documented in Reference [1]. The same limiting loading event, low temperature over-pressure (LTOP) that was used in the elimination of RPV circumferential weld inspections program, was used in this evaluation. The pressure for the LTOP condition is 1150 psi and the temperature is 88°F.

5.2 Design Inputs

This evaluation is intended to determine the effect of reducing inspection requirements on the probability of failure in the nozzle-to-shell weld and nozzle blend radius in BWR RPVs. As mentioned in Section 4.0, some of the design input is based on BWR fleet data. Other information is obtained from specific BWR plants as described below.

For the nozzle blend radius region, since the nozzles are forgings, the number of fabrication flaws (due to the weld) was assumed to be zero. In the weld between the vessel shell and the nozzle, the number of fabrication flaws was assumed to be 1 per nozzle weld. For both locations, the number of stress corrosion initiated flaws was assumed to be 1 per nozzle or per nozzle-to-vessel shell weld.

All random variables are summarized in Table 5-1.

Table 5-1
Random Parameters Summary

Random Parameter	Mean	Standard Deviation	Distribution
Number of flaws per nozzle from weld fabrication, nozzle/shell weld	1	–	Poisson
Number of flaws per nozzle from weld fabrication, nozzle blend radius	0.001	–	Poisson
Number of flaws due to stress corrosion initiation	1	–	Poisson
Flaw size-fabrication	–	–	PVRUF
Flaw size-stress corrosion	Clad thickness		Constant
Weld residual stress Through-wall	Cosine distribution: 8 ksi on inside and outside surface	5 ksi on each surface	Normal
Clad stress	32 ksi	5 ksi	Normal
RPV % Cu	0.26	0.045	Normal
RPV % Ni	1.2	0.0165	Normal
Neutron fluence	Negligible	–	–
Initial RT_{ndt}	-20 °F	13 °F	Normal
Fracture Toughness	Mean K_{IC} vs RT_{ndt}	–	
Upper Shelf K_{IC}	200 ksi$\sqrt{in}$	5 ksi$\sqrt{in}$	Normal
Stress Corrosion Initiation	$time = 4.21^{20}\sigma^{-10.5}$	Residual y = 0.9248x-0.0003	Lognormal
Stress Corrosion Crack Growth Rate, da/dt	$da/dt = 1.18^{-13}\sigma^{4}$	Residual y= 0.9085x-0.3389	Weibull
Stress Corrosion Crack Growth Threshold	33 ksi$\sqrt{in}$	9 ksi$\sqrt{in}$	Normal
Fatigue Crack Growth Rate, da/dn	$\frac{da}{dN} = 3.817^{-9} K^{2.927}$	Residual Y = 4.155x-0.3712	Weibull
Fatigue Crack Growth Threshold, ΔK	ΔK = 0 ksi$\sqrt{in}$	0 ksi$\sqrt{in}$	n/a

5.3 Assumptions

Where possible, the analysis was performed consistent with the methodology and assumptions in Reference [1]. The following assumptions were used in the evaluation:

1. Fluence at all nozzle locations is negligible.
2. Fabrication flaws are due to the weld process only.
3. One stress corrosion initiated flaw and no fabrication flaws in the nozzle blend radius, since it is forged.
4. One fabrication flaw and one stress corrosion initiated flaw per nozzle-to-shell weld.
5. PVRUF [1] flaw size distribution is assumed.
6. Residual stress at the nozzle-to-shell weld is modeled using a cosine through-wall distribution with a mean of 8 ksi at each surface.
7. The standard deviation for surface residual stress is assumed to be 5 ksi.
8. Average upper shelf fracture toughness is 200 ksi$\sqrt{in}$ with a standard deviation of 5 ksi$\sqrt{in}$.
9. Nozzle material chemistry is assumed to be the same as the nozzle-to-shell weld chemistry.
10. No interaction between stress corrosion initiation and fatigue crack growth (either stress corrosion or fatigue).

The modified software for this project is identified as VIPERNOZ to distinguish from the original VIPER software in Reference [1].

5.4 Fatigue Crack Growth

The fatigue data for A533-B-1 and A508-2 in pressurized water reactor (PWR) primary water are reported in Reference [21] for weld metal testing at an R-ratio (R) of 0.2 and 0.7. Most of the test data in Reference [21] are reproduced and presented in Figure 5-1. To produce a fatigue crack growth law and distribution for the VIPERNOZ software, the data for R= 0.7 was fit to a form of the Paris Law. The R= 0.7 was chosen for conservatism. The curve fit results of the mean fatigue crack growth law is presented in Figure 5-2 with the Paris Law shown as follows:

$$\frac{da}{dn} = 3.817 * 10^{-9} (\Delta K)^{2.927} \qquad \textbf{Equation 5-1}$$

where

a = crack depth

n = cycle

$\Delta K = K_{max} - K_{min}$

A comparison to the ASME B&PV Code, Section XI [22] fatigue crack growth law for reactor water environment is also presented in Figure 5-2. This figure shows a very reasonable comparison and shows the ASME Code Section XI data is more conservative on growth rate at high ΔK values.

Using a rank ordered residual plot, it was shown that a Weibull distribution was a better representation of the data. The Weibull residual plot with the linear curve fit of the data is shown in Figure 5-3, and represented by the following curve:

$$y = -0.3712 + 4.15x \qquad \textbf{Equation 5-2}$$

where

$y = \ln[\ln(1/(1-F))]$

$x = \ln[((da/dn)_{actual}/(da/dn)_{mean})]$

F = cumulative probability distribution

This crack growth rate relationship was used in the crack growth calculation portion of the PFM analysis.

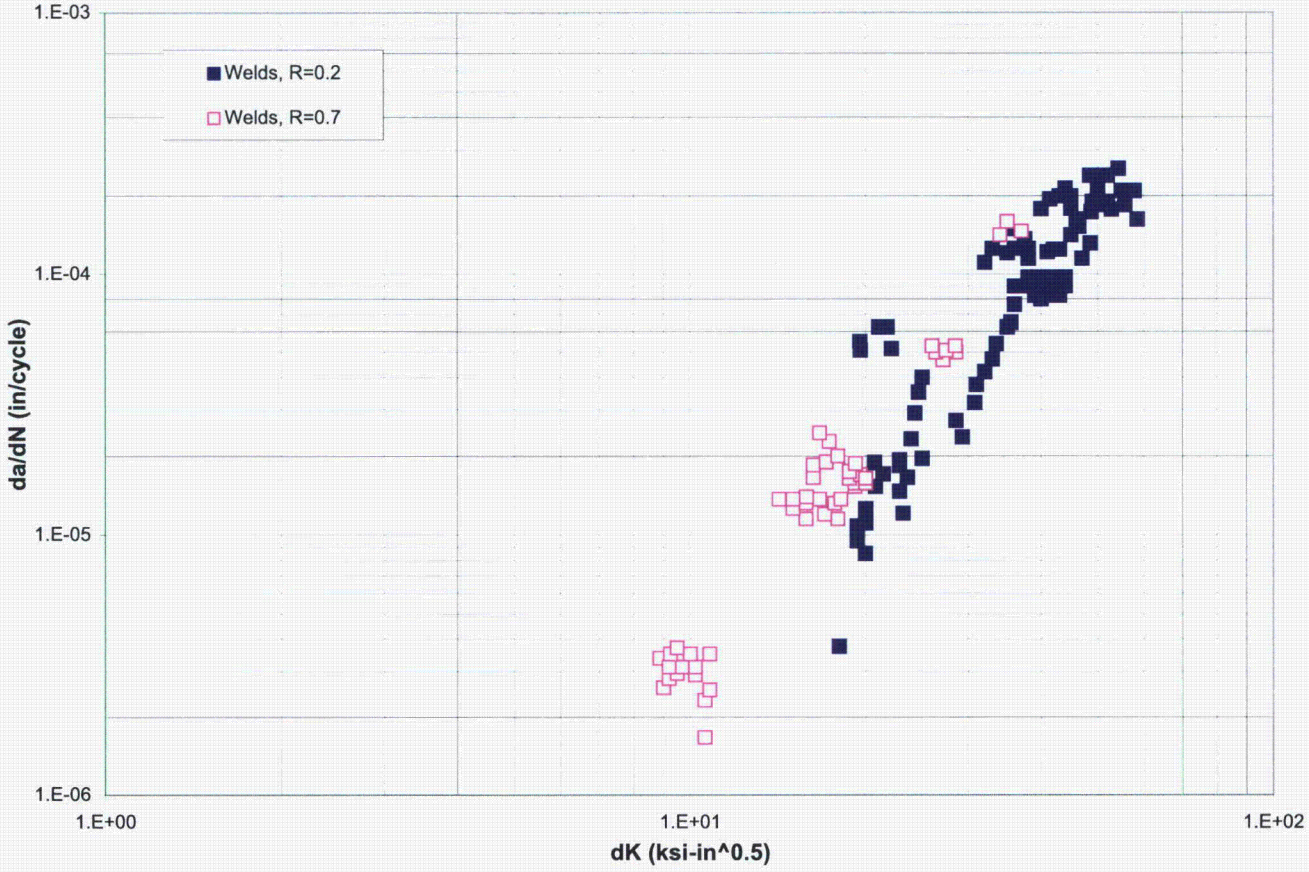

Figure 5-1
Fatigue Crack Growth Data

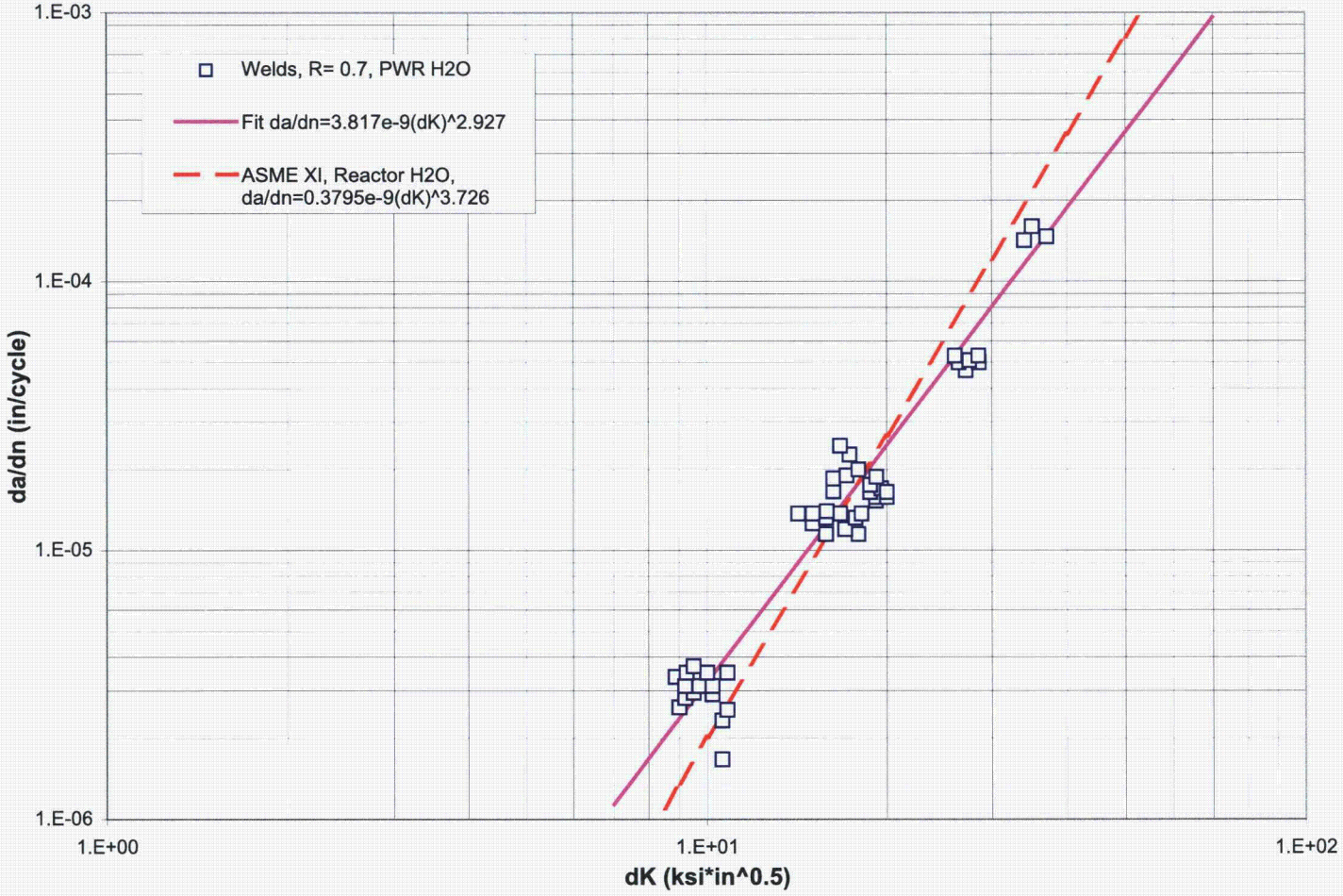

Figure 5-2
Curve Fit of the Fatigue Crack Growth Data

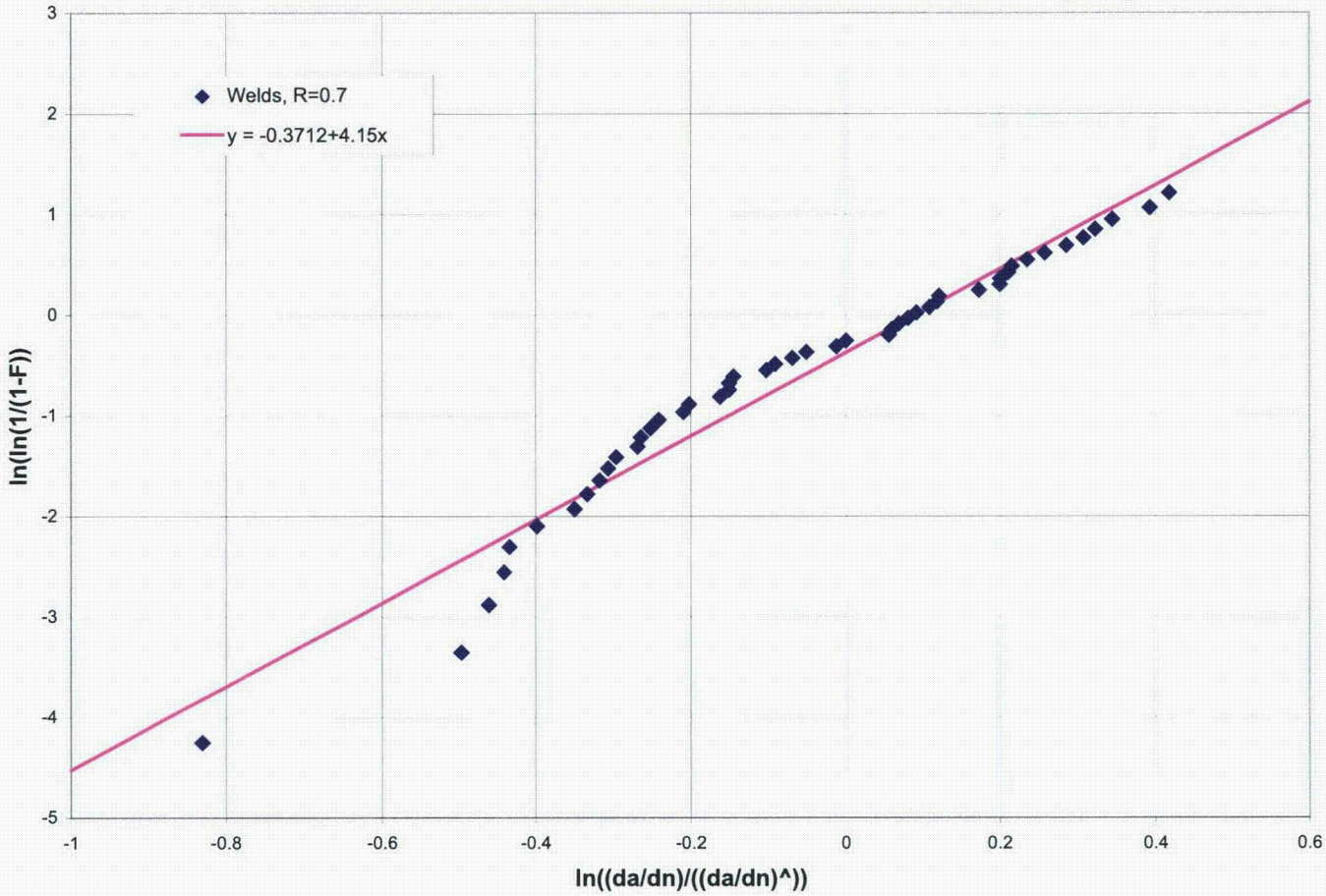

Figure 5-3
Residual Plot of Fatigue Crack Growth Data

5.5 Stress Results and Fatigue Cycle Loadings

The stress analyses for the nozzle-to-shell weld and the nozzle blend radius for the four nozzles were presented in Section 4. The stress analyses were performed for the load cases of unit pressure, unit moment, unit axial load, and the appropriate thermal transients for each nozzle. The through-wall sections were selected based on the stress results and postulated crack location. The locations of the through-wall stress sections and the azimuth locations are shown in Figures 4-1 and 4-2. The azimuth locations are 0°, 90°, 180° and 270° of the nozzles. Two through-wall sections were selected. Section C corresponds to the nozzle-to-shell weld. Section D corresponds to the nozzle blend radius.

The load cases analyzed for all the nozzles include:

1. Unit pressure
2. Unit axial load
3. Unit in-plane moment
4. Unit out-of-plane moment
5. Thermal transients depending on the nozzles as described in the previous sections

For the two sections of interest in the nozzles (nozzle blend radius and nozzle-to-vessel shell weld), the stresses due to the actual nozzle axial and moment loads in general are small compared to the stresses caused by the pressure and thermal loadings. Therefore, only the pressure and thermal stresses were used in the evaluation.

5.5.1 Core Spray Nozzle

The thermal transients for the core spray nozzle are presented in Figure 4-12 and 4-13 corresponding to heat up and emergency shut down transients, respectively. The pressure is 1050 psi and 0 psi at the beginning and at the end of the emergency shut down transient, respectively.

For the nozzle blend radius (Section D), for the thermal transients, only the maximum and minimum through-wall stress profiles that produce the largest stress ranges are used in the evaluation. For Section D, the maximum hoop stress (at 90° and 270°) among the four azimuth locations was conservatively used.

For Section C, the maximum stress is at the 90° and 270° in the hoop direction for the combination of pressure and thermal stresses and is used for this evaluation.

The thermal cycles for the core spray nozzle are summarized in Table 5-2. The number of heatup/shutdown cycles is 40 [23] for a design life of 40 years. The number of emergency cool down cycles is 10 for a design life of 40 years, [23].

Table 5-2
Nozzle Thermal Cycles

Nozzle	Transient	Cycles in 40 years
Core Spray	Heat Up/Shut Down	40
	Emergency Cool Down	10
Main Steam	Heat Up/Shut Down	40
Recirculation Inlet	Heat Up/Shut Down	40
	Sudden Pump Start of Cold Recirculation Loop	16
Recirculation Outlet	Heat Up/Shut Down	40
	SRV Blown Down	47
	Loss of Feedwater Pump	26

5.5.2 Main Steam Nozzle

The thermal transients for the main steam nozzle are presented in Figure 4-14 and 4-15. For the thermal transients, only the maximum or minimum through-wall stress profiles that produce the largest stress ranges were used in the evaluation. For Section D, the maximum hoop stress (at 90° and 270°) was conservatively used.

At Section C, the maximum stress is at the 90° location in the hoop direction for the combination of pressure and thermal stresses.

The thermal cycles for the main steam nozzle is summarized in Table 5-2. The number of heatup/shutdown is 40 cycles, [23] for a design life of 40 years.

5.5.3 Recirculation Inlet Nozzle

The thermal transients for the recirculation inlet nozzle are presented in Figures 4-16 and 4-17. The pressure is maintained at 1050 psig for the sudden pump start transient.

At Section D, for the thermal transients, only the maximum or minimum through-wall stress profiles that produce the largest stress ranges were used in the evaluation. The maximum hoop stress (270°) was conservatively used.

At Section C, the maximum stress in the hoop direction is at 90° and 270° for the combination of pressure and thermal loads.

The thermal cycles for the recirculation inlet nozzle are summarized in Table 5-2. The number of heatup/shutdown cycles is 40 [23] for a design life of 40 years. The number of sudden pump start of cold recirculation loop is 16 cycles for a design life of 40 years.

5.5.4 Recirculation Outlet Nozzle

The thermal transient for the recirculation outlet nozzle are presented in Figure 4-18 and 4-19. The minimum pressure for the loss of feedwater pump is 240 psig.

At Section D, for the thermal transients, only the maximum or minimum through-wall stress profiles that produce the largest stress ranges for thermal fatigue crack growth are used in the evaluation. The maximum hoop stress (90° and 270°) was conservatively used.

At Section D, the maximum stress is at the 90° and 270° in the hoop direction for the combination of pressure and thermal stresses.

The thermal cycles for the recirculation outlet are summarized in Table 5-2. The number of heatup/shutdown cycle is 40 [23] for a design life of 40 years. The number of SRV blow down transient is 47 cycles over the 40 year design life. The number of loss of feedwater pump transients is 26 cycles over the 40 year design life. Since there are 3 smaller cycles within each loss of feedwater pump transient, the total number of cycles used in the PFM analyses was 78 cycles.

5.6 Probabilistic Fracture Mechanics Evaluation Results

The probabilistic fracture mechanics evaluation was performed for the case of 0% inspection sampling (no inspection), 25% inspection sampling and essentially 100% (90%) inspection sampling during each 10 year interval for the four nozzles. The POD curve shown in Figure 2-1 ("Pass Plus Fail") was used in the evaluation to simulate the inservice inspection of the RPV.

For the nozzle blend radius region, a nozzle blend radius crack model was used in the evaluation of the RPV reliability. For this location and crack model, the applicable stress is the stress perpendicular to any section cut parallel to the nozzle longitudinal axis (axial crack with respect to nozzle centerline). The maximum stress among the four azimuth locations (0°, 90°, 180° and 270°) was selected for use in the PFM evaluation.

For the nozzle-to-vessel shell weld, either a circumferential or an axial crack could be initiated due to component fabrication (i.e. considering only the welding process) or stress corrosion cracking. From Reference [1], it is shown that the probability of failure for a circumferential crack is much less than an axial crack, due to the difference in the RPV stress (hoop versus axial) and the influence function of the crack models. It is also shown in the stress results that the difference between the thermal hoop stress and the thermal axial stress is less than the difference between the pressure hoop stress and the pressure axial stress. Therefore, the PFM evaluation for the nozzle-to-vessel shell weld concentrated on an axial crack (with respect to the vessel). The maximum hoop stress among the four azimuth locations is used and typically was from the 90° or 270° locations.

The results of the PFM evaluation are dependent on the fracture mechanics model used to represent the specific cracking being analyzed. As discussed in Section 2.0, there has been very limited observed indications at this location. Based on the fact that any flaws at this location would be very limited, any flaws that are postulated to be present are assumed to have an aspect ratio (ratio of depth to length, a/l) of 0.5.

The inspection POD curve shown in Figure 2-1 ("Pass Plus Fail") was used with an inspection interval of 10 years. The crack size distribution, PVRUF, is shown in Figure 5-4 and is the same as the distribution used in the BWRVIP-05 effort. The calculation of stress intensity factor is at the deepest point of the crack.

The analyses were performed using VIPERNOZ, a modified version of the program VIPER, [20], with the modifications as described in Section 5.3.

The number of simulations varied from 1 million to 10 million depending on the reliability.

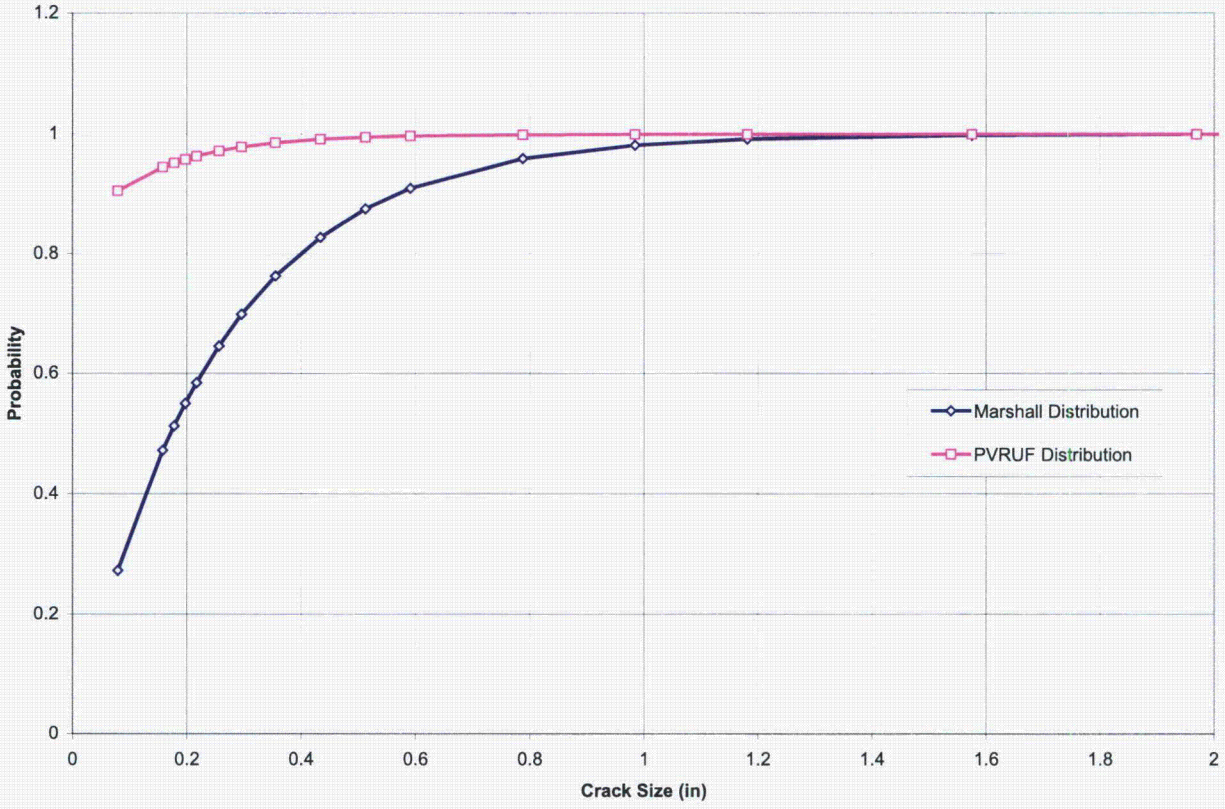

Figure 5-4
PVRUF Flaw Size Distribution

5.7 Results of Analyses

The reliability evaluation results are presented for the three cases (0%, 25% and 90%) of inservice inspection sampling level discussed above. The probabilities of failure are summarized in Tables 5-3 to 5-5 and described below.

Table 5-3
Probability of Failure Results Summary for 0% Inspection Sampling

Nozzle Blend Radius Results			
Nozzle	**# Simulations**	**# Fractures**	**Probability of Failure**
Core Spray	1 million	0	$<1x10^{-6}$
Main Steam	1 million	0	$<1x10^{-6}$
Recirculation Inlet	1 million	0	$<1x10^{-6}$
Recirculation Outlet	1 million	0	$<1x10^{-6}$
Nozzle-to-Vessel Shell Weld			
Nozzle	**# Simulations**	**# Fractures**	**Probability of Failure**
Core Spray	10 million	0	$<1x10^{-7}$
Main Steam	1 million	0	$<1x10^{-6}$
Recirculation Inlet	1 million	0	$<1x10^{-6}$
Recirculation Outlet	1 million	0	$<1x10^{-6}$

Table 5-4
Probability of Failure Results Summary for 25% Inspection Sampling, 10 Year Interval

Nozzle Blend Radius Results			
Nozzle	**# Simulations**	**# Fractures**	**Probability of Failure**
Core Spray	10 million	0	$<1x10^{-7}$
Main Steam	10 million	0	$<1x10^{-7}$
Recirculation Inlet	10 million	0	$<1x10^{-7}$
Recirculation Outlet	1 million	0	$<1x10^{-6}$
Nozzle-to-Vessel Shell Weld			
Nozzle	**# Simulations**	**# Fractures**	**Probability of Failure**
Core Spray	1 million	0	$<1x10^{-6}$
Main Steam	1 million	0	$<1x10^{-6}$
Recirculation Inlet	1 million	0	$<1x10^{-6}$
Recirculation Outlet	1 million	0	$<1x10^{-6}$

Table 5-5
Probability of Failure Results Summary for 90% Inspection Sampling, 10 Years Interval

Nozzle Blend Radius Results			
Nozzle	**# Simulations**	**# Fractures**	**Probability of Failure**
Core Spray	1 million	0	$<1x10^{-6}$
Main Steam	1 million	0	$<1x10^{-6}$
Recirculation Inlet	1 million	0	$<1x10^{-6}$
Recirculation Outlet	1 million	0	$<1x10^{-6}$
Nozzle-to-Vessel Shell Weld			
Nozzle	**# Simulations**	**# Fractures**	**Probability of Failure**
Core Spray	1 million	0	$<1x10^{-6}$
Main Steam	1 million	0	$<1x10^{-6}$
Recirculation Inlet	10 million	0	$<1x10^{-7}$
Recirculation Outlet	1 million	0	$<1x10^{-6}$

5.7.1 Inspection Sampling of 0% (No Inspection)

For the nozzle blend radius, the evaluation shows that the conditional probabilities of failure due to an LTOP event are insignificant ($<1.0x10^{-6}$) for the four nozzles evaluated (no failures predicted in one million iterations). Considering the LTOP occurrence probability at $1x10^{-3}$ per year, the total probability of failure for the nozzles would be less than $1x10^{-9}$ for the 40 year design life.

For the nozzle-to-vessel shell weld, using an axial crack model with a crack aspect ratio of a/l=0.5, the conditional probabilities of failure are small ($<1.0x10^{-6}$). No failures were predicted in 1 million simulations. The total probability of failure is less than $1x10^{-9}$.

5.7.2 Inspection Sampling of 25%

For any cracks in the nozzle blend radius region, the probability of failure due to the LTOP event is essentially insignificant, less than $1.0 x10^{-7}$ (no failures in 10 million iterations) for all nozzles. The total probability of failure is less than $1x10^{-10}$ for all nozzles except the recirculation outlet nozzle, which has a total probability of $1x10^{-9}$.

For the nozzle-to-vessel shell weld, the probability of failure for LTOP event is essentially zero, less than $1.0 x10^{-6}$, Table 5-4. This corresponds to a total probability of failure of less than $1x10^{-9}$.

5.7.3 Inspection Sampling of 90%

The probability of failure for any cracks existing in the nozzle blend radius region of the four nozzles evaluated is essentially insignificant, less than 1.0×10^{-6} with an in-service inspection coverage of 90% every ten years. The total probability of failure is less than 1×10^{-9}.

Similarly for the nozzle-to-vessel shell weld for an axial crack model the conditional probability of failure is less than 1.0×10^{-6}, corresponding to a total probability of failure of less than 1×10^{-9}.

6
DETERMINISTIC FRACTURE MECHANICS EVALUATION

Section 5 contained the PFM analysis of the four nozzles of interest. The PFM analysis takes the variation of key parameters into consideration. The PFM method can also take into account combinations of parameters that could result in limiting conditions. The ASME Code Section XI standard practice is to perform a deterministic fracture mechanics analysis.

In this section, a deterministic fracture mechanics evaluation is described. The DFM analysis uses average type parameters for the calculations and can also be performed using limiting parameters to produce conservative results. The DFM analysis can be useful in cases where a bounding type evaluation is required, but cannot take into consideration of the variation of independent parameters that can significantly impact the results. For the deterministic analysis, the same stress results (from Section 4) and the other input from the probabilistic analysis were used assuming these values to be the average values instead of variable values. An initial flaw depth of 0.15 inch was assumed for the DFM analysis.

Tables 6-1 and 6-2 present the results of the deterministic calculations for the four nozzles being considered. Results of the evaluation show that fracture of the two locations using the average values is not expected since the crack growth is not significant if the average growth rate is used.

Table 6-1
Nozzle Blend Deterministic Fracture Mechanics Analysis Results

Nozzle	Initial Crack Depth (in.)	Final Crack Depth (in.) (@ 40 Years)
Core Spray	0.15	0.51
Main Steam Line	0.15	0.41
Recirculation Inlet	0.15	0.57
Recirculation Outlet	0.15	0.53

Table 6-2
Nozzle-to-Shell Weld Deterministic Fracture Mechanics Analysis Results

Nozzle-to-Shell Weld	Initial Crack Depth (in.)	Final Crack Depth (in.) (@ 40 Years)
Core Spray	0.15	0.39
Main Steam Line	0.15	0.74
Recirculation Inlet	0.15	0.53
Recirculation Outlet	0.15	0.52

7
SUMMARY

An evaluation of RPV reliability as a function of nozzle inspection sampling was performed. The nozzles considered were the core spray, main steam, recirculation inlet and outlet nozzles. The analyses were performed using the worst weld chemistry from the BWR vessel fleet. Neutron fluence effects were assumed to be negligible. The stresses were conservatively selected from the limiting azimuth location in the nozzle. Any cracks were assumed to occur at the highest stressed locations around the nozzle azimuth (usually at the 90° or 270°). Both stress corrosion and fatigue crack growth were included in the evaluation. Fabrication flaws and stress corrosion initiated flaws were considered at the nozzle-to-vessel shell weld. Only stress corrosion initiated flaws were considered at the nozzle blend radius region. The probability of detection curve was determined using up-to-date inspection capability information.

For any cracks in the nozzle blend radius region, the results show that the conditional failure probability of the nozzles due to the LTOP event are very small ($<1x10^{-6}$ for 40 years), even without any inservice inspection.

At the nozzle-to-vessel shell weld, the conditional probability of failure due to the LTOP event is also very small, $<1x10^{-6}$ for 40 years with or without any inservice inspection.

The results are based on the assumption of one fabrication and one stress corrosion initiated flaw in the nozzle-to-shell weld and one stress corrosion initiated flaw in the nozzle blend radius region. The results also show that the majority of the crack growth is due to the stress corrosion for the four nozzles evaluated. Crack growth due to fatigue is small.

All initiated flaws are assumed to occur at the highest stressed locations, which is very conservative. Another conservatism in the evaluation is the use of elliptical axial crack in the nozzle-to-vessel shell weld. The nozzle-to-vessel shell weld is a circular weld. The analyses assumed that the crack, if initiated in the axial direction, would propagate axially. This assumption would predict crack growth into the vessel shell base metal. The probable crack growth path is more likely along the contour of the circular nozzle-to-vessel shell weld. If the crack follows the contour of the weld, it will grow into a lower stressed region.

Reference [1] shows that the circumferential crack in the vessel has probability of failure orders of magnitude smaller than the axial crack. This is due to the fact that the pressure stress in the hoop direction is twice as large as the axial stress. This condition is amplified for the pressure stresses in the nozzle region. Therefore, the evaluation of a circumferential crack in the nozzle to shell weld is not included.

From the evaluation, it is concluded that the failure probabilities due to an LTOP event at the nozzle blend radius region and the nozzle-to-vessel shell weld are very low for all inspecting sampling cases evaluated (0%, 25%, and 90%). In fact, no failures were observed in the analysis regardless of inspection sampling level, including the case where no inspection is performed.

Based on the results of this evaluation, it is concluded that the inspection of 25% of each nozzle type (e.g., 1 of 4 main steam nozzles) is technically justified.

8
REFERENCES

1. *BWR Reactor Pressure Vessel Shell Weld Inspection Recommendations (BWRVIP-05).* Electric Power Research Institute: September 1995. TR-105697.
2. ASME Boiler and Pressure Vessel Code, Section XI, Division 1, Section XI, Division 1, 1989 Edition, 1989 Addenda, Appendix VIII.
3. Gosselin, S. R., Heasler, P, G., Doctor, S. R., Simonen F. A., Becker F. L., "NDE Performance (POD) Curves for Fatigue Cracks in Piping Based on Industry Performance Demonstration," Topical Letter Report, Prepared for the U.S. Department of Energy, Pacific Northwest National Laboratory, Richland WA, 2001.
4. Nichols R. W., Crutzen S., "Ultrasonic Inspection of Heavy Section Steel Components – The PISC II Final Report," Elsevier Applied Science, 1988.
5. ASME Boiler and Pressure Vessel Code, Code Cases: Nuclear Components, 2001 Edition, Code Case N-552, "Alternative Methods – Qualification for Nozzle Inside Radius Section from the Outside Surface, Section XI, Division 1".
6. NUREG-0619, "BWR Feedwater Nozzle and Control Rod Drive Return Line Nozzle Cracking", U.S. Nuclear Regulatory Commission, 1980.
7. Bamford W. H. et al, "Technical Basis for Elimination of Reactor Vessel Inner Radius Inspections", ISI-99-26, ASME, Section XI.
8. ANSYS/Professional, Revision 5.7, ANSYS, Inc., December 2000.
9. General Electric Company APED Drawing No. 232-567, Revision 7, "Nozzle Details-Vessel," SI File No. GPUN-27Q-203.
10. General Electric Company APED Drawing No. 232-566, Revision 6, "Nozzle Details-Vessel," SI File No. GPUN-27Q-203.
11. Carolina Power and Light Specification No. 248-156, Revision 0, "Design Specification For Reactor Coolant Recirculation System N2 Nozzles, Safe End, and Thermal Sleeves," SI File No. CPL-05Q-200.
12. Chicago Bridge and Iron Company, Drawing R-10, Revision 0, "Forging Measurements," SI File No. W-EPRI-180-203.
13. Pilgrim Reactor Pressure Vessel Cyclic Load Analysis, Technical Report No. 93177-TR-03, Revision 0, SI File No. PNPS-02Q-211.
14. General Electric Company APED Drawing No. 232-565, Revision 5, "Nozzle Details – Vessel," SI File No. GPUN-27Q-203.

15. Combustion Engineering, Inc., Stress Report No. CENC-1143, "Analytical Report for Jersey Central Reactor Vessel," Nuclear Components Department, CE Contract 264, GPU Nuclear Company, SI File No. GPUN-27Q-204.

16. Structural Integrity Associates, SIR-89-033, Revision 0, "Design Report for Brunswick Recirculation System N2 Nozzle Safe End and Thermal Sleeve Replacement," SI File No. CPL-05Q-400.

17. ASME Boiler and Pressure Vessel Code, Section II, Part D, "Materials – Properties," 1995 Edition.

18. RPV Nozzle Stress Analysis, Revision 0, SI File No. GPUN-27Q-304.

19. General Electric Company APED Drawing No. 135B9990, Sheet 5, Revision 0, "Nozzle Thermal Stress Cycles (Drain-Core Spray and Head Spray)," SI File No. CPL-35Q-245.

20. VIPER, Vessel Inspection Program Evaluation for Reliability, Version 1.2 (1/5/98), Structural Integrity Associates.

21. Bamford, W.H., "Application of Corrosion Fatigue Crack Growth Rate Data to Integrity Analysis of Nuclear Reactor Vessels," Journal of Engineering Material and Technology, Volume 101, 1079.

22. American Society of Mechanical Engineers, Boiler and Pressure Vessel Code, Section XI, 1986 Edition.

23. "Reactor Vessel Thermal Cycles Design," and "Rector Vessel Nozzle Thermal Cycle Design," SI File NYPA-50Q-215 and SI File NYPA-50Q-216.

Export Control Restrictions

Access to and use of EPRI Intellectual Property is granted with the specific understanding and requirement that responsibility for ensuring full compliance with all applicable U.S. and foreign export laws and regulations is being undertaken by you and your company. This includes an obligation to ensure that any individual receiving access hereunder who is not a U.S. citizen or permanent U.S. resident is permitted access under applicable U.S. and foreign export laws and regulations. In the event you are uncertain whether you or your company may lawfully obtain access to this EPRI Intellectual Property, you acknowledge that it is your obligation to consult with your company's legal counsel to determine whether this access is lawful. Although EPRI may make available on a case-by-case basis an informal assessment of the applicable U.S. export classification for specific EPRI Intellectual Property, you and your company acknowledge that this assessment is solely for informational purposes and not for reliance purposes. You and your company acknowledge that it is still the obligation of you and your company to make your own assessment of the applicable U.S. export classification and ensure compliance accordingly. You and your company understand and acknowledge your obligations to make a prompt report to EPRI and the appropriate authorities regarding any access to or use of EPRI Intellectual Property hereunder that may be in violation of applicable U.S. or foreign export laws or regulations.

The Electric Power Research Institute (EPRI), with major locations in Palo Alto, California; Charlotte, North Carolina; and Knoxville, Tennessee, was established in 1973 as an independent, nonprofit center for public interest energy and environmental research. EPRI brings together members, participants, the Institute's scientists and engineers, and other leading experts to work collaboratively on solutions to the challenges of electric power. These solutions span nearly every area of electricity generation, delivery, and use, including health, safety, and environment. EPRI's members represent over 90% of the electricity generated in the United States. International participation represents nearly 15% of EPRI's total research, development, and demonstration program.

Together...Shaping the Future of Electricity

Programs:

Nuclear Power

BWR Vessel and Internals Project

Printed on recycled paper in the United States of America

1016123

Electric Power Research Institute
3420 Hillview Avenue, Palo Alto, California 94304-1338 • PO Box 10412, Palo Alto, California 94303-0813 USA
800.313.3774 • 650.855.2121 • askepri@epri.com • www.epri.com